ABSTRACT

CLAUNCH, ELIZABETH-LANE CARSON. Smart Composites: Optical Sensors Embedded in 3D Orthogonal Woven Fabric for Structural Health Monitoring Applications. (Under the direction of Dr. Abdel-Fattah Seyam and Dr. Kara Peters).

Unexpected failure in structures such as airplanes, bridges, and dams can have catastrophic effects. Structural health monitoring (SHM) is a way to monitor the integrity of such structures so that any critical deformation can be detected and acted upon immediately. Compared to most current SHM systems, which are applied to a structure's exterior, this research aims to introduce a polymer optical fiber (POF) based system that is an integral part of the construction material.

Due to their fiber-like structure, optical fibers are well suited to be incorporated in textile composites. 3D orthogonal woven (3DOW) preforms are an excellent host for optical fiber sensors because the yarns are arranged in straight paths. During composite fabrication, a POF can be woven directly alongside yarns in the 3DOW preform, creating a smart composite. This allows access to interior locations where other sensing methods may not be able to detect.

The overarching objective of this research is to prove smart composites composed of POF sensors embedded in 3DOW composites can function as viable structural health monitoring systems. Testing of this system mimics accidental impacts that can occur during a structure's lifespan by exposing the smart composite specimens to multiple low energy impacts at a localized site. The composite sensor system efficacy is then evaluated by establishing a relationship between the sensor's location, composite damage, and the resulting POF signal. This is used to determine the best location for optical fiber sensors to be placed within the composite so that they can accurately predict structural damage before failure occurs.

More effort is needed to bring the optical fiber sensor technology to a fully mature readiness level. A market study also accompanies this work, which aims to identify technological trends and future end uses of the optical fiber sensors through a strategic text-based analysis method.

Smart Composites: Optical Sensors Embedded in 3D Orthogonal Woven Fabric for Structural Health Monitoring Applications

by
Elizabeth-Lane Carson Claunch

A dissertation submitted to the Graduate Faculty of
North Carolina State University
in partial fulfillment of the
requirements for the degree of
Doctor of Philosophy

Textile Technology Management

Raleigh, North Carolina

2019

APPROVED BY:

_____	_____
Dr. Abdel-Fattah Seyam Co-Chair of Advisory Committee	Dr. Kara Peters Co-Chair of Advisory Committee
_____	_____
Dr. Kavita Mathur	Dr. Trevor Little

DEDICATION

To my grandfather, William Claunch

for allowing me to be my best self

BIOGRAPHY

Elizabeth grew up in Versailles, KY. She attended Auburn University and graduated with a Bachelor of Science degree from the Department of Polymer and Fiber Engineering in May of 2011. She then attended Virginia Tech where her research involved renewable composite materials composed of self-assembling wheat gluten. She graduated with a Master of Science degree in Biological Systems engineering in May of 2013. After taking a year off she decided to join North Carolina State University in August of 2014 to pursue her PhD in Textile Technology and Management. During this time, she has worked as a teaching and research assistant.

ACKNOWLEDGMENTS

I am thankful for the abundance of support and encouragement that was given to me throughout my Ph.D. studies. I was fortunate to have a wonderful advisory committee, who provided me with guidance and support. I'm especially grateful to my advisor Dr. Seyam, I could not have accomplished all that I have without his guidance, sponsorship, and motivation. I'm thankful to my committee co-chair Dr. Peters for her input and feedback. I also appreciate Dr. Mathur, Dr. Little, and Dr. Jordan for their willingness to serve on my committee and for their suggestions. Great thanks to NC State University, Wilson College of Textiles, and the Graduate School, for providing resources and a great hands-on learning experience.

I would also like to acknowledge my wonderful colleagues, Hadir Eldeeb, and Prateeti Ugale. Rahul Vallabh. Thank you, Ang Li, for help with compression testing. Thank you to Tywanna Johnson and Robert Cooper in the TATM department for assisting with our administrative needs. Also thank you to Tri Vu, for his mechanical help to keep our machines running. I would like to extend a special thanks to Mohamad Midani for patiently teaching the lab techniques and procedures that I needed to complete this project and for an unceasing supply of encouragement. Also thank you to Anuradha Gupta for her daily support, optimism, and delicious food.

I am also always thankful for my family and friends especially, my graduate school crew, Mira Abed, Emily Lichtenberger, and Kelsey Boes for their continuous love, friendship, and support.

TABLE OF CONTENTS

LIST OF TABLES

LIST OF FIGURES

Chapter 1: Introduction

Man-made materials are continuously evolving. With the popularity of the internet of things, everyday structures can be connected to the world, gathering usage metrics, and alerting the user to potential structural danger. Structural health monitoring (SHM) is one method to achieve this and consists of an intelligent system incorporating sensors, data transmission, computational power, and processing ability inside structures for real-time monitoring of structural conditions. A successful SHM system will positively impact the structure by ultimately increasing the safety of the structure, increasing the structure's longevity, and reducing the cost of maintenance and inspections. It should also be accurate at predicting failure within the structure through the quantitative information provided [1, 2].

Safety and failure prevention are strong motivations for implementing SHM systems. Civil structures are often complex and expected to be fully functional under severe environmental conditions such as high winds, storms, and earthquakes. These incidents present extreme loading that may compromise the integrity of the structure and lead to total failure that results in casualties, social, and economic problems. Therefore, it is necessary not only to monitor structural status (stress, displacement, acceleration), but also environmental parameters (wind speed, temperature, and quality of the foundation) with a complete SHM system [3]. Another issue with structures is that many are being used to their maximum capacity or past their intended lifespan. For example, many structures built in the 1960s and 1970s are now considered deficient by today's design standards and present a need to be monitored more frequently. Systemic visual inspection, instrumentation, load capacity tests, field measurements, and long-term performance monitoring and assessment are all viable tests that may be performed on a civil structure to ensure its integrity throughout its lifespan. SHM can provide information and eliminate many of these specifications, allowing physical inspections to be need-based instead of scheduled.

Poor maintenance and inspection programs can also cause accidents. The Aloha airlines incident is one example in which the fuselage failed during flight [4]. The failure mechanism was multiple fatigue cracks that potentially could have been noticed with better inspection methods. Other modes of failure could be due to poor manufacturing and unexpected load conditions. The use of new materials in construction, such as composites also creates a need for monitoring

because real-world performance experience is still limited in many cases [1]. For important novel structures, sensors are often installed during the construction phase for early monitoring. Minor repair can then be performed to avoid major damages that require costly renovation or even reconstruction [1].

The overarching objective of this research is to prove smart composites composed of POF sensors embedded in the 3D orthogonal woven fabric can function as viable structural health monitoring systems. Three levels have been outlined in order to examine different aspects of this objective. The first aims to understand the relationship between a composite's impact resistance and POF signal loss, to identify if the embedded sensor is sensitive to a damaging event. The second level aims to determine the sensitivity of the sensor related to its location from the damage event. This will help achieve the best configuration for the desired sensing application. Since optical fiber sensors are not yet a mature technology, the third level aims to observe technological trends and potential markets for the sensors. Understanding these relationships is an important step toward the proposed smart composite system being implemented for industrial use and achieving the benefits associated with structural health monitoring of structures.

Chapter 2: Literature Review

2.1. Introduction

The concept of smart materials can be considered a step in the general evolution of man-made objects. Human production often follows a trend from simple to complex. This trend in structures started with the use of homogenous materials, supplied by nature, was followed by multi-materials (in particular, composite materials) which allowed the creation of structures adapted to specific uses. The next step in the evolution consists of making the properties of the materials sensitive, controllable, and adaptive so that they can adjust to changing environment conditions [4]. SHM systems fit into this step of evolution through making materials sensitive.

Structural health monitoring involves the integration of sensors, smart materials, data transmission, computational power, and processing ability inside structures. This research investigates a novel SHM system based on a sensor that consists of a polymeric optical fiber (POF) embedded in a 3D orthogonal woven (3DOW) composite. Signal loss in optical fibers serves as the basis to interpret the structure's current health. This review focuses on the components that make up successful real-time monitoring systems and discusses the current uses of SHM systems.

2.2. SHM Sensor

The sensor is a key component in SHM and can detect and measure several parameters by comparing the measured value to a known. There are many types of sensors both in use and being investigated for SHM applications including strain gages, accelerometers, ultrasonic sensors, optical fiber sensors, acoustic sensors, and piezoelectric sensors [5-7]. Some of these sensors are difficult to deploy over large structures or are unable to withstand harsh environments [6]. Traditional electric load monitoring systems, such as accelerometers and strain gages, often require cumbersome wiring, can be large and difficult to embed in a structure [7]. In some cases, the signal can't be discriminated from the noise because of the electromagnetic interference. A possible solution to these issues is optical fiber sensors which have distinctive advantages over other sensing methods such as multiplexing capability, flexibility, high sensitivity, immunity to electromagnetic interference, and the ability to embed such sensors into the structure [8]. The following sections discuss optical fiber sensors which are

especially interesting because of their fiber-like structure which can be easily integrated into a smart textile system.

2.2.1. Optical fiber characteristics

The term optical fiber indicates a special form of optical waveguide with a circular cross-section, which is flexible and can be produced at great lengths [9]. They are most well-known for their use in communication to transmit light over longer distances and with higher data rates than other forms of communication. Use and testing methods for standard telecom optical fibers have paved the way for current SHM systems. Today, optical fiber sensors have been established as a new and innovative measurement technology in several fields, such as material science, civil engineering, light-weight structures, and geotechnical areas [10].

All optical fibers are composed of a core, a cladding, and sometimes another outer protective layer shown in Figure 2.1 [11]. In order to transmit a light signal effectively through the core of the fiber, the core and cladding are composed of two optically dissimilar materials. The core is the interlayer and is typically made of a material with a high reflexive index. The cladding surrounds the core and is made of a material with a low reflective index. Light waves are trapped and carried within the core by reflection at the interface between the core and cladding of the optical fiber [9, 12, 13].

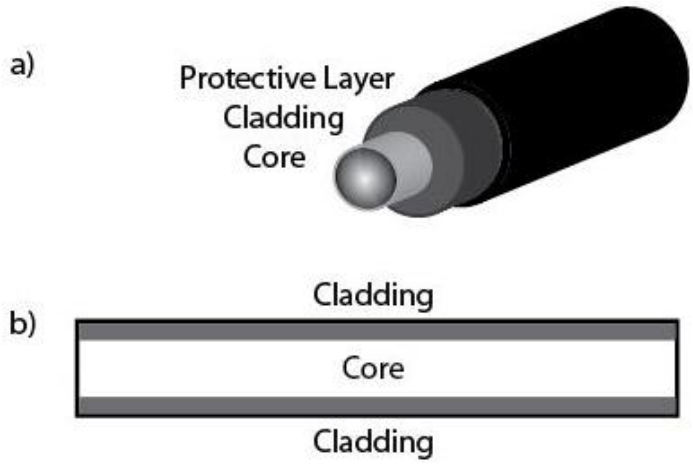

Figure 2.1. a) A typical structure of an optical fiber with the core, cladding, and optional protective layer. POF does not require a protective layer. b) Side view of an optical fiber

There are two classifications, single mode and multimode when it comes to light propagation in optical fibers. In single mode fibers, the light waves are all distributed in space the same way. Single mode fibers typically consist of a small core, and the light propagates nearly straight down the fiber at shallow angles relative to the core and cladding [14]. They are best suited for long distance communication, as they have only one strong propagation mode [14, 15]. Multimode fibers consist of a larger core, 50-100 μm, and contain more than one propagation mode [14]. Typically, larger cores simplify connection and allow for the use of lower cost electronics. However, the bandwidth to distance limit is lower and these fibers are typically better suited for shorter communication applications [15].

In multimode fibers, the refractive index profile can be uniform (step-index fibers, SI) or graded (graded-index fibers, GI). In a step index profile, the fiber has a constant refractive index across the entire cross-section for both the core and cladding. This causes light rays to travel in straight lines, shown in Figure 2.2a, which are completely reflected at the interface of the core and cladding. The individual rays travel different distances, resulting in varying transit times. Graded index profile, on the other hand, minimizes the difference in travel time. In GI, the core has a radius dependent refractive index and the cladding has a uniform index. As demonstrated in Figure 2.2b, rays in the middle of the core travel a short distance, but because of a higher refractive index at the center of the core, these rays also travel slower than the rays toward to edge of the core. The rays closer to the cladding in the core have a longer distance to travel, but they travel at a faster speed due to the lower refractive index near the cladding. Thus, the light rays are propagated at similar transit times. The refractive index profile is typically included in the naming system for optical fibers for its importance to the functionally, namely the transmission capacity of the optical fiber.

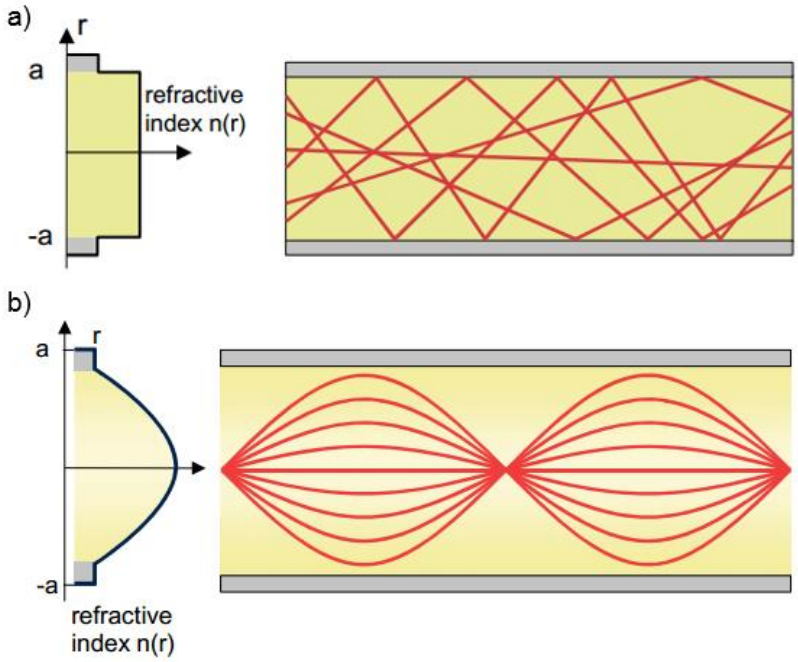

Figure 2.2. Refractive index illustration in a fiber with a) step index profile b) graded index profile [9]

Attenuation is a process encountered by light as it passes through a fiber. When light passes through a straight optical fiber, the power of the light decreases exponentially with length [9]. There are certain events that can cause more attenuation. These mechanisms can be classified as either intrinsic or extrinsic. Intrinsic losses typically originated inside the fiber and can include absorption of the constituent material and Rayleigh scattering. Both depend on the composition of the optical fiber and cannot easily be eliminated. Extrinsic losses, however, occur outside of the fiber and can more easily be avoided. Radiation losses which occur from bending are an example of an extrinsic loss. Macrobends occur from bends with large dimensions, such as rolling an optical fiber on a reel. As the bend radius decreases radiation losses increase. Small scale, fluctuations in the fiber axis are called microbends [15]. These losses can be detrimental to the power of light, thus the goal when dealing with optical fiber sensors is to minimize loss by careful manufacture and installation.

2.2.2. Optical fiber materials

Many of the characteristics of optical fibers are determined by their materials. There are two main material categories when dealing with optical fibers for use in sensing applications. The first and most widely used are silica optical fibers also known as glass optical fiber (GOF). GOFs have the benefit of having a high strength, small size, and low attenuation. They however also come with a low tensile strain and a tendency to be brittle. These optical fibers cannot handle bending and require multiple protective layers, such as a polymer layer to reduce abrasion and a protective outer jack to protect the core in situations where bending may be present [16]. When deployed as a sensor such protections can result in inconsistencies between the measurement of fiber strain and structural strain [17]. The addition of a third layer is also another step in the processing and an added cost.

The other category is polymer optical fibers (POF) in which the core is typically made from polymethylmethacrylate (PMMA), Polycarbonate (PC), Polystyrene (PS), or fluorinated polymer (PF).[18, 19] The cladding layer is generally made of fluorinated polymers. The first PMMA core was developed in the 1960s by Dupont [15]. POF technology, however, has been slow to take off because of high attenuation associated with PMMA, PC, PS cores. This limited them to communicate at a short distance. One of the main reasons behind the high attenuation is the C-H bond vibration absorption, which can be reduced by replacing hydrogen atoms with heavier atoms such as fluorine, chlorine, and deuterium. These polymers decrease the attenuation to <50 dB/km at the visible region of the spectrum, which is five times lower when compared to a PMMA optical fiber [19, 20]. It wasn't until 1996 that an optical fiber composed of amorphous fluorinated polymers was developed which exhibited a lower attenuation. PF has an attenuation that is five times lower when compared to a PMMA optical fiber [19, 20]. This makes it possible to extend the measurement length up to 500 m and allows POF to be more competitive with GOF in this aspect [20].

Generally, GOFs have better thermal stability and lower attenuation. POFs, however, have significant advantages in areas where GOFs fall short, exhibiting high elastic strain limits, high fracture toughness, high flexibility in bending, and high sensitivity to strain [11]. The main advantage of POF lies within the fracture resistance and flexibility. The elastic limit of a POF,

such as PMMA, is around 10% compared to silica at 1-3% [11, 18]. Plastics used in POF also have a lower density and lower cost than silica, resulting in overall lower weight, and typically less expensive optical fibers [11]. Unlike the GOF, POF can be fabricated with a large core diameter with less protected layers [21]. POF core diameter ranges from 50 µm to 1,000 µm, this is larger than the GOF core diameter which ranges from 10 µm to 100 µm [22]. The core, cladding, and overcladding dimensions of a perfluorinated POF are pictured in Figure 2.3. Using a large diameter core simplifies the light coupling through the fiber, but it can potentially create issues when embedding the fiber in a material if it is large enough to affect the properties of the material.

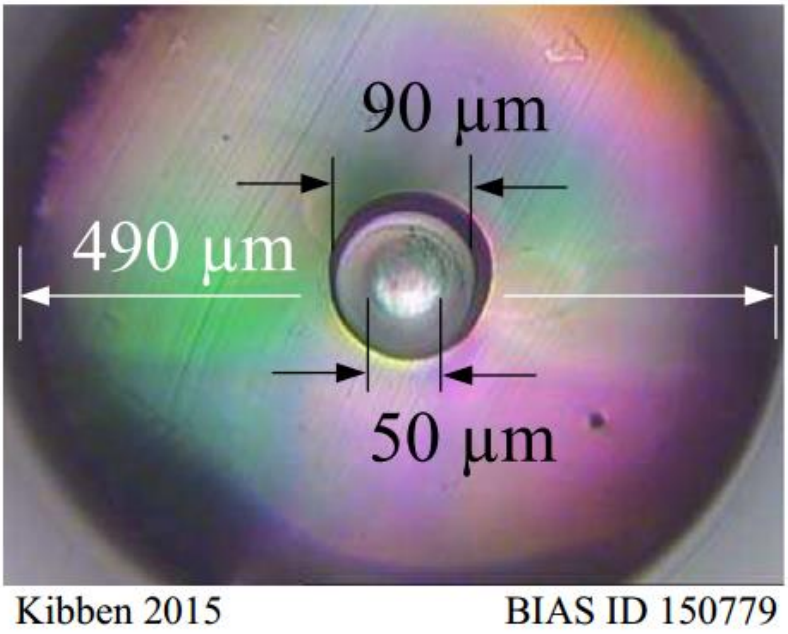

Figure 2.3. Cross-section of a graded index, perfluorinated POF with dimensions: core- 50 µm, cladding- 90 µm, and overcladding- 490 µm [23]

2.2.3. Optical fiber sensors

Based on their operating principle, optical fiber sensors can be categorized into three main types: interferometric, grating-based and distributed [6, 7]. Each category has a variety of types, targeting diverse measurement parameters and applications. In general, interferometric sensors are most suitable for single point detection. Grating-based and distributed sensors can be used for

quasi-distributed and distributed measurements respectively. Table 2.1 gives an overview of the major sensor types, and what parameters they typically are capable of measuring.
Sensors are either intrinsic or extrinsic. In an intrinsic sensor, the quantity being measured acts directly over the fiber and changes some physical properties of the optical fiber [14]. These changes produce a change in the properties of the light traveling inside the fiber. In this type of sensor, the light never exists the optical fiber. Two examples are curvature based sensors and Bragg grating sensors [14]. In an extrinsic sensor, the light modulation happens outside of the sensor. The fiber only carries light from the source to the sensing part and from the sensing part to the detector [14]. Fabry-Perot sensors are a typical example of an extrinsic sensor.

Table 2.1. Overview of optical fiber sensors

Category	Specific sensor type	Measurement parameters
Interferometric sensor	• Fabry-Perot • Mach-Zehnder • Michelson • Sagnac • SOFO sensors	• Strain • Refractive Index • Temperature • Velocity
Distributed sensor	• Ramen scattering • Rayleigh Scattering • Brillouin Scattering	• Strain • Temperature
Grating-based sensor	• Fiber Bragg Grating (FBG) • Long period Grating sensors	• Strain • Temperature • Vibration • Pressure

Interferometric sensors which detect optical phase differences between two light waves with the same frequency [6]. In this type of sensor, the measurements depend on the intensity of the light passing through the optical fiber and on the occurred interaction inside the optical fiber [24]. Sensors based on Mach-Zender and Michelson interferometers use long period gratings and photonic crystal fibers [25, 26]. These sensors have been used to measure refractive index [27], temperature [28], and velocity [29]. Sagnac type interferometers have mainly been applied to rotation measurements. Fabry-Perot is one of the more successful SHM sensors found in the

category and is typically used to monitor strain. Low coherent (SOFO) sensors are also very successful in the realm of SHM and have been deployed in bridges, buildings, oil pipes, and tunnels. They, however, are only suitable for the measurement of elongations and contraction at a low speed and are not capable of detecting impact damages [7]. Interferometric sensors have the advantage of being small and can be easily integrated into a structure without affecting its mechanical properties. They are also known for having high resolution. The major disadvantage, however, is that they have a low multiplexing capability which limits their application to measurement of a relatively low number of points [6].

Distributed sensors are a type of sensor in which the fiber is not directly affected by the measured parameter [19]. In distributed optical fiber sensing systems, the fiber itself becomes the sensor by detecting changes in the characteristics of the light scattered, caused by variation in physical parameters along the fiber length. The optical fiber is used to carry or transmit light to the outside of the fiber, where the light is influenced by the measurements, and then receive the light to measure the change in its intensity. Rayleigh, Brillouin and Raman scattering are types of light scattering used in these optical fibers. Rayleigh and Brillouin scattering are most commonly used for strain measurements and can be detected in both time and frequency domains [6]. Raman has been used mainly for temperature measurements [30].

Grating-based sensors have an inherent capability to measure a multitude of parameters such as strain, temperature, and pressure. This allows them to be a forerunner for SHM applications. Fiber Bragg grating (FBG) optical fibers, are considered the most mature grating based sensors and have been studied for a wide variety of mechanical sensing application including monitoring of civil structures (highways, bridges, buildings, dams, etc.), smart manufacturing and non-destructive testing (composites, laminates, etc.), remote sensing (oil wells, power cables, pipelines, space stations, etc.), smart structures (airplane wings, ship hulls, buildings, sports equipment, etc.), as well as traditional strain, pressure and temperature sensing. These sensors are often targeted as the major leading technology for SHM, in contrast to other competing optical fiber sensor technologies [7].

A Bragg grating is a periodic variation in the refractive index along the fiber core [1, 14]. The inscription is typically achieved using excimer lasers or UV sources and a method for generating the spatial pattern [6]. When a broadband signal passes through the optical fiber, a wavelength corresponding to the period of the index, known as a Bragg wavelength, will be preferentially reflected [11]. This leaves the rest of the incoming light to pass without altering its properties. An FBG can be used as an optical filter to block certain wavelengths or as a wavelength specific reflector [14]. When local deformation is present, the grating's period varies and the reflected wavelength changes accordingly allowing detection of strain. In fiber reinforced composites, FBGs are one of the most popular and reliable solutions for stain monitoring [8]. The main advantage of fiber gratings for mechanical sensing is that these devices perform a direct transformation of the sensed parameter to optical wavelength, independent of light levels, connector or fiber losses, or other FBGs at different wavelengths [6].

The production of FBG has proven more difficult for POF compared to GOF because the physical mechanisms for grating fabrication are different in POFs and have not been as widely researched. With POF, the dominant mechanism for inscribing gratings is through photopolymerization [11]. Gratings have been generated in POF, but several reports use polymer cores associated with higher attenuation, such as PMMA [1]. Recently Koerdt et al. [23] has demonstrated that Bragg gratings can also be generated on a perfluorinated POF, Figure 2.4. The gratings in the core were done with a krypton fluoride excimer laser and the phase mask method. The created polymeric optical fiber with Bragg gratings has a higher failure stain than GOF due to the polymeric nature. This is essential for SHM application where high strain may be observed. These fibers have promising stability, reliability and are a positive step toward polymeric FBG sensors for use in SHM applications.

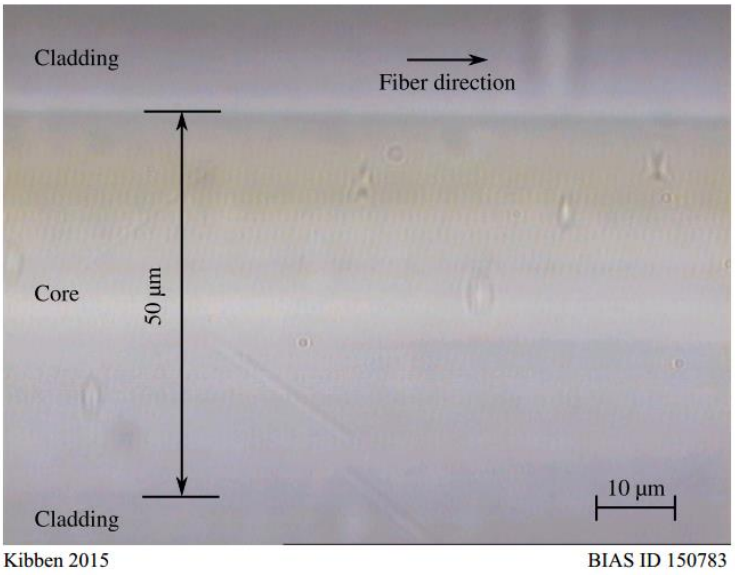

Figure 2.4. A grating period of 1µm perpendicular to the fiber direction and a yellowing core region are observable in the POF [23]

Di Sante suggested that one of the main challenges for both FBG-based and distributed sensing techniques is the development of reliable methods to monitor key structural parameters related to damage inception and growth over large structures [6]. Large scale adoption of these sensors for SHM is also hindered by issues regarding sensor performance, detection capabilities, size and the lack of a standardization and certification framework. But if designed and packaged properly, optical fibers can be a very robust sensing method [1]. With further advantages in research and development of the sensor technology, these issues are expected to improve.

2.3. Optical fiber loss testing method

All load-bearing structures will experience some level of damage during their lifespan. Using a parameter to evaluate the effect of damage on the structural performance, such as in SHM, can be fully achieved only when the nature of the damage is understood and characterized [13]. The basic steps of SHM in the case of damage monitoring are that the damage is detected by a sensor, the damage is then located and identified, and then the severity of the damage is determined. After this, the damage is reported and the necessary steps are taken, such as sending out a warning or making repairs. In this process, one of the most challenging steps is identifying the location and type of damage. Non-destructive techniques such as X-ray or ultrasonic inspection

are often used and can give important information about local damage, but do not have the ability of real-time monitoring needed for SHM and often require disassembly of the structure or of a part for further inspection [5].

In the case of optical fiber sensors, there are several methods for testing attenuation and optical fiber quality. These test methods, such as optical signal loss test and optical return loss test, measure the loss of optical fiber using end to end loss technique, where damage may be detected by a fiber breaking and transmission going from on to off, but this does not tell the user the location of defects that cause such power loss [16]. For decades, measuring optical fiber transmission loss was the only avenue for measuring optical fiber signal loss. These loss tests consist of a light source such as a laser device and power meter. Helem Neon (650 nm) is often used as a light source and located on one end of the optical fiber. An optical detector is located on the other end and is connected to a power meter. This loss test can be used with glass or polymeric optical fibers but can only measure the transmitted loss through the optical fiber without determining the location of the problem or identifying the reasons behind the loss. The main disadvantage of the loss test is that the test is maintained on both ends of the fiber, which means the light source has to be connected to one end and the detector and the power meter have to be connected to the other end. This test method can't be used to determine the location of the problem so this test has to be repeated at different lengths in order to determine the location of the defect or the problem.

2.3.1. Optical time domain reflectometry

Optical time domain reflectometry (OTDR) is a technique based on time domain detection. OTDR using Rayleigh scattering was initially developed for fault detection in the telecom field, based on loss of light at the damage location [6, 31]. Since its development OTDR has been used for testing optical fibers during installation, maintenance and restoration of optical sensor based systems by monitoring fiber attenuation, micro-bending loss, diameter fluctuations, and fiber length [32, 33]. Advanced OTDR can be used to determine the fiber signal loss, return signal loss at each connector, fusion splices, the location of defects, and may assist in defining the causes of the fiber signal loss [10, 16, 34]. It is often used to measure attenuation in distributed glass optical fiber sensors and has been used in research to physically sense bending and

clamping mechanisms [34]. The use of OTDR has had less popularity with POF sensors because of its high attenuation and expected large dispersion [35]. The increased physical flexibility, however, of POF material is particularly valuable when using OTDR in confined regions [13]. Therefore, OTDR still serves as a possible method for a POF distributed sensor and is being used in research settings [34-36].

There are two light levels in OTDR, a constant low level created by the fiber called Rayleigh backscattering and a high-reflection peak at connection points called Fresnel reflection. Rayleigh backscattering is used to calculate the level of attenuation in the fiber as a function of distance. It is a result of light hitting impurities and defects inside the optical fiber, depicted in Figure 2.5. When this happens the impurities can cause the light to scatter and be redirected, resulting in both signal attenuation and backscattering. Fresnel reflections detect physical events along the fiber and occur when a sudden change happens to fiber refractive index (i.e. change from fiber material to air). This causes the light to reflect back on the fiber and appears as a spike in the OTDR trace. These reflections typically occur at connectors, fiber breaks, and the ends of the optical fiber [37]. Fresnel reflections lead to what is known as dead zones, the length of time during which the detector is temporarily blinded by a high amount of light. This occurrence is like when a human eye receives a strong flash of light from the camera in the dark, or light from the headlights of a car at night. The eye is temporarily blinded and needs some time to recover. In OTDR, time is converted to distance, and more reflection causes the detector to take more time to recover, resulting in a longer dead zone.

One of the main advantages of OTDR is the single end nature of the test method, requiring only the operator and instrument to qualify the fiber and find defects. In OTDR based on Rayleigh scattering, the backscattered light signal is measured. To perform the measurement, short light pulses are coupled at one end of the optical fiber. The light is transmitted through the fiber and undergoes Rayleigh scattering along the fiber length, illustrated in Figure 2.5 [9]. A proportion of the light is backscattered and results in a reflected pulse detected at the input [32, 34]. A reflection or excess loss is observed in the spectra when there are defects, disturbances, or discontinuities in the fiber [32, 35]. The total time duration for the light to travel from the input

to reflect the input again is also measured [38]. From this backscattering measurement, statements about the attenuation curve and local disturbances can be made.

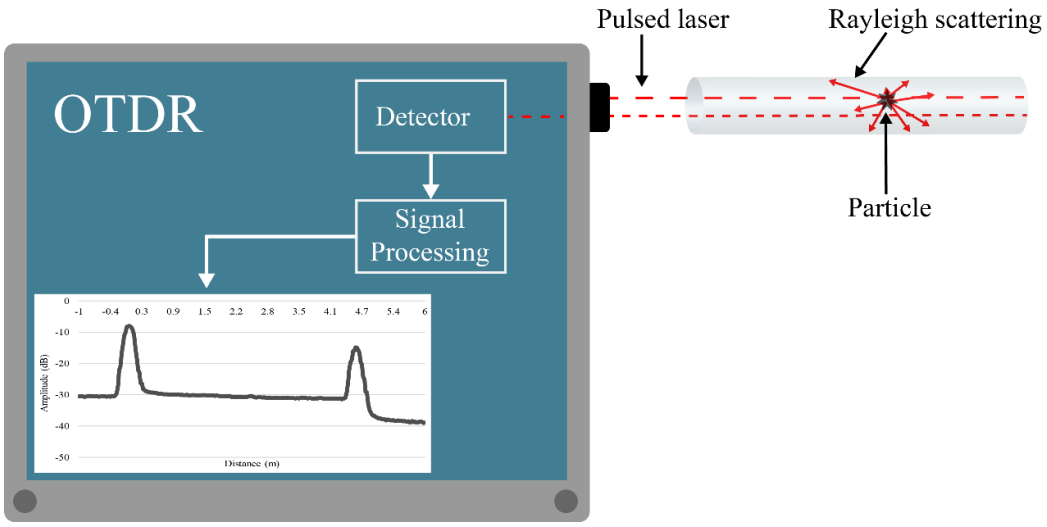

Figure 2.5. Illustration of OTDR function, Rayleigh backscattering in the optical fiber, and the resulting spectra

The major restriction of OTDR, especially related to SHM is low spatial resolution of 1 m. With OTDR, the low spatial resolution in necessary to achieve a higher dynamic range. By increasing the laser pulse width, the signal to noise ratio increases, hence the dynamic range increases, while the spatial resolution of the OTDR system decreases by increasing the laser pulse width and increasing the bandwidth of the photodetectors [40, 41]. For certain distributed sensing requirements such as crack detection in building materials, a crack width less than millimeters in width can be an issue for the OTDR to detect because of the spatial resolution [39]. Regardless, researchers have found ways to use OTDR based on Rayleigh scattering in SHM applications. One approach is to use a “zig-zag” method to detect cracks in a structure. In this method, the optical fiber sensor is embedded in a zigzag pattern and monitored by OTDR [3]. When a crack forms within a structure, such as the bridge deck, the optical fiber intersecting with the crack at any angle other than 90° has to bend to stay continuous [12]. This disruption in the fiber is considered micro bending and results in a sharp drop in the optical signal. The light intensity loss is detected and located by means of the OTDR equipment, therefore locating the position of the crack within the structure.

OTDR is the first generation of fiber optic distributed sensors and allows damage location monitoring, but its use and application are limited. OTDR based on Raman (ROTDR) and Brillouin (BOTDR) scattering are more recently being employed for distributed sensing applications. In both mechanisms, spectral components are affected by environmental parameters, which allows observation of temperature and strain. Table 2.2 provides a comparison of these distributed sensing methods. In ROTDR evaluating the intensity ratio between the anti-Stokes and Stokes components of the spectra can provide information about temperature [7]. Brillouin scattering is produced by the interaction between light and sound [39]. The frequency of light scattered in BOTDR is dependent on temperature and strain and thus evaluating the spectra, can determine changes in the external environment [7].

Table 2.2. Distributed sensing methods

	OTDR	**ROTDR**	**BOTDR**	**OFRD**
Sensing Parameters	• Fiber loss • Break location	• Temperature	• Temperature • Strain	• Temperature • Strain
Spatial resolution	• 1-10 m	• 1 m	• 1-5 m	• 10 μm-10 mm
Advantages	• Wide applications • Long range	• Infinite sensing points	• Infinite sensing points • Long range	• Faster rate • High spatial resolution • Large dynamic range
Disadvantages	• Detection limitations • Large Bandwidth	• Temperature only • High Cost	• Cross sensitivity	• Shorter range

2.3.2. Optical frequency domain reflectometry

OTDR does have some limitations including uncertainty in measurement location, and the need for a very large frequency bandwidth [6]. These limitations may be overcome using a Rayleigh scattering based technique called optical frequency domain reflectometry (OFDR). The mechanism of the OFDR technique is to obtain the backscatter information of a fiber in the frequency domain by measuring the complex transfer function of the fiber and subsequently calculate the impulse response in the time domain by conducting an inverse fast Fourier

transform [42]. By repeating the measurement process along the fiber length, it is possible to obtain a measurement of strain [6]. This method provides a distributed measurement of multiple reflections along the fiber with high spatial resolution but also enables detection of loss and fiber attenuation at a quality comparable to OTDR [42]. OFDR has advantages over OTDR for applications that require a combination of high speed, sensitivity, and resolution over intermediate length ranges [41]. OTDR, on the other hand, is better suited for longer range, low-resolution system-level applications.

A study by Liehr, Nother, and Krebber [42] presents the use of OFDR with multimode GOF and perfluorinated POF. In OTDR, changes in the backscattering of light can be used to locate and detect strain along the length of a POF. The authors show that this change is also observed with the OFRD technique, Figure 2.6, and at a faster rate of 1 second measurement time compared to existing OTDR devices which operate at 2-minute measurement times. This measuring technique is an important improvement of current POF strain sensor technologies for applications in SHM where real-time results are critical for strain detection and it opens the door for new SHM applications due to dynamic measurement possibilities and increased accuracy over traditional sensing methods.

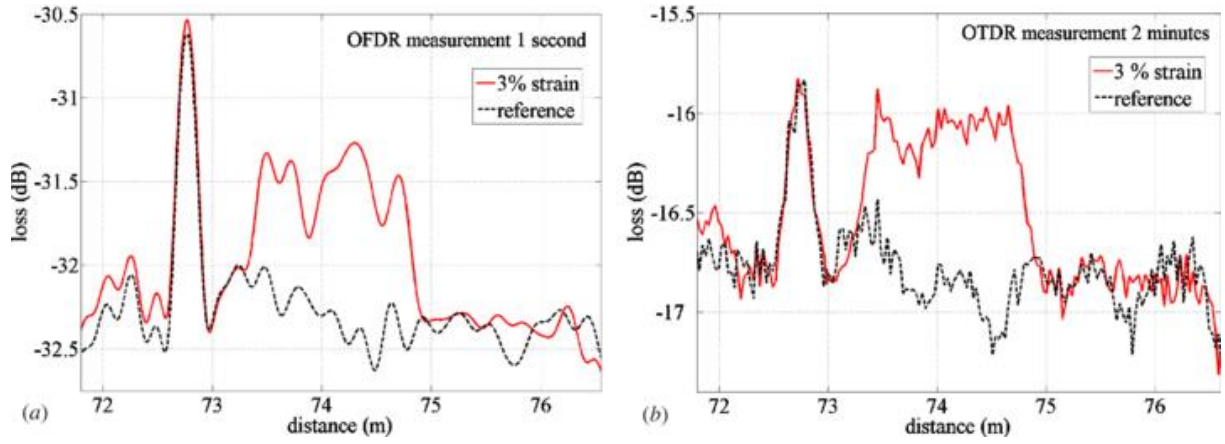

Figure 2.6. a) OFDR measurement compared to b) OTDR measurement for a 1.5 m section of perfluorinated POF strained to 3% [42]

2.4. Composite design

Composites are a combination of two materials, the filler, and the matrix, that optimize and leverage the advantages of each. The bond between these constituents, known as the interface, is a region with distinct properties that plays an important role in mechanical performance and must be also considered during fabrication. The choice of material for the filler and the matrix is determined by the desired combination of properties, intended application, and method of manufacture. In many industries, such as aerospace and marine, there is a high value placed on lightweight, high strength, and corrosion resistant materials. The low density of composites compared to traditional structural materials meets this high standard, and also provides the added benefit of lower fuel consumption and faster speeds for aircraft and ships. The structure of the Boeing 787 Dreamliner, for example, is composed of 50% composite materials by weight and is one of the first aircraft which is clearly designed to allow SHM systems to be embedded, particularly for impact detection [4, 6]. Figure 2.7 shows where composites are currently being deployed in the Boeing 787.

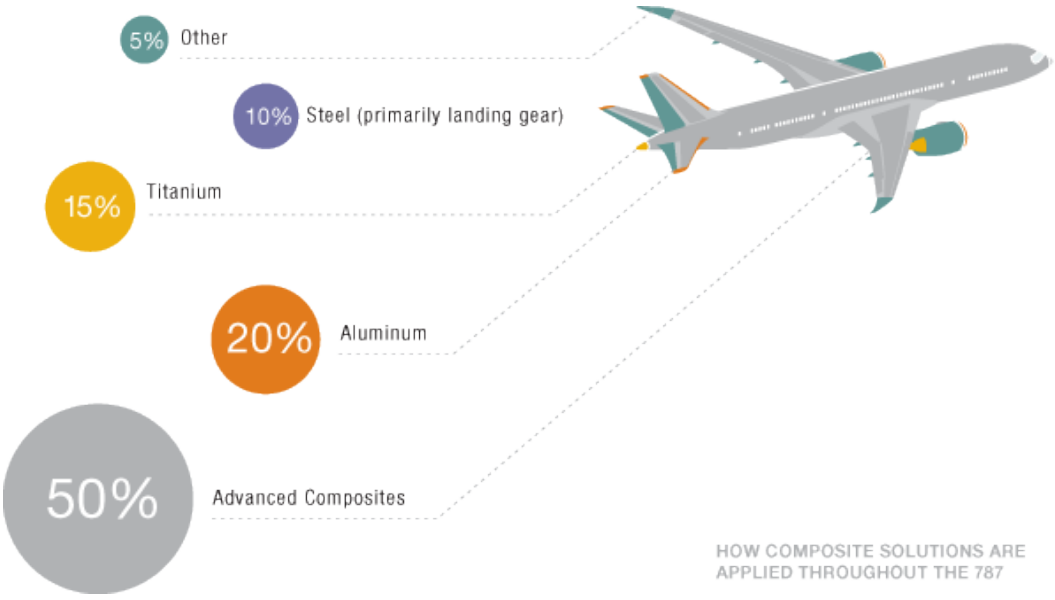

Figure 2.7. Use of composite materials in Boeing 787 [43]

Boeing also claims that composite structures require less scheduled maintenance than non-composite structures. For example, the Boeing 777 composite tail is 25% larger than the 767

aluminum tail but requires 35% fewer scheduled maintenance labor hours, because composites have a reduced risk of corrosion and fatigue compared with metal [43]. With the use of metal, there is the risk of fatigue cracking and corrosion experienced with traditional aluminum floor beams. The 777 model has been flying for more than 10 years with more than 565 airplanes in the fleet and to date has not replaced a single composite floor beam [43]. Composites are a perfect candidate for SHM systems since they offer unique, tailorable advantages over traditional materials and help meet the goals SHM by lowing overall maintenance time and costs and increasing the safety of the structure. This section discusses the materials and practices used to create these materials and how sensors can be embedded to create a smart composite material.

2.4.1. Composite properties

Conventional engineering materials are usually classified into metals, ceramics, and polymers. Like composites, each single phase material has advantages and disadvantages which dictate their end use and application. Metals tend to be heavy, but they are chosen for their high strength and toughness. Ceramics are brittle, but they are often used for strength and thermal resistance. Conventional polymers tend to have low strength, but they are often chosen for situations which require ductility and lightweight. Industries are increasingly requiring materials to have unusual combinations of properties that cannot be met by conventional metal alloys, ceramics, or polymeric materials. A unique advantage of composites is that their properties can be tailored to fit different types of loading conditions by changing the materials involved or the structure of the matrix.

Property maps are a convenient way to compare the property combinations offered by composites with those of conventional materials [44]. Relating two properties of material was pioneered by Ashby and resulted in diagrams similar to the one found in Figure 2.8 which shows Young's Modulus (E) as a function of density (ρ) [44]. These diagrams are useful for comparing ratios of two properties, and from them, a material of maximum performance can be selected. Steel and concrete are widely used traditional building materials for their high strength, but as shown in Figure 2.8, carbon fiber reinforced composites (CFRC) offer a similar E value to steel but with reduced density and glass fiber reinforced composites (GFRC) have a similar E value to concrete with a reduced density as well.

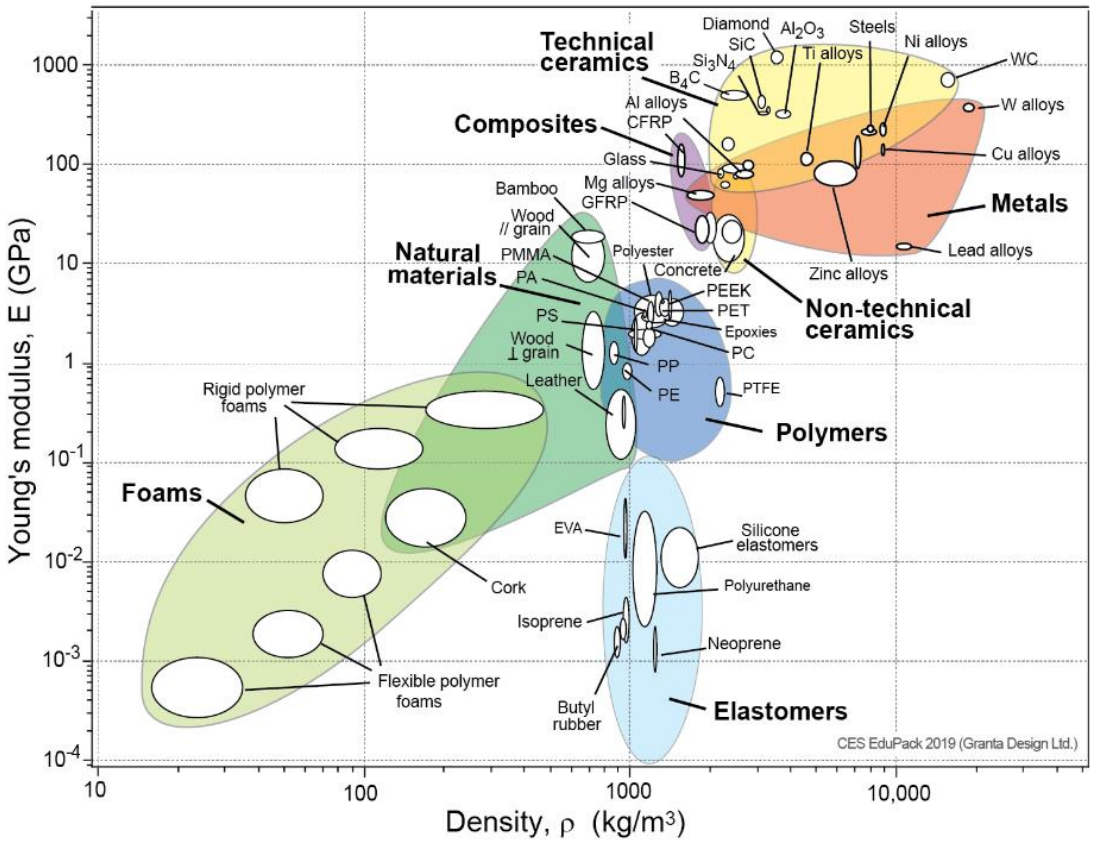

Figure 2.8. Diagram of Young's modulus as a function of density which demonstrates that composite materials (CFRC and GFRC) are competitive with traditional materials such as steel and concrete [45] (Chart created using CES EduPack 2018, Granta Design Ltd.)

Despite the advantages and success of composites their adoption as a common building material has not been widely accepted. Composites are more complex than their traditional counterparts, and durability and safety issues are a concern for some industries. One of the major concerns with implementing composites as a structural component is their reaction to damage. In a composite, large anisotropies in stiffness and strength are possible and must be considered during design. This represents a departure from conventional engineering practice, in which an engineer designing a component commonly considers material properties to be isotropic [44]. The mechanical differences in the materials used for the matrix and reinforcement can result in relatively unpredictable behavior involving the initiation and propagation of damage. Failure of composites is a multistage process in which the failure may be triggered in a certain mode, but propagation and final failure mode may differ for the initial mode [44]. In many cases, composite failure gets initiated internally and only once the failure has propagated cannot be observed

externally. Internal failure of composites can manifest as breaking of fibers, microcracks in the matrix, debonding between fiber and matrix, and delamination [44]. This type of failure can be difficult to observe and monitor through routine external inspections. It is also difficult to estimate the remaining strength and residual life of the structure [6]. A significant amount of research has been conducted in order to investigate the influence of defects, especially those caused by impact, on the strength and life of composite structures [6]. SHM can play a critical role in aiding this research and can offer insight, through sensor feedback, about the material during the design and construction phases.

2.4.2. Classification of Composites

Composites are often classified by their matrix and filler materials. In industry, there are three main classes of composite based on the matrix material. The most common are polymer matrix composites (PMCs) that usually consist of a polymer matrix embedded with glass, carbon, or aromatic polyamide fibers such as Kevlar [46-48]. Another class is metal matrix composites (MMCs) which are most often implemented for high-temperature use. The third class is the ceramic matrix composites (CMCs). CMCs function opposite to PMCs in which the filler contributes to toughness and the matrix provides the majority of the strength [44, 49].
Three main categories are typically identified when discussing composite reinforcement: particle, fiber, and structural. Particle reinforced composites consist of particles distributed within a matrix [50]. Large particles are often used to restrain movement of the matrix and impede crack propagation. With smaller particles (0.01-0.1μm), known as dispersion strengthened composites, the particle-matrix interaction occurs on an atomic or molecular level. In this type of composite, the matrix bears most of the load. Concrete is the most common example of a particle reinforced composite.

Structural composites are those which consist of several two-dimensional (2D) layers bonded together. The properties of structural composites depend on both the constituent material and on the strategic geometric design of the layers. Laminar composites and sandwich panels are two of the most common types of structural composites. Laminar composites are composed of 2D layers of aligned fibers, randomly distributed fibers, or woven fabric [44, 50]. The layers are stacked and bonded together such that the strength direction varies with each layer to achieve the end

property goal. Sandwich panels are designed to be lightweight beams or panels having relatively high stiffness and strength. A sandwich panel consists of two outer sheets that are separated by an adhesively bonded core. Typically, the outer sheets are made of a stiff material and the core material is lightweight and has a low modulus of elastically. These stacked composite structures have found use in a wide variety of applications including roofs, wind turbine blades, and aircraft wings.

Fiber reinforced composites are composed of fibers embedded in a matrix material. The design goal of fiber-reinforced composites is typically to create high strength at a reduced weight. The filler consists of either continuous fibers or discontinuous fibers which can be aligned or randomly oriented. Discontinuous fiber composites contain short fibers, nanotubes, or whiskers as the reinforcement and can be anisotropic if the fibers are aligned, or quasi-isotropic if they are randomly oriented. Continuous fiber composites consist of long fibers which can be parallel, oriented at right angles to each other (crossply or woven fabric), or oriented along several directions (multidirectional continuous fiber composite) [50]. The fiber in this type of composite is responsible for a significant percentage of the applied load. The matrix typically has a lower stiffness and strength than the fiber and serves to protect, align, and stabilize the fibers, as well as transfer stress from one fiber to another [51].

Continuous fibers can be produced in a variety of geometric preforms using technology originally developed for textile processes: knitting, braiding, and weaving. With knitting, the yarn is arranged in a repeating series of intermeshed loops so that the orientation of fibers is changing continuously in three dimensions [44]. There are many knitting configurations possible. The volume fraction of fibers in knit composites, however, is relatively low and large matrix pockets cannot be avoided [44]. The 2D fiber arrangements produced by braiding are similar to woven fabrics and are typically used to create flexible tubes. Woven fabrics can be configured into many designs such as plain, satin, and twill weaves. These fabrics are flexible and allow draping so that nonplanar structures can be created. Both braided and woven structures also lead to pockets in the matrix at cross-over points, and thus the maximum fiber content is often less than in laminated composites made by stacking unidirectional plies [44]. Weaving for

use in composites can also have unfavorable characteristics in terms of mechanical properties, fiber interlacing, and crimp.

2.4.3. 3D woven preforms

Textile methods can be configured into 2D fabrics, often used as layers in laminar composites, or for the production of three-dimensional (3D) fabric preforms [52]. In 3D techniques, the goal of research has been to develop processes that can produce complex performs in an automated, cost-effective manner [53]. One of the most prominent features that separate 2D fabrics from 3D are that they have a substantial dimension in the thickness direction formed by layers of fabrics or yarns [54]. The manufacturing of thick composites lowers fabrication costs due to reduced labor time when multiple layers of 2D fabric plies are replaced by one or a few 3D woven plies providing the same required thickness in a composite structure.

3D woven preforms can be classified into those that can be manufactured on conventional weaving technology and those that require specially made weaving machines/devices [54]. The most common multiply and multiaxial 3D weaves are a type of angle interlock performed on 2D weaving machines that use cam, dobby, or Jacquard shedding mechanisms [55, 56]. Multiply weaves can be created by stitching through the raising and lowering of harnesses with a conventional loom. One significant drawback of the process of weaving multilayer fabrics on conventional 2D weaving machines is that it creates a high level of yarn interlacing. This leads to a high degree of fiber crimp which can negatively affect the mechanical properties of the composites [57]. Another drawback is fiber damage that can be caused by the moving parts [56]. This type of weave is acceptable for some types of applications, but for some others, having zero crimp is more desirable.

The second type of 3D woven preform is known as a 3D orthogonal weave and is produced on a special 3D weaving loom, which requires three sets of yarns compared to the conventional two. The structure of the 3D orthogonal weave is shown in Figure 2.9. The X-yarns (red) are orthogonal to the Y-yarns (blue) and do not interlace. Since there is no interlacing, there is minimal crimp between the X- and Y-yarns which results in increased properties of the final composite. The Z-yarns (green) interlace through the entire thickness of the preform, binding the

layers together. One concern with composites is that they are susceptible to damage, mainly delamination in the Z direction between layers. Interior delamination significantly affects performance by degrading stiffness and reducing the load bearing capability of the structure [13]. An additional benefit of 3D orthogonal weave is that it adds reinforcement in the thickness direction and prevents delamination. Two of the goals of SHM are to increase the longevity of the structure and reduced maintenance time and cost. This orientation of fibers helps SHM meet its goal by providing added reinforcement and preventing one type of common damage from occurring.

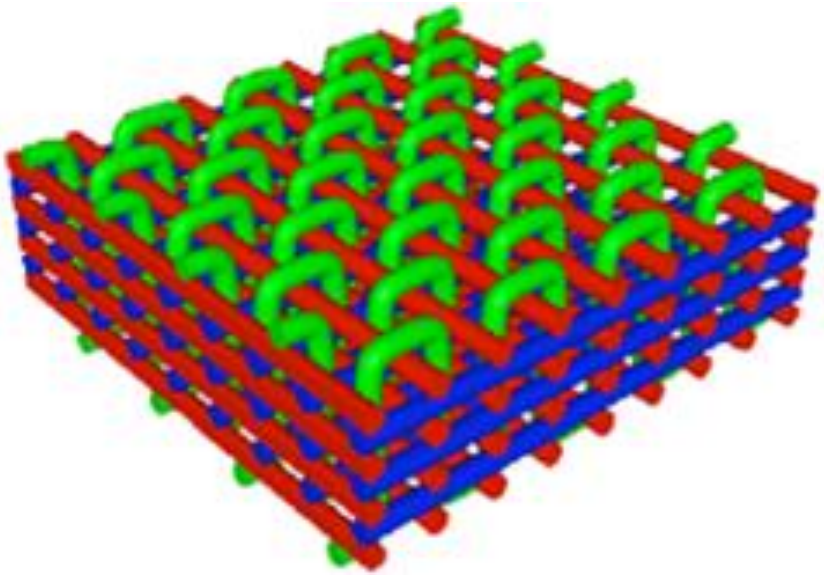

Figure 2.9. Structure for 3D woven orthogonal preform: X-yarns: red, Y-yarns: blue, Z-yarns: green [58]

Since the 1970's a wide range of processes have been developed to produce 3D orthogonal woven preforms. These range from techniques using relatively conventional weaving mechanisms but with multiple weft insertions, to processes that have very little in common with the traditional weaving process. Generally, with 3D orthogonal weaving machines, the warp ends are not required to be drawn through the heddles of the shedding mechanism, which reduces the amount of fiber damage during the weaving process. Only the Z fibers have to be moved up and down, thus they are drawn through heddle eyes. The first 3D looms were patented in 1974 by Fukuta [52] and Greenwood [59]. Most of the 3D looms that came later closely resemble these two designs with slight improvements. The earliest 3D weaving machines were only capable of

creating solid rectangular fabric sections with a fixed width and it was not possible to cut such a product to the desired shape because of the lack of interlacement. These drawbacks were overcome by Mohamed and Zhang in 1992 [60], Figure 2.10. This loom was one of the first to produce commercial 3D orthogonal woven preforms and has the ability to create a 3D fabric with a desired cross-sectional shape. This set up differs in the way that Y- and Z-yarns are supplied and fed through the loom. The Y-yarns are supplied from a creel instead of a warp beam and feed through dents in the reed in a matrix form arranged according to the desired cross-sectional shape of the product. Thus, the shape of 3D woven fabrics can be arranged during the weaving process, producing near net shape fabrics such as I-beams. This fabric can then be placed straight in a mold without any additional labor work.

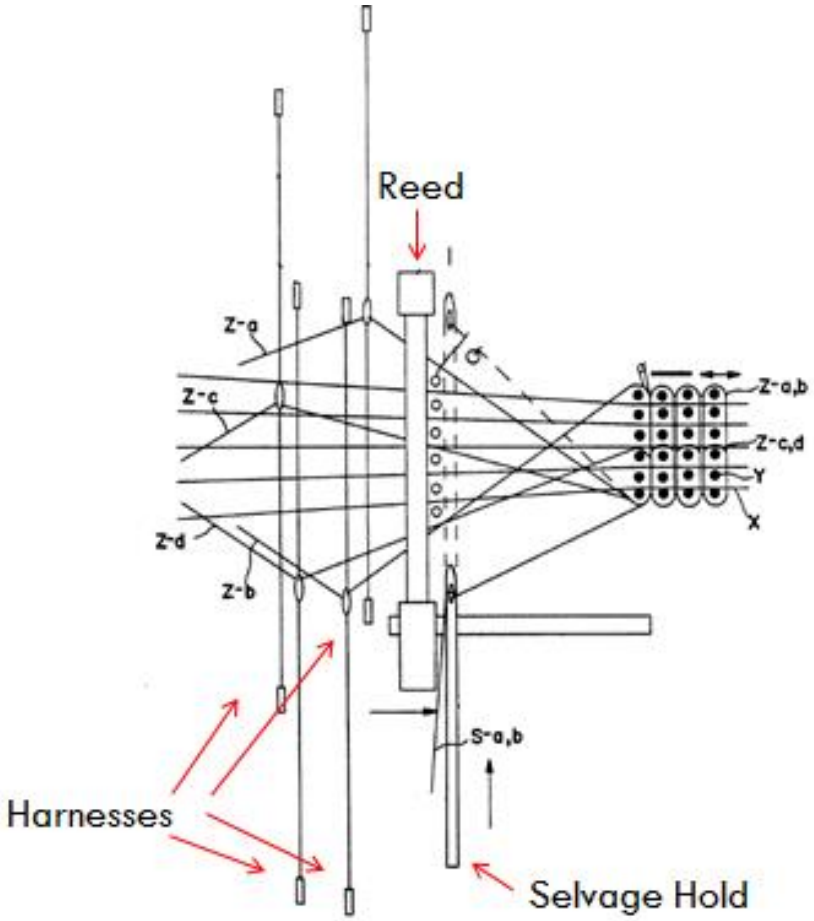

Figure 2.10. Side view and 3D weaving loom patented by Mohamed and Zhang [60]

The Z-yarns are split into groups along the fabric width operated by separate heddles. The X-yarns are inserted from both sides of the machine based on the length of yarn needed to form the desired shape [61]. The loom features the simultaneous insertion of all filling yarns, thus the machine productivity (in terms of the product volume, not length) can be fairly high even at low speed. A similar version of this machine was donated to the college of textiles by 3TEX and has been used in several research projects [36, 58].

Despite the potential benefits of 3D woven composites, their commercial use has been limited to a number of niche applications in aerospace and civil engineering fields where the use of traditional composites was most readily accepted. When comparing relatively new 3D woven preforms to well-established 2D preforms there are many challenges that hinder their widespread use. The main issue inhibiting 3D woven composite structures is that the cost is currently higher than the 2D prepreg or fabric laminates for many applications [62]. There are many reasons behind the high cost such as the use of special machines that increase the initial cost of production. Production speed is also low 20-30 cycles per minute compared to conventional 2D looms that operate at 200-300 cycles per minute or higher, sacrificing time and money [57]. There are also challenges with the material itself when compared to traditional materials. 3D products do not fully satisfy all the desired criteria for the composites sector in areas such as high energy adsorption, good impact resistance, good formability, good through thickness stiffness, strength, and fatigue resistance to flexural and torsional strains. This makes use of these less desirable than the well-established materials for some applications. Mouritiz et al. lists several of the issues affecting the use of 3D woven fabrics in very demanding applications and suggests that they may be better suited for less demanding applications such as in automobiles and containers [63].

Since 3D weaving is a relatively new technology, there are also many challenges associated with being a new and not well-established industry. Commercial applications in composite sectors usually require well-established design strategies that relate the functional properties of a product with its structural parameters and material properties [53, 61]. There is a high cost associated with certifying 3D and other new materials for use in load-bearing structures, such as bridges, when compared to 2D composites that have been well established for decades. Along with this,

most design engineers are unfamiliar with this type of reinforcement and use of a 3D reinforcement may not even be part of their knowledge base. These challenges are only likely to be resolved with time, use, and research.

Although the structure is not yet produced in large commercial quantities at low-cost Chen, Taylor and Tsai state that "3D woven fabrics as composite preforms have an important role to play in the development of advanced textile composites" [54]. A great deal of effort is being expended into reducing the costs associated with the manufacture of these preforms. Education of designers and manufacturers in the correct use of these composite materials will also be critical to their introduction into new products. This can be addressed by educational institutions and industrial conferences. If the cost can be reduced there are potential markets in the areas of protective armor, infrastructure, industrial and biomedical components [53]. These markets would also allow room for interesting SHM applications.

2.4.4. Embedding Optical fiber in a composite

Due to their small size and flexibility, optical fibers are well suited to be incorporated in textile structures, such as the preform component of a composite. The advantages of embedding an optical fiber in a composite are the enhanced protection of the fragile fiber sensor and the possibility of strain monitoring and damage detection in different interior locations where other sensing methods may not be able to easily examine [6, 8, 12, 13]. This combination of advanced composite material and optical fiber sensor results in a smart composite structure that offers advantages over traditional sensors. Sensor integration in composites, however, can present a number of issues and shortcomings that need to be addressed. This section discusses the use of 3D orthogonal woven composites as a host for optical fiber sensors and the potential benefits and difficulties associated with embedding optical fiber sensors in this material.

In order to prevent movement of the fibers within a composite, the fiber optical sensors can be woven into the structure either by 2D, 3D, or 3D orthogonal weave (3DOW) structure. In this setting, 3DOW has advantages over others because of its structure. As noted in section 2.2.1, optical fibers exhibit high attenuation when subject to bending. With 2D weaving an optical

fiber would be incorporated as a warp or weft yarn and therefore experiences micro bending in the form of crimp as part of the weave type. With 3DOW, the warp and weft yarns are on straight planes in the X or Y direction and woven together with a third Z-yarn. The POF can be part of the X- or Y-yarn plane and therefore avoid unnecessary bending. This structure is depicted in Figure 2.11 in which the POF is incorporated as an X-yarn in the 3DOW structure. The X-yarns (red) are orthogonal to the Y-yarns (blue) and do not interlace. Since there is no interlacing, there is no crimp between the X- and Y-yarns which results in increased properties of the final composite and a level surface for the POF to travel. The Z-yarns (green) bound the layers together.

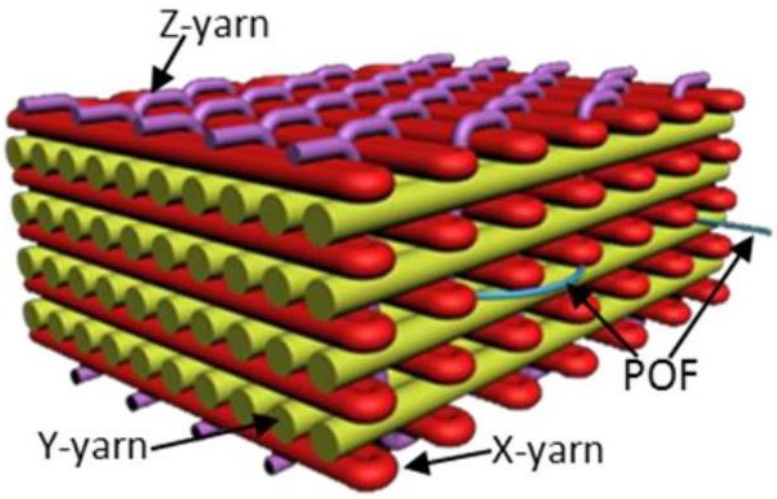

Figure 2.11. 3D orthogonal woven structure with embedded POF allows minimal bending and better performance of the optical fiber for use in SHM [36]

Despite the many advantages of embedded optical fiber sensors, integrating them into structures can also lead to several issues. One issue is the distortion of the composite structure. Even though optical fibers are small, and have a fiber-like appearance, a standard telecom fiber has a diameter of 125 μm which is much larger than common fiber reinforcements such as carbon fiber (5-10 μm) and glass fiber (4-32 μm) [6]. Smaller diameter fibers (40-60 μm) have been developed for sensing purposes, but even these have a noticeable size difference compared to their host fibers. It has been demonstrated, however, that these optical fibers do not produce any significant modification of the mechanical properties of the host structure if positioned well in

the composite [6, 64]. Even the 125 μm fibers exhibit low distortion of the hosting material when embedded parallel to the composite fibers in the laminate [65].

POF tend to have larger diameters than GOF. When embedded, this fiber can create matrix rich pockets due to the size difference. Schukar et al, [66] studied the effect of large diameter (1000 μm) on a laminate structure composed of glass fiber and epoxy resin. Multi-mode PMMA POFs with 1,000, 500, and 250 μm diameter were used. The POF was aligned parallel to the reinforcing fibers so that the composite glass fibers were not bent by the POF. Voids around the POF of 500 and 250 μm were less than that of 1,000 μm diameter fiber. As expected, the 250 μm POF created the least disturbance to the structure geometry, but this fiber produced more attenuation than the standard 500 μm size [66]. These results conclude that smaller diameters optical fibers are less disruptive to the structural integrity of the host material, but may be more sensitive attenuation caused by the preform structure. GOF is constructed with comparatively small diameters, but they are too fragile to be incorporated into many structures. POF produced using perfluorinated polymer can be constructed with a smaller diameter than PMMA. As advances in POF technology result in smaller diameters, there will be greater opportunities for POFs to become an integral part of materials.

Another problem area is the entry and exit point of the optical fiber in the composite material, which is prone to breaking [8]. These points are especially sensitive during composite manufacturing processes such as vacuum bagging, which can result in micro bending losses from the stresses of the curing process. Care must be taken to avoid sharp curvature of the fiber and prevent high optical loss. Several authors have explored options for mitigating this problem. The simplest solution is the use of small plastic tubes, often referred to as furcation tubes, which protect the fiber along short sections both inside and outside the material. The tubes are usually made of polytetrafluoroethylene (PTFE also known as Teflon) material of polyvinylidene fluoride (PVDF) [6]. Di Sante exhibited success with this method while implementing the vacuum bagging technique to manufacture composites with embedded FBG sensors for use as a sailboat mast composite [67]. Another solution is to integrate a fiber connector at the edge or surface of the laminate. Embedded connectors are specially designed so that the female part of the connector is embedded, and are often miniaturized to be less invasive [6]. The embedding of

the connector can, however, potentially decrease the strength of the composite. Even though the optical fiber is protected when embedded, the optical fiber is very delicate and may break outside of the composite materials as well. Luyckx et al. has a unique solution to this problem and suggested that research should focus on eliminating the entry point entirely by wireless transmission of data from the embedded sensor to the readout unit [8].

2.5. Applications of Optical fiber in SHM

Composites were originally developed for the aerospace industry, but increasing focus on industries outside of aerospace is resulting in a reassessment of how and where composites can be used [53]. Today, they are found in the aerospace, transportation, marine, energy, infrastructure, biomedical, and recreational industries. Since composites are already being used for many applications, implementing SHM systems involving optical fibers embedded in a composite component would result in a simple transition. This section provides an overview of both glass and polymeric optical fiber based SHM systems and the applications in which they are currently being explored in research and industry.

2.5.1. SHM in Civil engineering

Civil structures are often complex and expected to be fully functional under severe environmental conditions such as strong winds, storms, and earthquakes. These incidents present extreme loading that may compromise the integrity of the structure and lead to total failure that results in casualties, social, and economic problems. Therefore it is necessary not only to monitor structural status (stress, displacement, acceleration), but also environmental parameters (wind speed, temperature, and quality of the foundation) with an SHM system [3]. Another issue with structures is that many are being used to their maximum capacity or past their intended lifespan. The average bridge in the United States is 43 years old and of all bridges in the united states 9.1% were found to structurally deficient in 2016 [68]. SHM systems can provide real time information on the integrity of such bridges to ensure their safety for the future. According to a recent report on the global distributed optical sensor market, civil engineering is widely adopting the use of distributed OF sensors to enhance the inspection accuracy and efficiency. [69] With the implementation of optical fiber systems, high cost is a concern, but severe environmental

conditions and the large scale of civil infrastructures make these systems beneficial alternatives for several structural systems such long-span bridges, railway bridges, tall buildings, and pipeline systems [70].

Bridges

Bridges are subject to environmental derogation, extreme loading, and impacts caused by cars or ships that can result in significant damage to the structure. In addition, many bridges, especially those made with reinforced concrete, are deteriorating faster than they can be repaired or replaced [12]. The American society of civil engineers states that 9.1% of bridges in the USA were structurally deficient in 2016 [71]. Fortunately, the most established application of structural health monitoring technology is for use in newly built and existing bridges. Monitoring systems have been implemented on bridges in several countries including Europe, the United States, Canada, India, Japan, Korea, China [3, 72].

Identifying damage to a bridge when it first occurs can be beneficial to its overall integrity. The key parameters monitored with these systems are strain, temperature, cracking, and corrosion of the reinforcement [12]. In long span steel-concrete bridges, cracks may develop due to structural behavior, materials, and/or construction flaws. They may also be caused by overload, thermal loading, concrete shrinkage, and creep [14]. Crack openings, larger than 0.15-0.2 mm allow excessive penetration of water and chloride ions, leading to corrosion of steel reinforcements. [12] Conventionally, crack detection and monitoring for bridges have been carried out by visual inspection. The procedure is time-consuming, expensive, and sometimes unreliable. Optical fiber based crack sensors have the ability to monitor and locate several cracks with one fiber. Studies have been conducted for measuring crack propagation in concrete [73], but they can also be used in composites.

In one of the earliest studies for strain sensing, Takeda [74] investigated using PMMA POF sensors embedded in a carbon fiber-epoxy composite structure to detect and monitor crack propagation. This study depended on the occurred local deformation of POF during the transverse crack and its effect on the optical signal loss of POFs sensors. A tensile test was conducted on the prepared samples to obtain a relationship between the optical power, strain, and

transverse crack density. An end to end loss technique using a light emitting diode (LED) was conducted to measure the optical power in parallel with a strain gauge to measure the strain. Embedded POFs sensors were found to be a powerful and inexpensive way to detect and monitor the local crack density in composite laminates [74]. Due to its high strain limit, the POF survived beyond the failure of the laminate. The sensor was shown to detect the presence of the cracks, but its sensitivity to spatial properties of the crack and other parameters related to failure were not evaluated. The most successful SHM systems require a sensitivity of multiple parameters in order to provide accurate damage assessment.

The appearance of widespread failures in bridges has highlighted the importance of effective monitoring systems, which are able to identify structural problems at an early stage, guaranteeing the safety of the public. After catastrophic failure of the I-35W Bridge in Minneapolis, which collapsed in rush hour traffic during a resurfacing project, a hybrid SHM system was implemented on the new bridge. The structure originally failed due to increased concrete surfacing load caused by construction supplies and equipment and resulted in 145 injuries and thirteen fatalities. A hybrid SHM system was installed on the new St. Anthony Falls Bridge to measure dynamic and static parameters and prevent future failures. It includes 323 sensors and continuously gathers data on the bridge performance and health evolution through approximate analysis [75].

There are many examples of SHM systems that have been established on currently used bridges. The first bridge to use carbon fiber composite pre-stressing tendons was a bridge in Calgary, Canada [12, 16]. Researchers at the University of Toronto embedded FBG strain and temperature sensors in both the composite and steel reinforced girders to monitor the behavior during construction and under serviceability conditions. In order to circumvent the limited extensional strain that glass optical fibers can withstand fiber sensors were attached to pre-stressing tendons after they were placed under tension [16]. If this step were implemented today and POFs were used instead, this step may not be needed because of the higher strain limit of POF compared to GOF. The objective of the sensors was to monitor the performance of the new carbon fiber composite material, compared to traditional steel, over time. Results from the Bragg grating optical fibers showed that the system was capable of measuring the global changes in the internal

strain distribution within the bridge associated with concrete aging and ground movement for both the carbon fiber and steel tendons [76].

Another notable bridge using optical fiber sensors is the Shenyang Boguan Bridge, Figure 2.12a, in North East China. It has a unique “ribbon” style with the highest arch being 67 meters [17]. To ensure the safety during construction and service, an SHM system, Figure 2.12c, consisting of five different types of sensors (FBG strain sensors, FBG temperature sensors, accelerometers anemometers, and global positioning systems (GPS) revivers) was designed and installed on it. These sensors collect the signals and deliver them to the PC-based data acquisition system providing information about the structure.

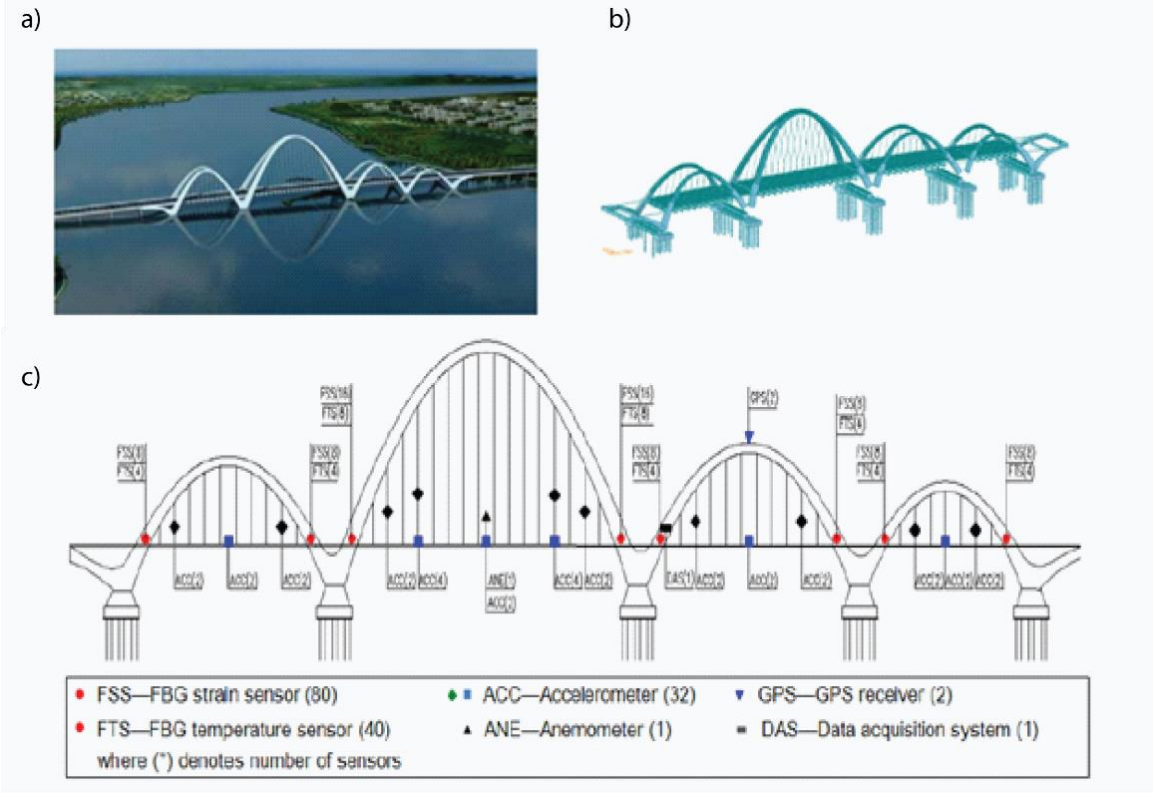

Figure 2.12. a) An aerial view of the Shenyang Boguan Bridge b) Full-scale FE model c) Distribution of sensors in the bridge [17]

A subcategory of bridges that has a high potential for SHM application is railroad bridges. In railways and railway bridges, SHM systems could be installed to measure rail imbalance and to

improve safety and measure parameters such as train speed and weight [75]. Systems such as these have already been established on several railroad bridges, such as the Han River railroad bridge, which is the biggest steel truss bridge in Korea [70]. A total of 46 sensors are installed on this bridge, 20 of which are FBG optical fiber sensors for measuring strain and temperature [70]. SHM are able to measure real-time responses from a railroad bridge under train-transit and environmental loadings, offering data about the use and integrity of the bridge. The research and application of SHM on railway bridges will provide useful data and prevent large scale failure and loss of property.

The application of SHM technology to bridges is very mature and will only continue to mature with technological developments and with confirmation of long term performance. Ko and Ni speculate that "the envisioned future for bridge health monitoring uses an array of inexpensive, spatially distributed, wirelessly powered, wirelessly networked, embedded sensing devices supporting frequent and on-demand acquisition of real-time information about the loading and environmental effects, structural characteristics and responses" [72]. As noted, many of these are already being successfully applied and perhaps widespread use of embedded optical fibers sensors is on the horizon.

Buildings

Along with the expected natural loading scenarios that one might predict for bridges; buildings and specialty structures may also be subject to unnatural hazards. A gymnasium, for example, may experience vibration from thousands of people jumping to music. In order to ensure the safety of the structure and the people in it, SHM would be a useful system to employ. An interesting example of this is the Sports center of Dalian in China [17]. The major buildings in this structure include the gymnasium, stadium, natatorium and media center, Figure 2.13a, which are all typical long-span special structures and have been equipped with SHM systems to survey the variation of key physical parameters and to provide the real-time observations of structural safety. In the gymnasium, the location of maximum stress was discovered based on the FE model, Figure 2.13b. More than 200 FBG sensors were installed on the cable anchor, the truss, and the strut to monitor the cable force, the stress and the compression stress [17]. Buildings and

specialty structures like this are maintained using SHM to add an extra safety factor for the patrons and to provide lower cost and more accurate monitoring of the structure.

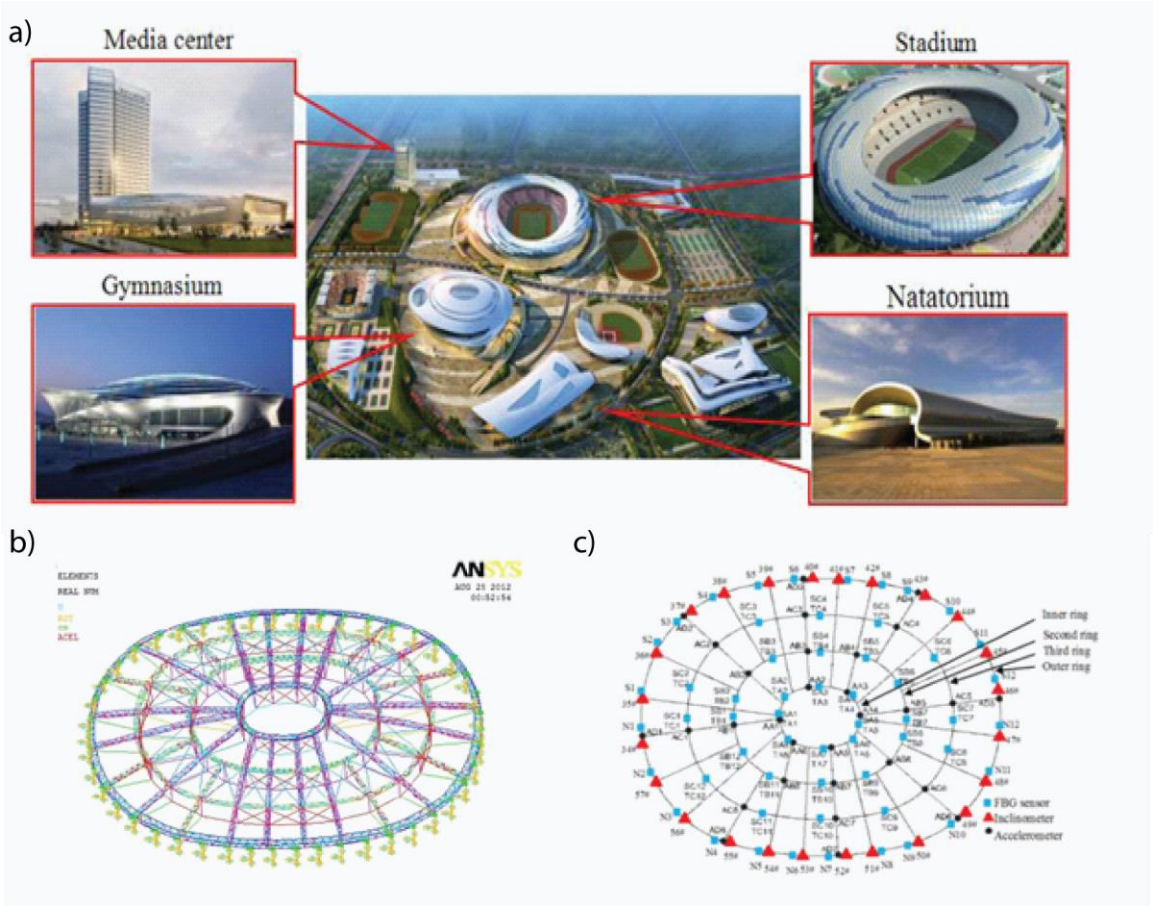

Figure 2.13. a) Sports center of Dalian in China b) FE model c) Location of sensors [17]

Another interesting application is the protection of historical buildings. In 2001, FBG sensors were installed on the primary arch of the Cathedral of Como in Northern Italy, built in 1396, to identify any significant structural deterioration and to protect the cultural heritage [3]. Another application is to protect historical buildings from earthquake damage. The motivation is to strengthen the masonry body and to detect the condition of the structures damaged or endangered by earthquakes. In this application, mainly vertical cracks are detected and monitored. Habel and Krebber suggested that smart textiles embedded with polymer optical fibers are the perfect system for this task because POF sensors have a high breakdown strain and the ability to resolve the location of the crack [10]. Many buildings are being used past their intended lifespan and

exhibit a need to be preserved for reasons of cultural significance. SHM could prove to be the perfect systems for these tasks.

Beams

Most mature SHM systems use glass FBG sensors for structural monitoring. The use of POF is relatively new in the industry and in many cases still in the research phase. One group, for example, conducted research on POF attached to composite beams for use on civil structures. Kuang and Cantwell [77] attached POF sensors to a composite beam to monitor the free vibration response after low energy impact. The composite beam material was made of eight layers of woven carbon fiber reinforced with epoxy resin. A 1 mm diameter PMMA POF adhered to the surface of a composite beam. Optical transmission efficiency was studied to check the integrity of the POF sensor after the bonding process and this showed no effect on POF properties. Impact tests were conducted away from the POF sensors to prevent damaging the sensor and at energies ranging from 2 to 8 J. After each impact test, a residual flexure test was conducted for each damaged specimen. Results showed a significant effect of the impact test on the residual flexural test results and that POF sensors are capable of characterizing and monitoring the damping of the damaged sample [77]. 3DOW preforms would also be beneficial for use in beams and would combat some of the challenges associated with the method used by Kuang and Cantwell. With 3DOW, all layers can be woven together in the shape of a beam, minimizing the processing time. The structure of 3DOW also allows the optical fibers to be embedded in the composite for better sensor damage protection.

In another study, Kuang and Cantwell [78] investigated the use of POF sensors for monitoring the dynamic response of both cantilevers and simply supported beams under dynamic load conditions. POF sensors were attached to the surface of a plastic beam and were also embedded in carbon fiber composites. A flexural loading condition test was conducted on the prepared cantilever. For the two sensors, one end of the POF was attached to a light source and the other end was connected to a light detector. Cantilever vibration was created by putting different weights on the tip and POF sensor data signal was collected during the beam vibration. An impact test using a free weight drop test was also conducted to evaluate out of plane deflection of the composite beam. Impact tests on simply supported carbon fiber reinforced beams

demonstrated the sensor's ability to monitor out-of-plane deflections during the impact event. Results from flexure strain versus POF signal showed a decrease in the light intensity as flexure strain increases. Authors in both above studies only evaluated the impact energy that caused failure. They did not investigate other impact energy levels or the relationship to sensor data for partial damage. This is an important parameter to consider for SHM applications as one of the objectives is to alert to possible failure before it occurs. The ability to implement optical fibers in beams is an important step toward widespread use of SHM as damaged or outdated beams on an existing structure can be easily replaced with more advanced materials.

Pipeline and offshore platforms

Another major application for SHM is in the oil and gas industry to measure temperature, pressure, chemical composition, acoustics, strain, and to detect and minimize leaks within pipelines [75, 79]. Land pipelines are subject to damage from landslides, excavation, theft, corrosion, and earth movement [3]. A leak could cause large scale environmental damage and economic losses. Optical fiber sensors can be used to identify when and where failure occurs [80]. A success story of an SHM equipped pipeline in Indonesia proves that this technology is useful to the industry. This pipeline had been equipped with a vibration sensor and the system operator was alerted of a major event that caused damages to the pipeline. Upon further inspection, it was discovered that a landslide had occurred and a section of 24-inch pipeline was fully exposed [3]. The author of this article notes that "the monitoring technology demonstrated its unique potential in health monitoring of long pipelines since such accidents to pipelines could not be easily detected by other conventional methods" [3]. Clearly, this incident proves the necessity of embedding sensors on pipelines.

Offshore pipeline systems are the main platform to send the oil from offshore to onshore. Offshore platforms carry their own unique risks such as collisions with supply boats and ocean waves which can negatively affect the structural safety [17]. It is therefore beneficial to monitor the real-time strain variation of the platform with SHM. After reviewing SHM systems being used in offshore engineering applications, Li et al. concluded that systems based in the FBG sensors exhibit unique advantages in the field of offshore engineering ranging from its long-term durability, good reliability, and flexibility of installation [17]. Kwon et al. performed a

feasibility study on oil leakage monitoring for offshore pipelines using Brillouin optical time domain analysis sensors and found them to be successful at monitoring these factors as well [80]. Composites with embedded optical fiber may also prove to be a good candidate for this application because of their resistance to corrosion that may occur from contact with the ocean. Although there is not currently widespread use of SHM systems in pipelines, it is considered one of the fastest growing applications for optical fiber sensors [69]. They are beneficial to this industry and have the ability to prevent large scale environmental damage and economic loss.

2.5.2. SHM in Aerospace

Like many structures, aircraft, especially military aircraft fleets around the world are operating beyond their designed life cycle. This poses a need for the health of the structure to be monitored in real time to reduce the cost and need for rigorous on-ground inspection and maintenance [7]. With SHM it is possible to monitor many aspects of an aircraft's flight to ensure a safe journey for crew and passengers. Wings can be fitted with a system to monitor in-flight wind loads such as dynamic strain. Landing gear loads, flap deformation, and cracking can also be monitored with sensors [75]. The majority of the research related to SHM systems for aerospace use concludes that FBG sensors are the most promising sensor for this application [6, 7, 75, 81]. Continuous, real-time monitoring will not only increase operational safety, but also increase understanding of fracture mechanics of composites, and lower the cost associated with manual inspections [81].

The adaptation of composites in the aerospace industry could make the implementation of composite based SHM with embedded optical fibers a relatively simple and necessary transition. Composites also increase the need for SHM due to the relatively unknown nature of composite damage progression discussed in section 2.4.2. Damage can occur at any stage during the use of the aircraft. Impact damage can result from tools dropping during manufacturing and servicing, runway stones hitting the aircraft during take-off, bird strikes during flight, and weather-related issues such as hail and lightning [6, 82]. Among the strategies to reduce the consequence of a bird strike, flight crews should be provided with useful information to detect a bird strike while in flight, in order to take appropriate action and maintain control of the airplane [6]. Low-velocity impacts often caused by dropping tools can generate barely visible impact damage. This

can result in indentation, delamination, or fiber/matrix cracking, which can lead to severe reduction in the strength and integrity of composite structures [81, 82]. Hence there is a great concern to detect such damage and assess its extensiveness. The ability to monitor these conditions will likely result in increased use of composites in aircraft because it will increase the confidence in their structural capabilities, and lower the cost associated with their use since approximately one-third of acquiring and operating composite structures is associated with inspection.

Since impact damage is a critical concern to aircraft design, several research groups focus on impact detection systems. Tsutsui et al. [83-85] have been developing an impact damage detection system based on the use of both embedded multi-mode and single-mode small diameter optical fibers. The detection system relies on the optical loss due to bending of the structure and the embedded fiber after impact events. It has been found that the maximum amplitude of optical loss in a multi-mode fiber is related to the impact load. The authors also used several small diameter FBG sensors in the systems to estimate the impact location from the difference in time of arrival of the shock waves to the sensors locations. This is a highly important parameter in SHM and is one of the areas where optical fibers offer advantages over other sensors. Vella et al. used a full spectrum interrogator of FBG for detection of impact loading [86]. The authors used the system to detect low energy impacts (11.6 J) in a 24 layer composite specimen with an FBG sensor embedded at the midplane, 16 mm from the impact location. The specimen was impacted repeatedly until perforation and spectral measurements were taken and analyzed [86].
Güemes et al. [87, 88] reported a series of experiments on CFRP panels to detect delamination and changes in strain caused by impacts. A sensing grid was created by arranging optical fiber over the entire structure to monitor with spatial resolution down to a few millimeters. The chances of detecting the damage location increased substantially with respect to the use of quasi-distributed techniques which also require more complicated schemes of detection based on multiplexing techniques. Each time damage causes a change in the strain field, it is possible to visualize it through images representing the strain level over the structure and its local gradients, thus creating a map of strain distribution.

SHM is also an important feature to incorporate in the space side of aerospace as well. Fiber optical sensors have been considered for use in satellites, launchers, and atmospheric entry vehicles [89]. Space is a very challenging environment for any sensing system and is characterized by microgravity, vacuum, radiation, large thermal variations, and mechanical vibration from launch [89]. Fiber optical sensing systems offer many advantages in this environment such as insensitivity to electromagnetic interference, lightweight, flexible, efficient multiplexing for high sensor capacity, multi-parameter sensing, and the potential to embed in composite structures [89].

In spacecraft, SHM could be implemented during processing to access the quality of manufactured parts, monitor the temperature during the propulsion stage, or monitor the integrity of the spacecraft exterior during reentry into the atmosphere [75]. It is envisioned that SHM will provide near real-time information on structural integrity and report abnormal behavior to astronauts and support personal [90]. Figure 2.14 shows how sensors, in this case, small piezoelectric sensors, may be attached or embedded into the spacecraft structure to enable passive and active detection of structural damage. A system based on optical fiber sensors would appear similar to this set-up, especially in terms of data transfer and analysis. SHM may also help to address the safety of commercial space vehicles in development since it would record structural integrity during all stages of space flight. SHM could also play a prominent role in space vehicle recertification for the next flight and potentially reduce turnaround time. SHM technology is seen as an important element in improving the safety of space travel and reducing spacecraft operation cost and has the potential to revolutionize assessment and qualification of space vehicles [90]. The aerospace industry may be the next big industry to incorporate widespread use of SHM systems due to the need for continuous monitoring and ease of incorporation of SHM systems.

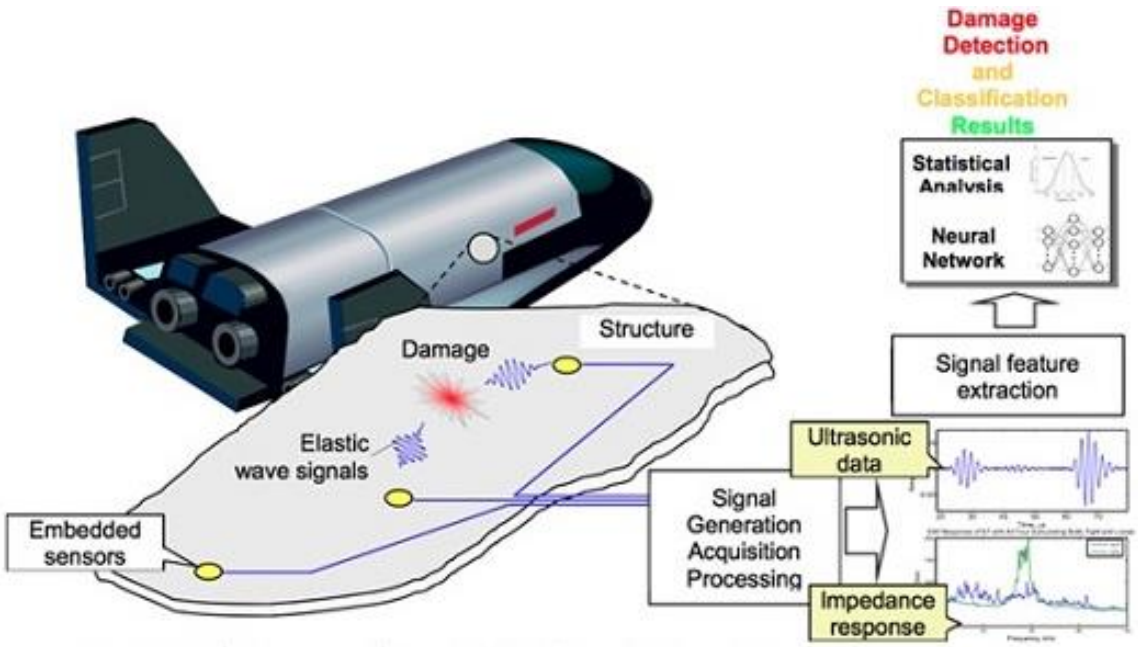

Figure 2.14. A concept of a spacecraft structural health monitoring system [90]

2.5.3. SHM in Other applications

Wind Turbines

Renewable energy, such as wind energy, is an important and popular topic, and even SHM has a place within this topic. A wind turbine is a vertical structure with many critical points that should be monitored to ensure the best performance of the structure [75]. In order to make wind energy more economically competitive with traditional fossil fuels, wind turbines should operate as continuously as possible. One of the main challenges in completing this goal is a component failure, which can lead to considerable long stoppages and cause significant economic loss and social impact [91]. The most common type of damage is blade damage and tower damage [75]. It is reported that wind turbine rotor blades are failing at a rate of around 3,800 a year, 0.54% of the 700,000 blades that are in operation worldwide [91]. The blades are made of fiberglass, which has a low modulus and can be damaged by moisture absorption, fatigue, wind gusts, or lightning strikes [91-93]. As shown in Figure 2.14, materials, manufacturing process, structural design and loads are all interactive factors that may play into the failure of a blade. The blades are the key element in a wind power generation system and account for 15-20% of the total turbine cost [75]. Wind turbines often provide minimal initial warning when they fail, and sometimes continue to operate for a large number of cycles with little reduction in strength and elastic properties.

Damage will then propagate quickly to failure that has the potential to cause significant damage to the wind turbine as a whole [75, 92]. This window of time where the turbine continues to operate allows the perfect opportunity of SHM to detect damage and signal for repairs because total failure and damage to a wind turbine are inflicted.

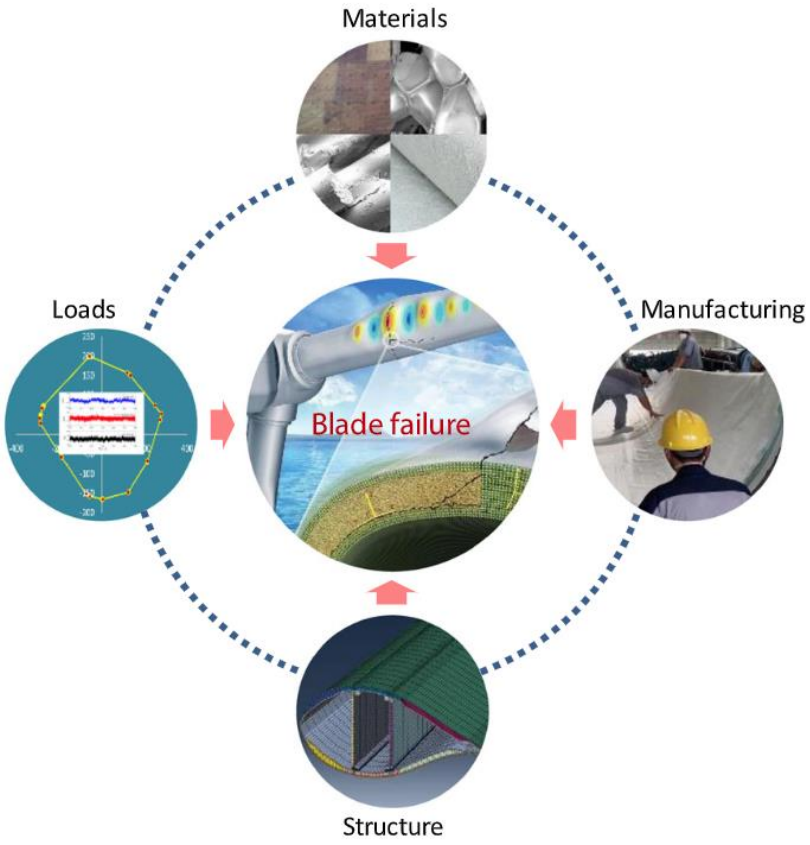

Figure 2.15. Factors contributing to wind turbine blade failure [91]

Currently, the damage and fatigue lifetime associated with the wind turbine blade is difficult to access and sometimes results in blades being retired before their life is over. Most of the research with relation to wind turbines is related to manufacture and production with minor research related to SHM [93]. The SHM research that is being accomplished mainly focuses on vibration detection and monitoring. For these reasons Liu, Tang, and Jiang suggested that optical fiber sensors are promising to measure strain in wind turbines for lifetime prediction and the monitoring of the stress level in the blades [93]. Sensors could measure temperature and strain in critical points of the blades of wind turbines, and alert of minor damage before it is able to

become critical [75, 92]. Similar to other examples mentioned in this review, a condition-based maintenance program using SHM information could minimize the time needed for inspection of components, prevent unnecessary replacement of components, prevent failures, and improve the availability of power, resulting in higher availability and lower cost of this renewable energy resource.

GeoTextiles

Another SHM application with positive environmental impact involves geotextiles. Due to complex geological conditions and nonlinear properties of soil and rock, geological structures such as foundations, tunnels, and dams are too complex to be accurately understood [16, 94]. The existing technologies to monitor these structures have drawbacks such as a large number of cables for multi-point measurements, electromagnetic interference, signal loss in long distance transmission, and low reliability making this application a good candidate for SHM with embedded optical fibers [95]. A group in Switzerland, led by Inaudi, made the point that a well-designed bridge should not require active monitoring during most of its lifetime [16]. This group instead put their focus in underground civil projects, such as pilings and tunnels, because of the poor understanding of the surrounding geological structures. Piles, consisting of a pre-stressed steel bar, reinforcement stirrup, and high strength concrete are used as reinforcement in geotechnical structures such as slope, excavation, and highway pavement. They are also important because they support structures and protect them from shocks and earthquakes. Damage can occur to piles during installation, or at the interfaces between the pile and the surrounding environment, thus increasing the need to monitor the stress distribution of piles [95]. Monitoring structural deformation in these systems could provide useful information. Audi's group has equipped anchoring cables used to stabilize rock slides with OF measuring devices [16]. It has also been proven that deformation of geotextiles can be evaluated by measuring the POF elongation using the optical time-domain reflectometry analysis [10]. Landslides are a common natural disaster in the eastern countries. Monitoring for landslides will allow for earlier warnings and a reduction in loss of property and lives [95].

Biofouling

Another environmental application of POF sensors is for monitoring the environmental parameters including flow, biofilm growth, turbidly, toxicity, humidity, rotation, and fluorescence [96]. Biofouling is when unwanted organisms attach to a surface and are most frequent in marine and medical industries. One example is that barnacles use a protein-based cement to adhere to ship hulls which create drag and results in higher fuel consumption. Scale, calcium carbonate deposits that form on surfaces and interfaces when hard water is heated or cooled, is a problem in heat exchangers because it reduces heat transfer and restricts flow [96]. Wong et al. investigated the ability to use a POF sensor to measure the very early stages of biofilm growth and found the sensor to be very effective at early detection for biofouling [96]. POF sensors were embedded in a woven carbon fiber epoxy prepreg composite. End to end loss technique was used to measure the power loss using an ultra-high luminescent LED as a light source and light-dependent resistor and a low-cost commercial data acquisition system. Biofouling and scale can cause reduced performance of systems that are in contact with water, and it would be beneficial to monitor, detect, and remove the build-up with an SHM system before it can become a problem.

2.6. Conclusion

This section reviewed background information on the components used to create smart materials for SHM systems including optical fiber sensors, optical fiber loss testing methods, and composite materials. SHM systems can be very beneficial to the industry with the ability to be incorporated in a wide variety of applications, reduce scheduled maintenance, and improve safety.

Optical fiber sensors are a very diverse sensor in terms of use and application. Current, industrial use of optical fiber sensors is most prominent in bridges. Many groups are researching other applications and optical fiber sensors appear to have a promising not too distant future in aerospace, wind turbines, and geotextiles. FBGs are the most common optical fiber sensor for use in many SHM applications. POF sensors are still mainly in the research phase and most research has not taken advantage of newer perfluorinated polymer optical fibers which offer lower attenuation and smaller diameter sizes than traditional PMMA material. Some of the more

interesting systems combine multiple sensors, such as FBG sensors, accelerometers, and GPS. There is also some indication that the future of SHM may be wireless, which would reduce some of the issues associated with embedding optical fibers in a material.

In order to be fully mature for structural health monitoring of structures critical issues such as robustness and maintainability need to be addressed. For example, replacing a damaged fiber is relatively complicated especially if embedded. This issue can be overcome if redundancy is built into the system to bypass the damaged optical fibers. Additional research and development are also required to ensure highly reliable detection capability, in order to avoid fiber breakage and signal loss. As technology improves the usability of optical fibers and their use in SHM will become more prevalent.

Chapter 3: Objectives

3.1. Incentives

Composites are subjected to accidental impact loading of various kinds during the manufacturing process and service life. The presence of damage can result in a considerable reduction in composite stiffness and compressive strength. Thus, it will be important to examine failure modes, specifically the response to localized impact loading, which has been identified as one of the most significant limitations of composites [51]. Composites have unique failure characteristics compared to monolithic materials such as fiber and/or matrix breakage, fiber debonding, and delamination [97]. These can precede the ultimate failure of the composite and present difficulties of analysis. Embedding composite structures with an SHM system will allow better monitoring of failure modes, provide real-time information about the integrity of the structure, and could lead to more widespread use of composites as they are further understood.

It was indicated in the literature review that most of the optical fiber based SHM research focuses on the use of FBG sensors for SHM. These have many advantages such as the capability to measure a multitude of parameters, but they are composed of glass, which tends to be brittle. POF sensors are more flexible and better for embedding in a material. Prior research in monitoring composite structures does not take full advantage of POF, a 3D orthogonal woven structure, and high-resolution OTDR as an SHM unit. Hamouda proved the feasibility of manufacturing such structures [36, 64, 98-100]. This research intends to build on his work by further characterizing the smart composite's ability to sense damage and to explore potential SHM end uses. Hamouda investigated the tensile strength, flexural strength, and low-velocity impacts of 3DOW composites embedded with POF [36, 98]. This research extends the work of Hamouda's impact tests to understand the relationship between signal loss and damage progression. This allows characterization of the composite's response to damage and provides an understanding of the sensor accuracy at measuring damage.

3.2. Objectives

There are three main objectives of this research:

I. To demonstrate that smart composites composed of POF sensors embedded in the 3D orthogonal woven fabric can function as viable structural health monitoring systems.
II. To characterize the sensors and their signal relationship to the induced damage.
III. To understand the trends of optical fiber as sensors in the industrial market.

In order to meet these objectives, the experiments are structured as follows:

I. To monitor the relationship between impact damage, residual strength loss, and POF, which is integrated into 3DOW glass fiber composites, signal loss.
II. To measure the sensitivity of the POF sensors at varying locations within the 3DOW structure of the fabric.
III. To predict technological trends and potential market of smart composite.

Chapter 4: Experimentation

4.1. Introduction

All load-bearing structures will experience some level of damage during their lifespan. Using a parameter to evaluate the effect of damage on the structural performance, such as in SHM, can be fully achieved only when the nature of the damage is understood and characterized [13]. The basic steps of SHM in the case of damage monitoring are to detect the damage, locate the damage, and determine the severity of the damage. After this, the damage is reported and the necessary steps are taken, such as sending out a warning or making repairs. The first three steps were investigated in this work and outlined in Figure 4.1. The smart composites were formed using a two-step process, first preforms were woven with embedded POFs and second the preforms were infused with the resin system and allowed to cure. OTDR was used after each formation step to assure the integrity of the optical fiber remained intact. Next, a series of destructive impact tests were performed. A signal was obtained using OTDR after each impact event to detect and locate the damage and lastly, severity of the damage was determined by evaluating the residual compressive strength after exposure to repeated impact events. The following sections outline the materials and test methods needed to carry out this process.

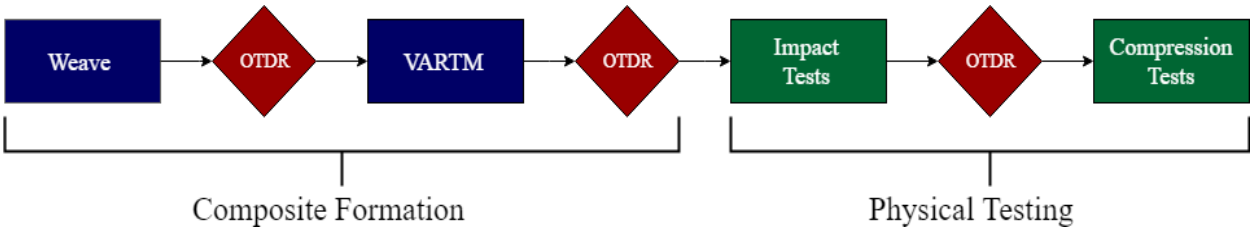

Figure 4.1. Flow chart of composite formation and physical testing events

4.2. Materials

4.2.1. Polymeric optical fiber

The POF (GigaPOF-62LD) sensor that was used in this study was a low attenuation, multi-mode, IR-transparent POF with a high bandwidth graded index (GI), acquired from Chromis Fiberoptics, Inc. The properties of this polymeric optical fiber are listed in Table 4.1. The core

and cladding of the POF were made of a perfluorinated polymer (PF) (Polyperfluoro-butenyvinyleether). This material was noted in the literature review as having low attenuation compared to other polymer materials used for POF. The core diameter was 62.5 μm, which is a common diameter for multi-mode optical fibers. Bending radius is an important parameter to consider in order to minimize attenuation loss due to bending when embedding an optical fiber in a material. Seyam and Hamouda determined that the critical bending radius, i.e. the minimum bending radius at which the optical fiber exhibits no signal loss, for this specific optical fiber to be 19 mm [100].

Table 4.1. Properties of POF

Property	Value
Core diameter	62.5 ± 5 μm
Cladding diameter	750 ± 5 μm
Numerical Aperture	0.185 ± 0.015
Max. tensile load	15.0 N
Long-term bend radius	7.0 mm
Critical bending radius	19 mm

4.2.2. Glass fiber

The material used to form the 3DOW composite preform was electrical glass fiber (E-glass), supplied by PPG Industries. Glass fibers have high tensile strength, high heat resistance, high chemical resistance, and a low cost compared to other high-performance fibers. These properties allow glass fibers to be used in a variety of fiber reinforced composite applications. Three different linear densities of glass fiber were acquired for the X-, Y-, and Z-yarns. The linear densities are 735 (g/km or tex), 2400 (g/km or tex), and 276 (g/km or tex), respectively.

4.2.3 Epoxy resin system

The resin system used to form the 3DOW composites was the Epoxy 2000 and 2120 hardener combination, distributed by Fibre Glast Developments Corporation. This resin system was mixed

in a 100:27 weight ratio and had a pot life of two hours at room temperature, which allowed enough time for the vacuum bagging process. It was selected for its high tensile strength (67 Mpa) [101], high modulus (2.8 Gpa) [101], and harmless effect on the POF and its sensing abilities [99]. It is critical that the resin not interact with the POF material to ensure the performance of the sensor in the composite.

4.3. Formation of 3DOW preforms and composites

Many composite properties are strongly dependent on the arrangement and distribution of fibers in the preform. This section outlines the fiber arrangement of the preform created by 3D orthogonal weaving, composite formation, and the fiber volume fraction of the resulting composite.

4.3.1. Weaving parameters

A series of samples were woven on the 3D weaving machine donated by 3TEX, Inc. available at the Wilson College of Textiles, North Carolina State University. The process of drawing-in Y-yarns into the machine, inserting the POF into the preform, and the completed woven preform is shown in Figure 4.2. Experimental design variables and levels of the 3DOW preforms are given in Table 4.2. In total 34, 1 m preforms were woven and infused. These were cut into about 200 total specimens for testing.

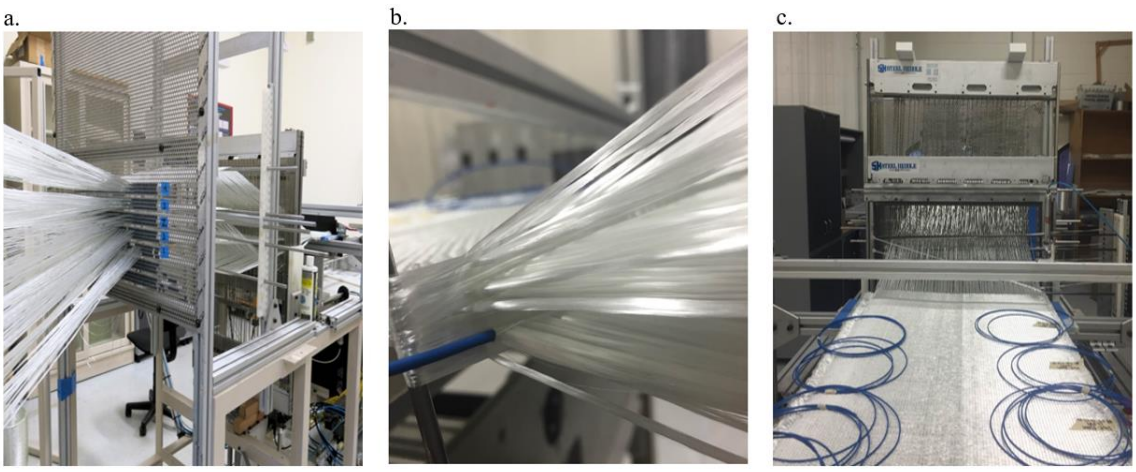

Figure 4.2. The process of weaving on the 3D weaving machine, a) drawing in of glass fiber Y-yarns, b) POF inserted into the fabric as an X-yarn with a protective tube placed over the section of POF protruding from the preform c) The woven fabric on the 3D weaving machine

Table 4.2. Design of experiment

Parameter	**Value**			
Sample Grouping	I	II	III	IV
Y- layers	4			
X-yarn density (pick/cm/layer)	1.57	4.72		
Position of POF	Middle	Middle	Top	Bottom
Total # of specimens	30	70	54	46

The weave structure for every preform was plain weave with four Y-yarn layers and five X-yarn layers. Each preform was formed using 102 Y-yarns per layer. The Y-yarns were drawn through the reed so that there was one yarn per layer in a reed dent. The reed density was 2.36 dents/cm (6 dents/inch). X-yarns were inserted simultaneously between Y-yarn layers with a double insertion per shed. A total of 102 Z-yarns bound these layers together with the plain weave

design and there was one Z-yarn per reed dent so that they were positioned evenly between Y-yarns.

During weaving, the POF was manually inserted into the preform in the X-direction. The optical fiber was inserted in 5 m segments with approximately 1.5 m embedded in the preform. About 1.75 m of POF protruded from each side of the preform to account for reflection at the fiber input and output during optical time domain reflectometry (OTDR), Figure 4.3. The POF is very fragile and underwent a lot of handling during the composite fabrication. The portion of POF outside of the preform was threaded into a 2 mm furcation tube to provide extra protection during weaving, infusion, and testing. Figure 4.2b demonstrates a POF inserted after the X-yarns have been inserted with a protective furcation tube placed over the section of POF protruding from the preform. A distance of 3.8 cm was kept between the POF insertions to accommodate the bending radius (19 mm) at both selvages of the 3D orthogonal woven preform.

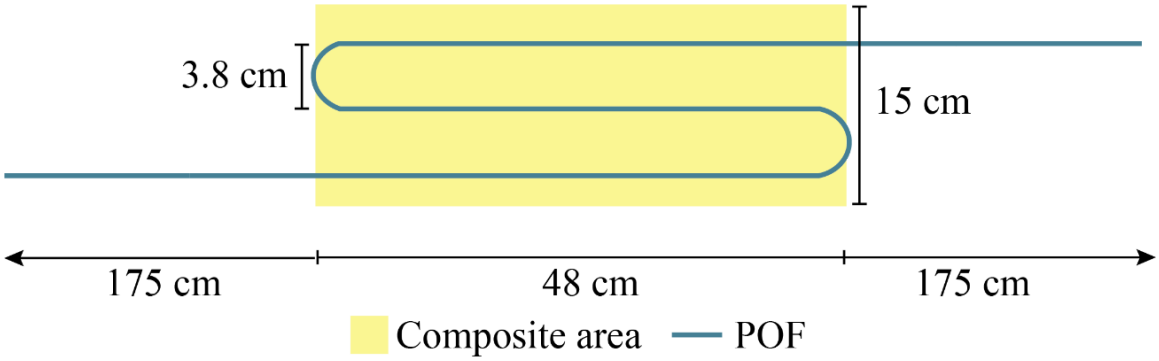

Figure 4.3. Schematic of POF embedded in the smart composite

Four test groups, shown in Table 4.2, were set up to compare pick density (groups I and II) and POF structural position (groups II, III, and IV). Specimens in group I, had a low pick density of 1.57 picks/cm/layer (4 picks/in/layer), Figure 4.4b, and specimens in groups II, III, and IV were woven with a maximum pick density of 4.72 picks/cm/layer (12 picks/in/layer), Figure 4.4a. The pick densities reported accounts for double pick insertion. To understand how optical fiber sensors react to a damage event based on their location to the event the position of the POF in the composite was varied between layers. The pick density and number of layers remained constant

while the POF was inserted in either the top (between 1st and 2nd Y-layers), middle (between 2nd and 3rd Y-layers), or bottom (between 3rd and 4th Y-layers) layers, as shown in Figure 4.5.

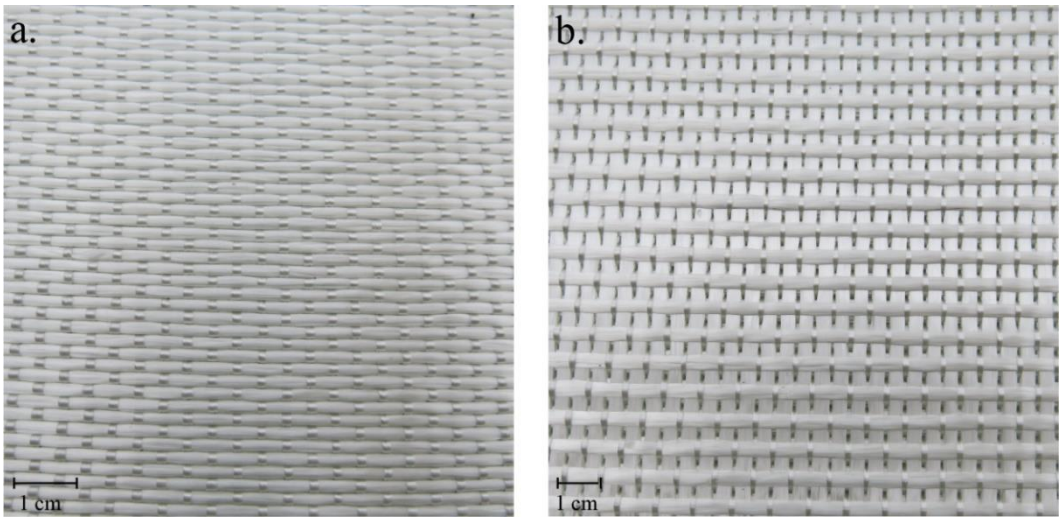

Figure 4.4. Weave structure showing density of a) 4.72 picks/cm/layer and b) 1.57 picks/cm/layer

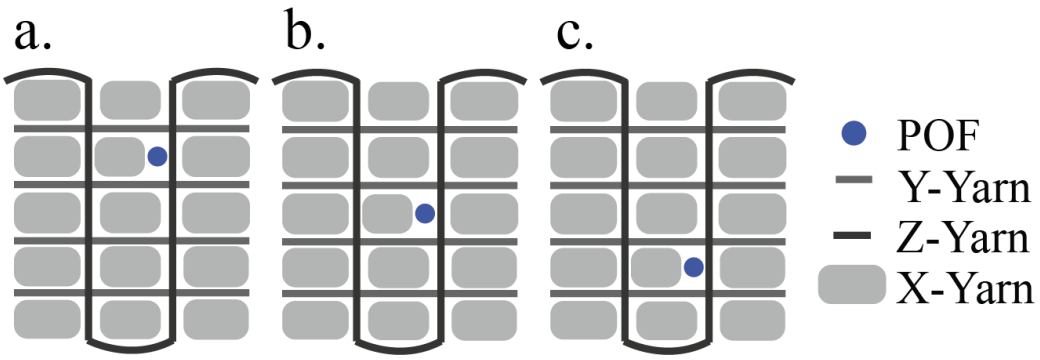

Figure 4.5. Representation of POF structural position a) POF located in the top layer b) POF located in the middle layer and c) POF located in the bottom layer

4.3.2. Resin treatment

3DOW preforms were treated with a resin system using the vacuum assisted resin transfer molding (VARTM) technique. The furcation tubes were placed on top of the sticky tape and an additional small piece of sticky tape was placed on top to prevent any air leakage during the resin treatment process, Figure 4.6. This also prevented excess resin from curing on the ends of the POF which needed to be connected to the OTDR. A vacuum pressure of 100 kPa was achieved

using a VacMobiles® 20/2 vacuum pump system. The prepared resin mixture was placed in a vacuum desiccator for degassing for about 20 minutes to remove the air bubbles created during stirring and thus decrease the potential for voids within the composite. The panel was left on the table to cure at room temperature. Specific steps for the VARTM technique with special consideration of the optical fibers are included in Appendix C. After the panel was cured, the panel was cut into specimens with dimension 48 cm x 15 cm, figures 4.3 and 4.7.

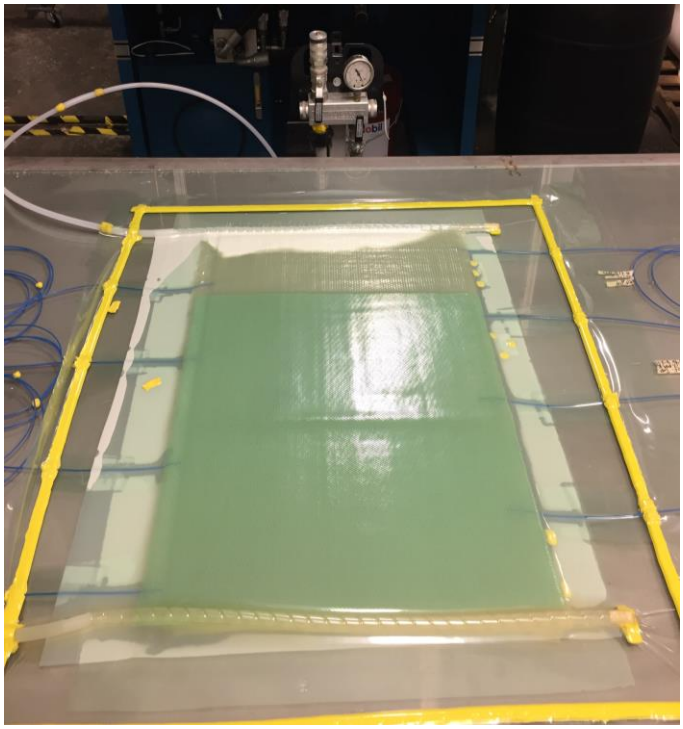

Figure 4.6. Set-up for the vacuum bagging process

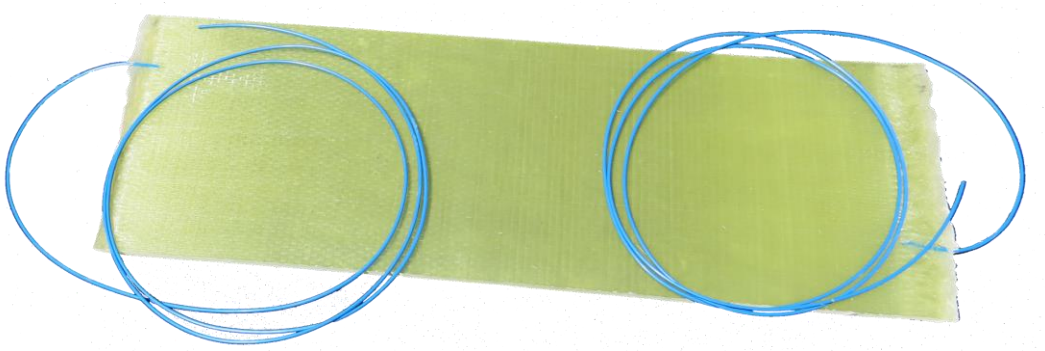

Figure 4.7. Example of a composite specimen after being cut

4.3.3. Fiber volume fraction analysis

The fiber volume fraction, percentage of fiber volume in the entire volume of a fiber reinforced composite, is an important parameter in composite engineering. The impregnation of resin around the fibers is dependent on the orientation and architecture of the fibers and a higher volume fraction typically results in better mechanical properties of the composites.
To determine the fiber volume fraction of the composite, the fiber weight fraction was converted to volume fraction using the weight and density of each component as shown in equation 1. The weight of the preform was measured before resin infusion and the weight of the composite was measured after the epoxy resin treatment. The density of E-glass was assumed to be 2.54 g/cm.

$$V_f = \frac{v_f}{v_c} = \frac{W_f/\rho_f}{W_c/\rho_c} \qquad (1)$$

where:
V_f = fiber volume fraction
v = volume,
W = weight
ρ = density
f = subscript for fiber
c = subscript for composite

The procedure for measuring the density of a composite is based on ASTM D792-00 [102] standard test methods for density and specific gravity of plastics by displacement. For this measurement, several 2.54 cm (1 in) by 2.54 cm (1 in) specimens were cut from the composite panel. First specimens were weighed in the air to the nearest 0.1 mg. Next, the universal specific gravity kit for an electronic scale produced by Mineralab was used to attach a specimen to an analytic balance with a thin wire. The specimen was weighed while the specimen and a portion of the wire were immersed in distilled water. The wire was also weighed alone, partially immersed up to the same point as in the previous step. The density of the material was then determined, using equation 2 as follows:

$$\rho = \frac{a}{a+w-b}(0.9975) \qquad (2)$$

where:
ρ = density (g/cm^3)
a = weight of specimen in air
b = apparent weight of fully immersed specimen and partially immersed wire
w = apparent weight partially immersed wire
0.9975 = density of distilled water at 23 °C

Four half meter panels were measured to determine the average volume fraction for the low density and high-density composites. The values obtained for each are provided in Table 4.3. The average fiber volume fraction observed in the low-density composite (1.57 picks/cm/layer) was 42% and the average volume fraction observed for the high-density composite (4.72 picks/cm/layer) was 52%.

Table 4.3. Fiber volume fraction for low density and high-density composites

		Low density (1.57 picks/cm)		**High density (4.72 picks/cm)**	
		Specimen 1	**Specimen 2**	**Specimen 1**	**Specimen 2**
Preform weight (g)	W_f	1023.5	825.0	1765.3	1977.8
Composite weight (g)	W_c	1627.7	1471.8	2354.1	2937.8
Density of E-glass (g/cm^3)	ρ_f	2.54	2.54	2.54	2.54
Avg. Density of composite (g/cm^3)	ρ_c	1.78	1.81	1.86	1.85
Volume fraction (%)	V_f	44.1	40.0	54.8	49.09
Avg. Volume fraction	V_f	**42%**		**52%**	

4.4. Testing

After composites were prepared, they were subjected to testing in order to create damage within the component and observe the POF sensor's response to the damage event. Composites offer several advantages over conventional engineering materials but still have a few limitations as well. One major area of investigation is examining failure modes, specifically in response to a localized impact loading event [51]. Donadon et al. and Richardson and Wisheart both cite four major failure modes related to an impact event: delamination, matrix mode, fiber mode, and total perforation [103, 104].

Impacts can be divided into two conditions: low-velocity impacts by a large mass, such as a dropped tool, and high-velocity impacts by a small mass, such as runway debris hitting an airplane body [51]. There is not a clear numerical distinction between these conditions, but it is suggested that they can be classified by the damage incurred. Under low-velocity impacts, the time of contact between the projectile and the target is relatively long allowing for the entire structure to respond to the impact event and energy is absorbed elastically [103-105]. This condition typically results in damage characterized by delamination, matrix cracking, fiber fracture, and debonding [106]. For higher velocity impacts, the impact event is short and the structure may have not enough time to respond, thus the damage is almost exclusively perforation with a delaminated area surrounding the hole [103, 104].

The goal of the testing was to monitor damage growth in the composite specimen and the response of the proposed SHM system. Accordingly, low energy impacts, simulated by a falling weight fixture, was chosen to create slow damage accumulation, and avoid completely penetrating the composite. OTDR signal was obtained after each impact to observe the POF sensor's ability to detect damage and residual compressive strength was obtained after the damage event to reveal the progression of damage.

4.4.1. Repeated impact testing

Damage to the composite structure was created by exposing composite plate specimens to multiple low energy impacts at a localized site. Such testing aims to mimic the accidental

impacts a structure may receive during its manufacturing process and service life, which have been shown to result in decreased compressive strength in the material. When low energy impact events are being considered, rupture does not occur after a single impact [107]. Single impact testing may not generate significant damage in a composite. This is especially true for 3D woven composites which have higher impact damage tolerance than 2D woven composites [108, 109]. It is thus more important to determine the evolution of the damage over several impacts rather than, solely the absorbed energy. To observe this evolution, the composite must not be completely penetrated and can be impacted multiple time. During drop weight impact tests, a weight falls from a pre-determined height to strike the specimen supported in the horizontal plane [51]. At low velocity, this test typically does not cause complete destruction of the test specimen. According to an early paper written by Jang, Kowbel, and Jang exploring the benefits of repeated impact testing, these events promote a clear damaged region even when impact energy is very low and represent a convenient method for assessing the damage tolerance of fiber composites [110].

Research on multiple, low-velocity impact responses of composites is limited. De Morais, Monteiro, d'Almeida have conducted a few studies using repeated impact testing. In these studies, a dart with mass 765 g and a semi-spherical nose of diameter 1.5 inches is used. The samples are 12.5 by 12.5 cm^2 and clamped before impact [97, 107]. Tooski et al. uses a specimen clamped between two steel frames having an opening area of 125 mm by 75 mm and impact energy of 6.8 J. A conical-shaped steel impactor with 1050 g weight and a hemispherical nose with a 6.35 mm radius were also used [111]. Several authors opt for a circular testing diameter of 76.2 mm [109, 112, 113], but these tests are not consistent in the type of striker or impact energy. Sevkat et al. uses an impact energy of 32 J, which is achieved with a velocity of 3.23 m/s, tup mass of 6.15 kg, and a diameter of 16 mm [113]. Baucom and Zikry used an energy of 18 J, which is achieved with a velocity of 2m/s, a tup mass of 9.0 kg, and diameter 19 mm [109]. Icten's study involves using a range of impact energies from 5-10 J and a 12.7 diameter hemispherical nose with mass 5.02 kg [112]. These studies do not suggest a consistent method for testing.

A high energy falling weight impact tester, CEAST 9350 was used to create damage in the composites as a result of impact forces. CEAST 9350 has maximum impact velocity 24 m/s with falling mass of 2 kg, max impact velocity 7 m/s with falling mass of 70 kg and maximum potential energy 1,800 J. A pneumatic clamping fixture with a 76.2 mm diameter opening secured the sample during impacts. A tup with diameter of 12.7 mm was used for each test. Impact energy levels of 9 J, 18 J, and 27 J were chosen to create slow damage accumulation in the composite. During the tests the total mass of drop weight remained constant at 4.93 kg, thus different energies were achieved by adjusting the drop height. Table 4.4 contains the parameters associated with the impact tests.

Table 4.4. Impact parameters

Property	Value		
Impact Energy (J)	9	18	27
Impact Velocity (m/s)	1.91	2.70	3.31
Falling Height (mm)	186	373	559
Total Tup Mass (kg)	4.93	4.93	4.93

The ASTM D7136 [114] standard for measuring damage resistance of a fiber reinforced polymer matrix composite to a drop weight impact event was followed with modification to the width of the sample. The standard recommends a flat rectangular composite plate of dimensions 15 cm x 10 cm be subjected to an out-of-plane, concentrated impact [114]. In these tests, specimens with dimension 15 cm x 48 cm were used to accommodate the critical bending radius of the POF and the use of the 3D weaving machine.

4.4.2. Optical time domain reflectometry

A major concern with low energy impact damage is that composites can contain barely visible impact damage which may escape detection during a visual inspection of the impacted surface of the component, but can severely reduce the structural integrity of the component [103, 109]. Thus, it is critical to detect the damage with embedded sensors. Before the impact events, one protruded end of the POF embedded in the composite was connected to the OTDR, depicted in

Figure 4.8, to measure backscattering level and signal loss before the impact (control sample) and after each impact event. Specimens were impacted in the same location followed by repeated number of impacts until signal damage were recorded. In some specimens, the POF was disconnected and reconnected to the OTDR between each impact event. It was later found that keeping the OTDR connected produced less noise and more consistent results in the OTDR signal.

Figure 4.8. POF connected to OTDR to monitor POF signal during impact testing

The LOR-220 from Luciol Instruments, a portable high-resolution scanning photon-counting OTDR was used to measure the integrity of the POF signal in these experiments. OTDR was used to test the quality of the POF after weaving and after resin treatment. During impact testing, one protruded end of the POF embedded in the composite was connected to the OTDR to measure the signal loss after each impact event. The OTDR settings listed in Table 4.5 were used for each measurement event. The OTDR was configured to emit a wavelength of 670 nm, with a time step resolution of 1.25 ns and signal pulse width of 1 ns. The optical pulse width, the time that the laser is on, on this technology is optimized for short range fiber testing since shorter pulse widths carry less energy [115]. This OTDR has a short dead zone, which is the minimum

distance after a Fresnel reflection where an OTDR can detect another event. The short dead zones (10 cm event dead zone and 40 cm attenuation dead zone) allow for detection of events such as fiber breaks and bend loss within the smart composite. A list of the OTDR specifications is included in Appendix B.

Table 4.5. OTDR settings

Property	Value
Wavelength	670 nm
Distance Range	1.25 km
Refractive Index	1.49
Backscatter Coefficient	-30
Insertion loss threshold	0.2 dB
Reflectance Threshold	-50 dB

A typical backscattering output signal of amplitude measured in decibels (dB) vs. distance measured in meters (m) is shown in Figure 4.9. It consists of a main slope which represents the signal attenuation according to Rayleigh backscattering and localized reflection spikes due to Fresnel reflection. Fresnel reflection at specific locations along the optical fiber. Fresnel reflection occurs when a sudden change happens to the fiber refractive index and causes the light to reflect back on the fiber. This Fresnel reflection appears as a spike on the OTDR waveform and is usually associated with connectors, fiber breaks, and the ends of the optical fiber [37]. The Rayleigh backscattering is used to calculate the level of attenuation in the optical fiber as a function of distance, which is shown by a straight line slope in an OTDR trace signature [37]. Attenuation is calculated by dividing the loss, by the length of the fiber, as the slope increases attenuation becomes higher. The dynamic range is the distance between the initial backscatter and the noise level. The higher the dynamic range, the higher the signal to noise ratio and the clearer the events will appear.

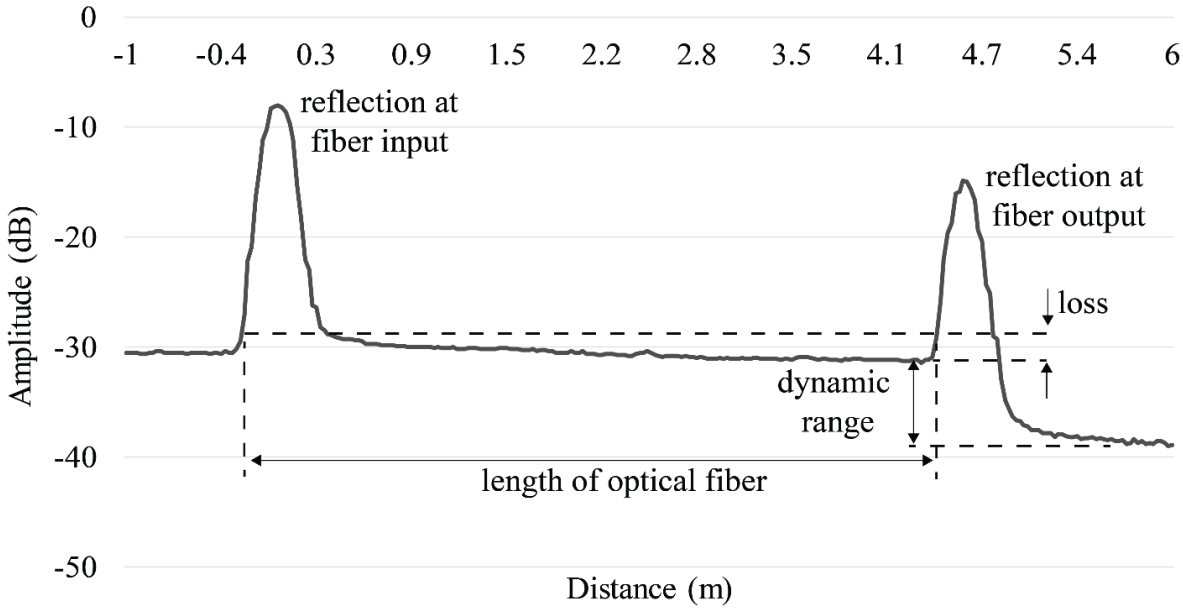

Figure 4.9. Characterization of a typical POF signal obtained from OTDR

The backscattered light is recorded as a function of time. Knowing the speed of light wave propagation through the optical fiber, the time of arrival of the backscattered signal can be converted into distance corresponding to a position along the fiber and is used to pinpoint damage to the fiber [32, 116]. A reflection or excess loss is observed in the spectra when there are defects, disturbances, or discontinuities in the fiber [32, 116].

4.4.3. Compression after impact testing

High strength reduction occurs under compression loading and thus it is an important problem to be considered in the design of composite structures [112]. Compression after impact (CAI) testing is an experimental method to obtain the degradation of the compressive strength of the composite plates due to impact loading. A compression after impact test was performed to detect damage resistance and damage tolerance properties of the composite specimens. Several articles use Boeing Specification Support Standard, BSS 7260 [117, 118]. There is now a compatible international ASTM standard for this test, ASTM D7137. Yan followed this standard. The main focus of this experimental investigation will be to characterize the damage within the composite due to impacts and determine the correlation of the reduction in compressive strength to the impact-induced damage [119].

ASTM D7137 [120] was followed to characterize the damage within the composite due to impacts. ASTM D7137 required a 150 mm by 100 mm flat rectangular composite sample that had been subjected to impact testing. After impact, the specimens were cut according to these dimensions (with the impact location in the center) using a computerized waterjet cutting technology available at ADR Hydro-Cut, Inc., Morrisville, NC. The waterjet cutting was very precise in terms of dimensions, with a very low coefficient of variation (less than 0.1%). The test was performed on the MTS model 370 servo hydraulic load frame using a compressive speed of 1 mm/min. The compression fixture associated with ASTM D7137 was used to hold the plate in place during the test. The test fixture was composed of adjustable retention plates to support the specimen edges and inhibit buckling when the specimen was end loaded. The side supports contained knife edges and the top plate sat on the top edge of the specimen. The specimen was placed in the fixture so that ends were flush with the ends of the fixture halves, the screws of the fixture were tightened, and then the fixture was placed and aligned between the flat platens on the testing machine, Figure 4.10. The thickness of each specimen was measured before each test using a Vernier caliper. There was slight variation in the thickness across the plate, thus the average thickness of 4 locations was used.

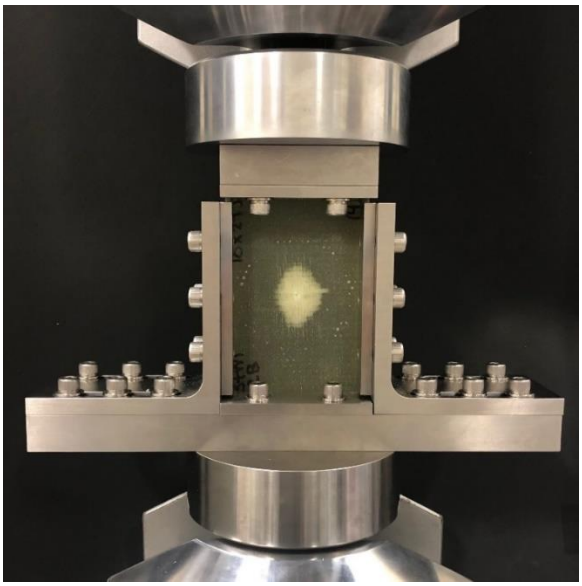

Figure 4.10. Specimen placed in CAI fixture

This test method can be used to test undamaged polymer matrix composite plates, but the standard suggests that historically such tests have demonstrated a relatively high incidence of

undesirable failure modes (such as end crushing). Test Method D6641/D6641M is recommended for obtaining compressive properties of undamaged polymer matrix composites [120].

4.4.4. Combined loading compression testing

To gather a baseline, undamaged compressive properties of the specimens, a combined loading compression (CLC) test was performed following ASTM D6641 [121]. This test method is used to determine the compressive strength and stiffness properties of polymer matrix composite materials. The specimen size was 140 mm x 13 mm and the specimens were also cut using the computerized waterjet for improved accuracy. The test was performed on the MTS model 370 servo hydraulic load frame using a compressive speed of 1 mm/min. The adjustable specimen fixture consisted of an upper half connected to a lower half by alignment rods. The test specimen was placed in the test fixture so that the ends of the specimen were flushed with the top and bottom surfaces of the fixture, and an unsupported 13 mm specimen gage length was present in the middle of the fixture, Figure 4.11. The assembled fixture was then placed and aligned between flat platens and the fixture was compressed between the two plates thus subjecting the specimen to combined end and shear loading.

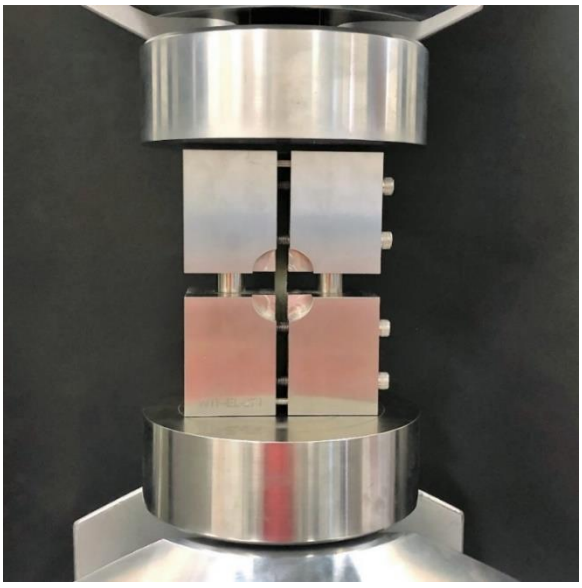

Figure 4.11. Specimen placed in CLC fixture

Specimen size typically changes the failure mode, and the specimen size for the CAI testing is much larger (150 mm by 100 mm) than for the CLC (140 mm x 13 mm). In an impact test, for example, the larger specimen would normally have more bending present due to impact. In 3D woven specimens, however, the amount of bending is much less (as compared to 2D woven specimens) and the damage is much more localized at the impact location, therefore changing the specimen size still allows for a reasonable comparison using the two test methods.

4.4.5. Tensile after impact testing

When a composite is subjected to low-velocity impacts, damages from this event can cause a reduction in structural stiffness and strength leading to growth of the damage and final fracture. Tensile properties are another important parameter to consider when observing the progression of damage and residual strength for composites [106]. Tensile after impact testing is a less common test method compared to compression after impact testing for determining residual strength. There does not exist a standard for tensile after impact testing, but various methods have been proposed.

Wang, Wu, and Ma investigated the low-velocity impact characteristics and residual tensile strength of carbon fiber composite laminates [106]. In this study a sample size of 76.2 mm x 277.8 mm was used to account for damage area, which is much larger than a typical tensile test. Two different stacking sequences were investigated, and degradation predicted by an FE model was compared with experimental results.

Caprino also conducted experiments to evaluate the residual tensile strength of composite panels after an impact event [122]. After impact, the specimens were visually inspected to evaluate the appearance of damage and identify the most relevant impact energy threshold. Caprino used specimens with dimensions 25 mm x 100 mm. In both studies, the trends of residual strength as a function of impact energy were divided into three stages: lower impact energy degradation stage, plateau trend, and higher impact energy degradation.

For this evaluation, specimens were tested following the guidelines of ASTM D3039 [123] standard test method for tensile properties of polymer matrix composite materials. This test

method is used to determine the in-plane tensile properties of polymer matrix composites and does not consider previous damage to the specimen. As suggested in the standard, specimens with dimensions 250 mm x 25 mm were used. These specimens were cut using a computerized waterjet for improved accuracy. The composite specimens were tested on the MTS hydraulic load frame. The specimens were aligned and mounted to grips on the MTS hydraulic load frame, Figure 4.12. They were then loaded in tension at a strain rate of 2 mm/min while recording the force.

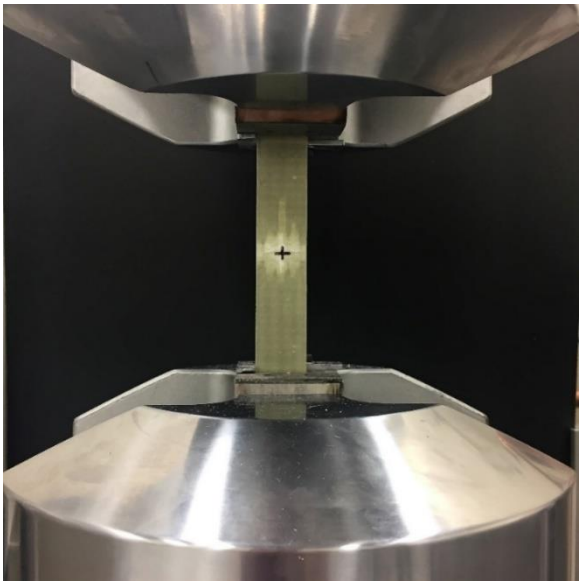

Figure 4.12. Specimen aligned in the grips of the MTS hydraulic load frame for tensile after impact test

Chapter 5: Results and Discussion

5.1. Smart composite manufacture and characterization

5.1.1. Characterization of embedded optical fiber

Smart composites were created by weaving a 3D orthogonal preform with embedded POF sensor and infusing the preform with resin. Table 5.1 shows a summary of the composite parameters after the manufacturing process. After resin infusion, the thickness of the composite panels was 3.2 ± 0.2 mm for 1.57 picks/cm/layer and 6.5 ± 0.3 mm for 4.72 picks/cm/layer. In the composite structure, the POF is located approximately 2 mm (Group I and Group III), 3 mm (Group II), 4 mm (Group IV) from the surface of the composite. Figure 5.1 shows a side view of the composite groups taken with digital optical microscope at 10x magnification. The POF in these images does not appear to have large resin pockets that sometimes occur when embedded in a composite. The average fiber volume fraction observed in the low-density composite (1.57 picks/cm/layer) was 42% and the average volume fraction observed for the high-density composite (4.72 picks/cm/layer) was 52%. Daniel and Ishai report that a typical 3D fabric E-glass/Epoxy composite has a volume fraction of 0.50 and a density of 1.90 g/cm [50]. The values for the measured composite are comparable to those reported, indicating that they are well-produced specimens and comparable to the typical composite of this type.

Table 5.1. Summary of composite parameters

Parameter	**Value**			
Sample Grouping	I	II	III	IV
Y- layers	4			
X-yarn density (pick/cm/layer)	1.57		4.72	
Position of POF	Middle	Middle	Top	Bottom
Distance of POF from the impact surface	2 mm	3 mm	2 mm	4 mm
Volume fraction	42%		52%	
Thickness	3.2 ± 0.2 mm		6.5 ± 0.3 mm	
# of specimens woven	30	70	54	46
% of specimens with good signal after manufacturing	13%	6%	20%	24%

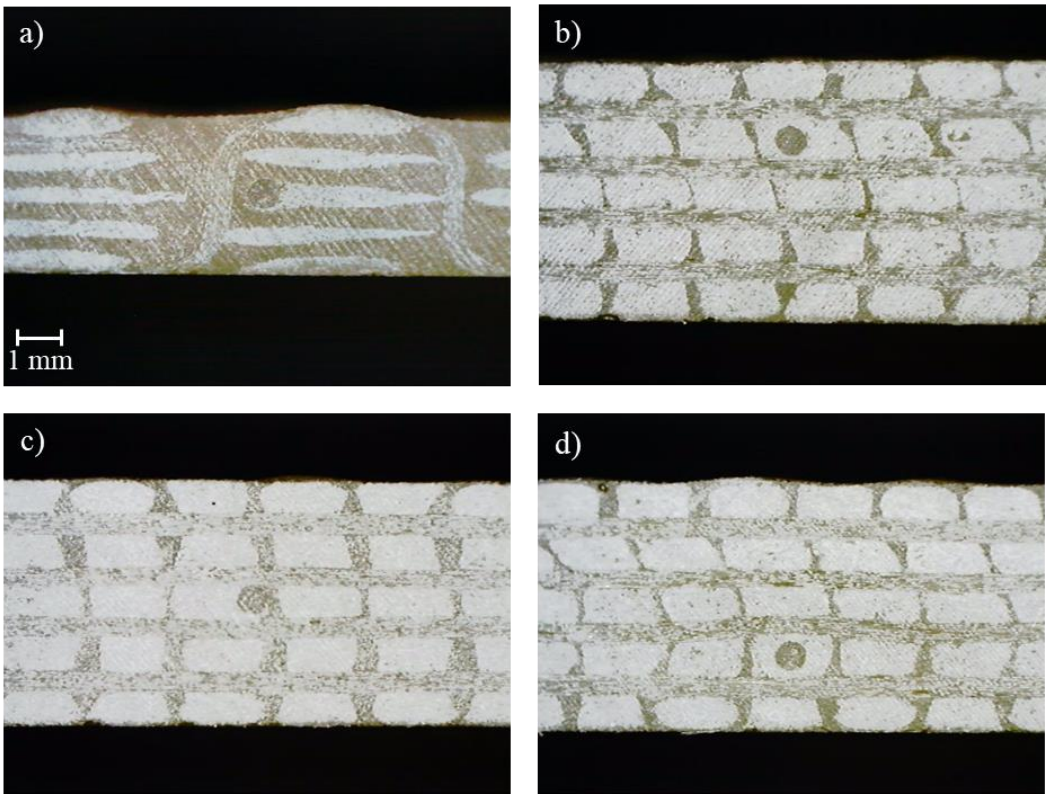

Figure 5.1. Side view of the 3DOW composite with the POF positioned in the a) top b) middle (high-density) C) bottom layer and d) middle (low-density) layer. Images taken with a digital optical microscope at 10x magnification

5.1.2. Fragility of embedded optical fiber

OTDR was used to test optical fiber embedded in the preform after weaving and after vacuum bagging to ensure the integrity of the fiber. Even though the POF is more flexible than GOF and precautions were taken to protect the optical fiber, such as the addition of furcation tubes, POFs were found to be very fragile and sensitive to the composite manufacturing methods. It was observed that POF was most likely to become damaged during the vacuum bagging procedure, especially at the point where the optical fiber enters the woven preform and at the selvage where the optical fiber is sometimes exposed due to turning the optical fiber to be woven back through the fabric. These areas are highlighted by the red rectangles in Figure 5.2. Some fibers were also damaged during the weaving process or while being transported/ stored.

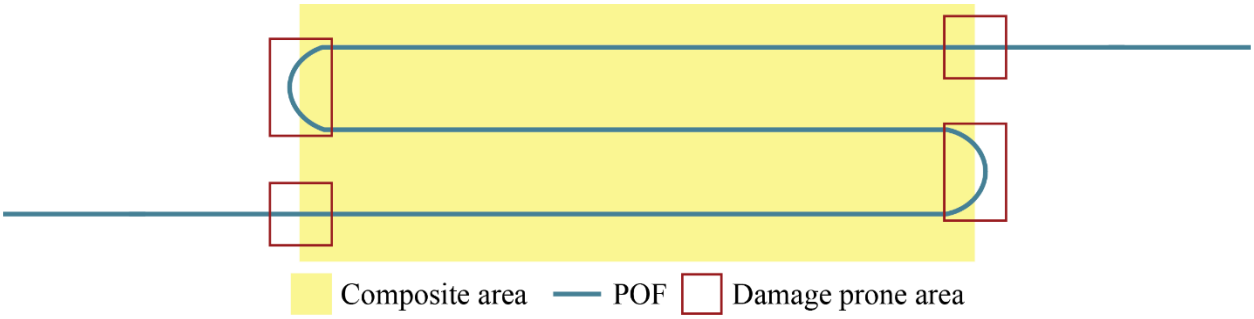

Figure 5.2. Areas in the specimen where the POF is most likely to experience damage

After vacuum bagging each POF signal was categorized as good or poor. A good signal is classified as a signal that remains roughly the same after vacuum bagging, has no major flaws in the slope of the signal, and has a large dynamic range. A large dynamic range is needed because it correlates with a high signal to noise ratio, thus the events in the spectra appear clearer. Figure 5.3a represents a POF with a good signal before and after vacuum bagging. Poor signals were classified as those in which the dynamic range was close to 0 dB, or signals which exhibited a major flaw such as a large reflection in the slope of the signal. Figure 5.3b represents a specimen with a poor signal resulting from a dramatic drop in attenuation. In this specimen, the dynamic range dropped from 9.1 dB before vacuum bagging to only 0.8 dB after vacuum bagging. The cause of this drop is unknown but may be related to micro-bending losses from the stresses of the resin curing process. It was mentioned in section 2.4.4 that micro-bending is a common problem in the manufacturing of composites with embedded optical fiber. During VARTM the removal of the peel ply also caused macro-bending issues when the optical fiber became adhered to it. Specimens, such as the one shown in Figure 5.3c have a large reflection in the middle of the signal that is most likely due to the POF breaking. As noted in section 2.3.1, Fresnel reflections such as this typically occur at connectors, fiber breaks, and the ends of the optical fiber. They also lead to dead zones where the detector is temporarily blinded by the high amount of light it is receiving. Signals with damage to the POF in the middle of the sample were no longer useable for the impact analysis because the dead zone would not allow other damage to be detected accurately. Both poor and good signals were found in the different varieties of specimens woven, regardless of the POF position or weave density.

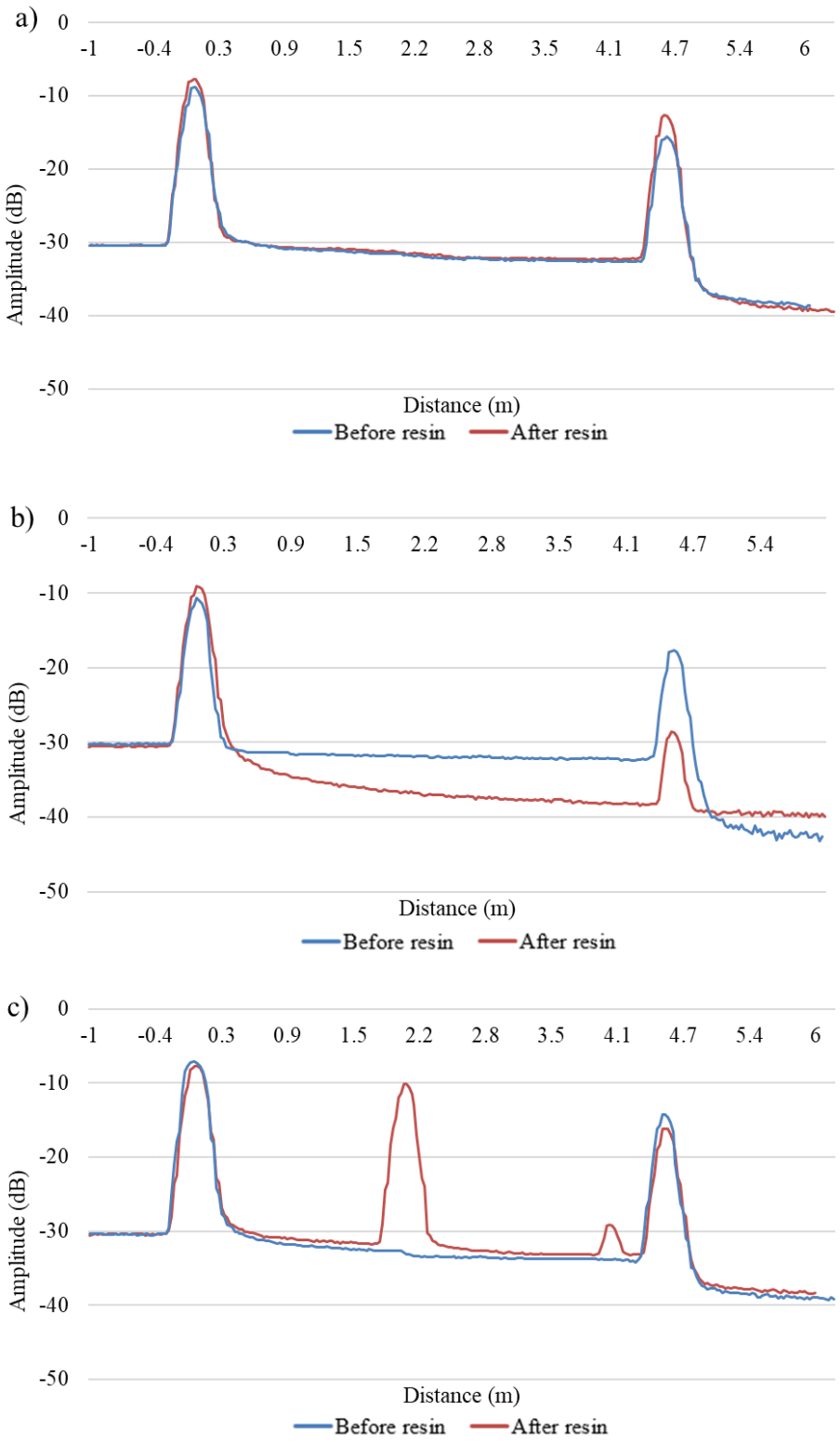

Figure 5.3. Examples of specimens before and after VARTM with a) good POF signal retention, b) poor signal due to a large attenuation drop, and c) poor signal due to a large reflection

One solution to the problem of excessive POF bending and breakage during VARTM was to secure Popsicle sticks, shown in Figure 5.4, at the ingress points of the fiber in the preform. As noted in section 2.4.4, these areas are highly sensitive to damage and the Popsicle sticks provided extra support and immobilized the optical fiber at these vulnerable points. Another solution was to position the spiral tube across the width of the preform instead of over the selvage, where it is traditionally placed during VARTM. This reduced pressure and movement of the POF during the curing process. These solutions were both implemented after several optical fibers had failed, and although not 100% successful they did improve the success rate for the optical fiber signal being retained through the manufacturing process.

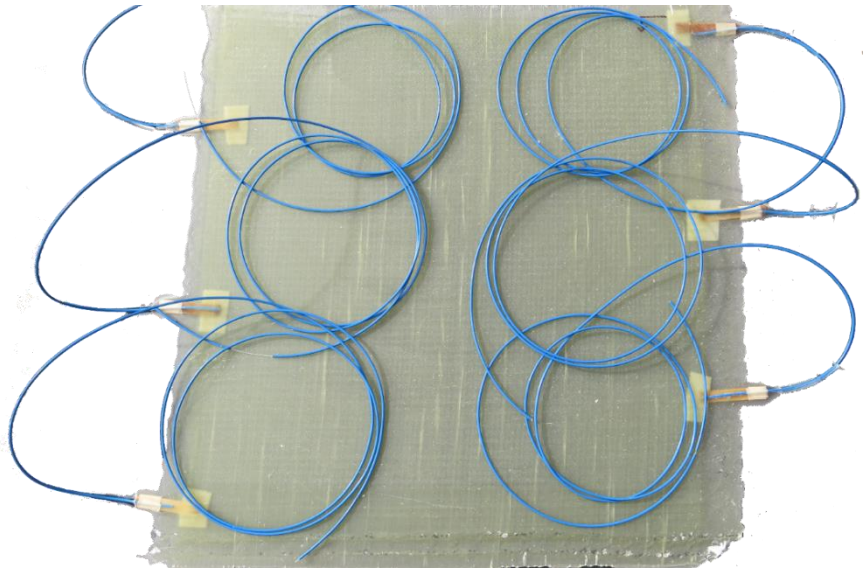

Figure 5.4. Demonstration of the use of Popsicle sticks to reduce breakage of the optical fiber where the optical fiber meets the woven fabric

Despite these modifications to the manufacturing process, the overall success rate of the POF embedded in the composite (specimens which were classified as having a good signal) was only 15% for all specimens created. The success rate also fluctuated for the different categories of specimens, Table 5.1. Specimens in category IV (POF positioned in the bottom layer) had the highest success rate of 24% and specimens in category II (POF positioned in the middle layer) had the lowest success rate of only 6%. The specimens in category II were the first to be woven and vacuum bagged before the procedure had been perfected. These specimens were also stored on the bottom of a pile of woven specimens and transported to several different storage areas,

therefore they had the highest probability of becoming damaged. Specimens in category IV, on the other hand, were woven last after changes to the vacuum bagging procedure had been made. The POF in this category was also closest to the table during VARTM, minimizing bending, which may have also contributed to the higher success rate.

5.2. Comparison of POF structural position

The composite sensor system was evaluated by establishing a relationship between the sensor's location, POF signal after impact damage, and residual composite strength. Due to the destructive nature of the testing and the fragility of the POF, all tests were conducted on individual specimens, which have inherent variation from one sample to another. The POF signal obtained from OTDR is also unique to the environment in which the POF is tested. Slight changes in the connection of optical fiber to the OTDR can produce shifts in the signal obtained. Therefore each signal tested must be considered on an individual basis. For the following data, the signal produced before the impact test was started, was considered the baseline. This measurement is labeled as impact 0. This baseline must be considered when comparing between POF embedded in 2 different composites.

Four test groups were set up to compare pick density (groups I and II) and POF structural position (groups II, III, and IV). This section covers the relationship between impact damage and POF positions in the structure (top, middle, or bottom layer) keeping pick density constant at 4.72 picks/cm. Impact energy levels of 9 J, 18 J, and 27 J were chosen to create slow damage accumulation in the composite. Specimens were impacted on the top surface and attenuation losses were calculated at approximately 3 m along the length of the POF.

5.2.1. POF signal results

9 J impact energy

The lowest impact energy used was 9 J. Figure 5.5 demonstrates a typical progression of damage for the composite impacted multiple times at this energy level. The area of the impact diameter grow with each impact, and was measured using image processing software. The impact damage area grew from an area of 2.92 cm^2 after 1 impact to an area of 6.75 cm^2 after 30 impacts, this is

an increase in damage size of 131%. The tup does not penetrate the back of the sample after impact 30. The impact diameter for each impact is listed in Table 5.2. Figure 5.6 represents the signal of a POF embedded in the top layer of a composite after being impacted 10 times and 20 times at an impact energy of 9 J. In this optical fiber, there was a loss of about 4 dB after 10 impacts and a loss of 10 dB after 20 impacts compared to the baseline. The loss is a uniform attenuation along the embedded section of the POF. This shows that the optical fiber was sensitive to the impact events, but it was not completely damaged. Complete damage to the optical fiber would result in a spike in the signal at the impact location, like the reflection observed at the ends of the optical fiber.

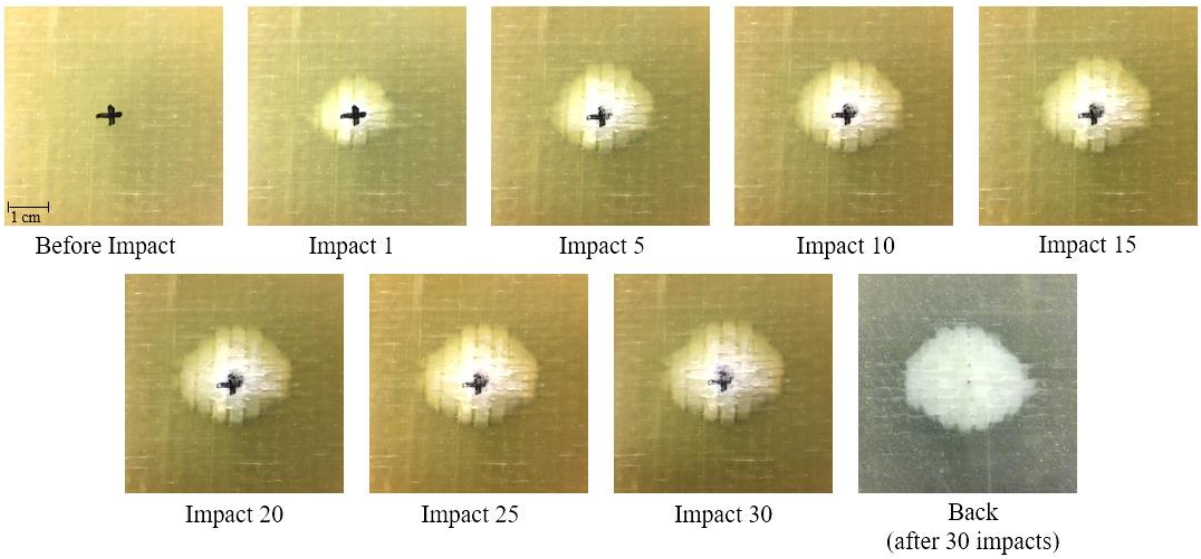

Figure 5.5. Progression of impact damage at 9 J on a specimen with pick density 4.72 picks/cm

Table 5.2. Impact damage area (impact energy: 9 J, pick density: 4.72 picks/cm)

Impact number	**Area (cm^2)**
1	2.92
5	4.62
10	5.30
15	5.90
20	5.98
25	6.71
30	6.75
Back (30 impacts)	7.65

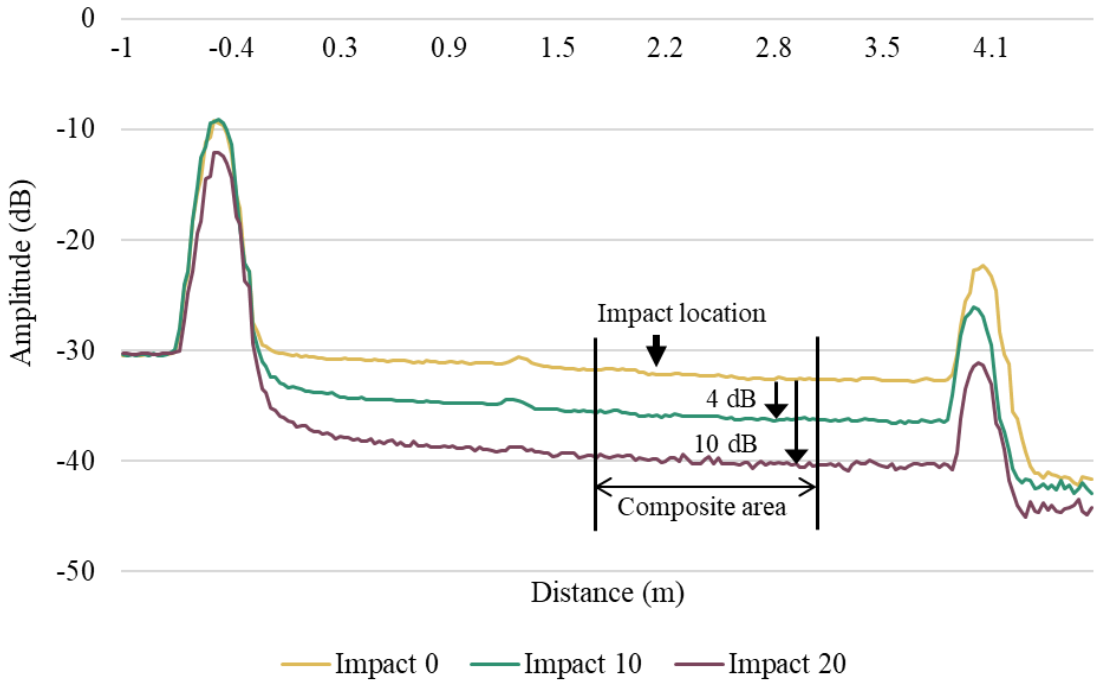

Figure 5.6. Signal of POF embedded in the top layer of the 4.72 picks/cm preform and impacted at a 9 J energy level

At the 9 J impact energy level, specimens with POF located in the middle and bottom layers were also tested. The signal for these POF did not change as drastically as the POF located in the top layer. At 9 J impact the POF located in the middle layer, Figure 5.7 showed a reduction of about 3 dB after 30 impacts. The POF located in the bottom layer, Figure 5.8 showed hardly any loss with a reduction of only 0.2 dB after 30 impacts and 2 dB after 50 impacts. However, this loss was localized to the impact location for the POF in the bottom layer, as seen in Figure 5.8. This localized change in attenuation is most likely due to bending induced residual crimping of the POF at the impact location. During the impact, the bottom side is in tension, and when the loading is released, some residual bending is present on the POF. This residual bending increased uniformly with additional impacts.

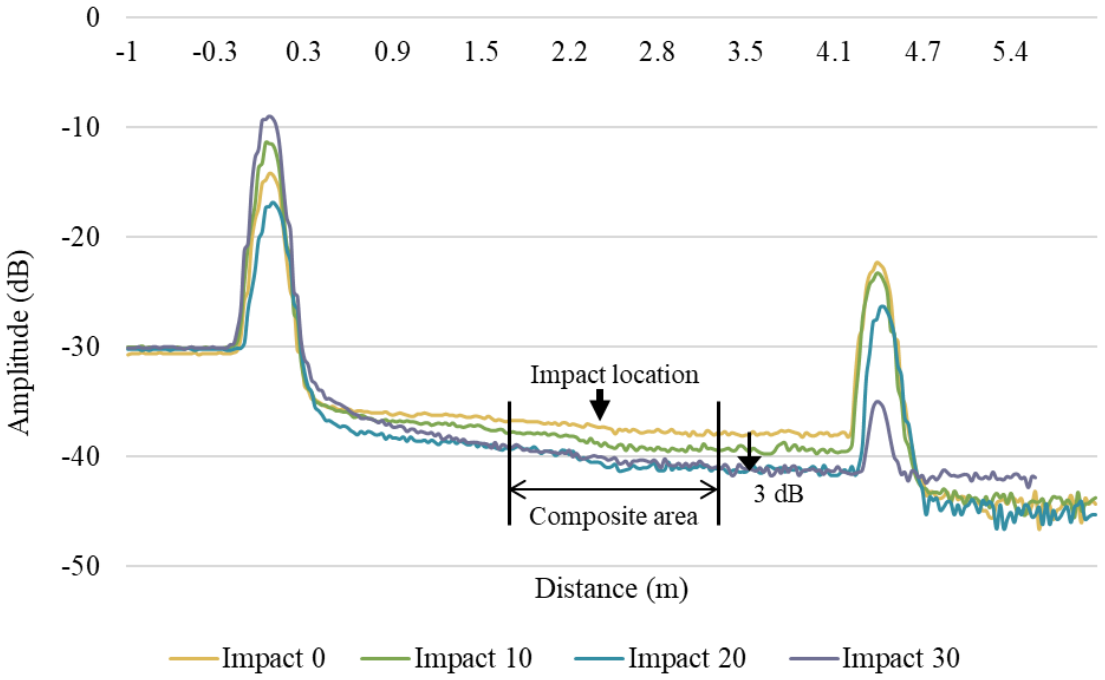

Figure 5.7. Signal of POF embedded in the middle layer of the 4.72 picks/cm preform and impacted at a 9 J energy level

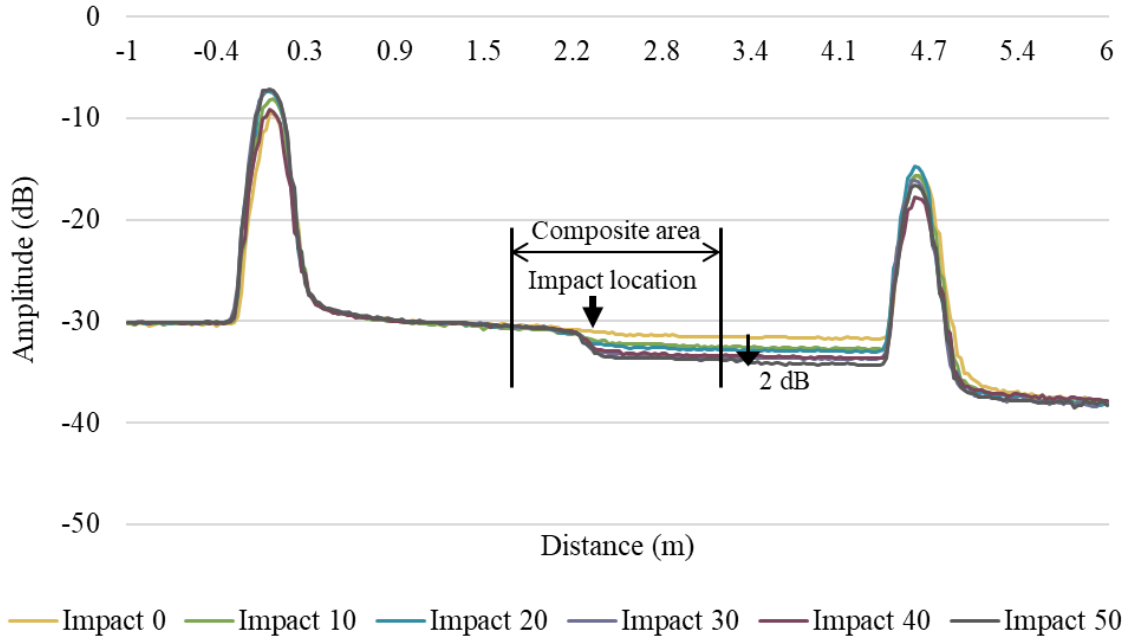

Figure 5.8. Signal of POF embedded in the bottom layer of the 4.72 picks/cm preform and impacted at a 9 J energy level

18 J Impact energy

An impact energy of 18 J was then used to create damage in specimens with the POF located in the top and bottom layers. Unfortunately, there were not enough specimens with POF located in the middle to test at 18 J and 27 J energy levels. Figure 5.9 represents a typical progression of damage for the composite impacted at 18 J. The impacted area grows from 4.48 cm^2 after 1 impact to 11.15 cm^2 after 30 impacts, an increase in the damaged area of 149%. The impact diameter for each impact is listed in Table 5.3. As expected, the damaged area is larger than the damaged area observed at 9 J and grows more rapidly. At 30 impacts, the tup does not penetrate the back of the sample.

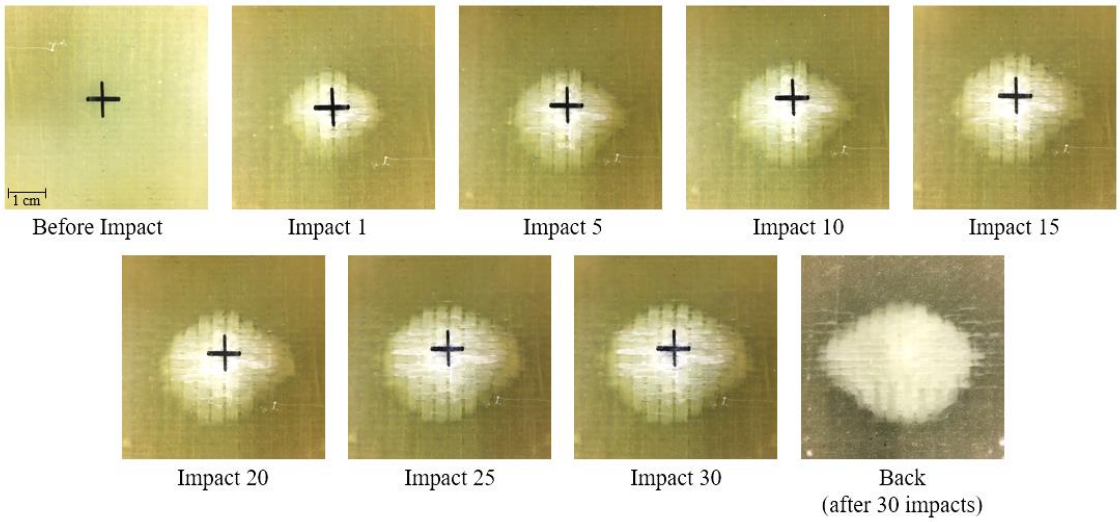

Figure 5.9. Progression of impact damage at 18 J on a specimen with pick density 4.72 picks/cm

Table 5.3. Impact damage area (impact energy: 18 J, pick density: 4.72 picks/cm)

Impact number	**Area (cm^2)**
1	4.49
5	6.38
10	7.15
15	8.56
20	8.71
25	9.98
30	11.15
Back (30 impacts)	12.32

A POF embedded in the top layer of the composite impacted at 18 J, Figure 5.10, shows a similar reduction in signal to the POF shown in Figure 5.6 for 9 J. During this impact event, there was a loss of 3.1 dB after 10 impacts and 5.8 dB after 20 impacts. This optical fiber shows a decrease in signal localized at the impact location, like that observed in the previous specimen. At 18 J impact energy a POF in the bottom layer, Figure 5.11 was also tested. The POF was not sensitive to the impact events and the signal was only reduced by 0.2 dB after 30 impacts and 6.5 after 50 impacts. However, localized signals, presumably due to the residual POF bending, are observed after 40 impacts.

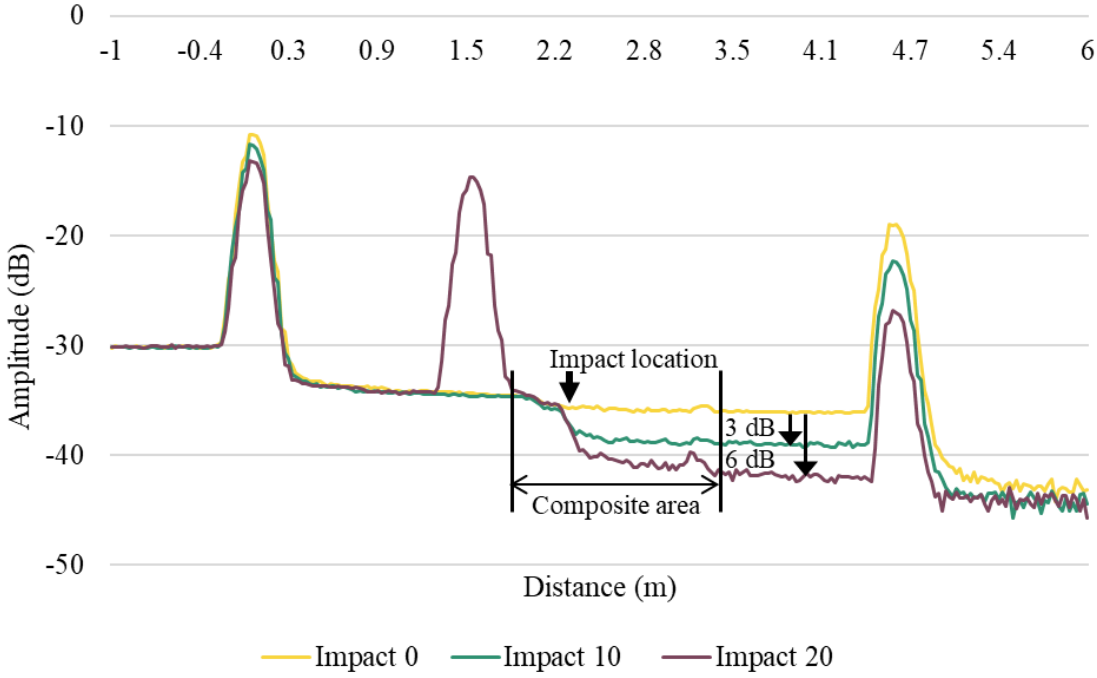

Figure 5.10. Signal of POF embedded in the top layer of the 4.72 picks/cm preform and impacted at 18 J energy level

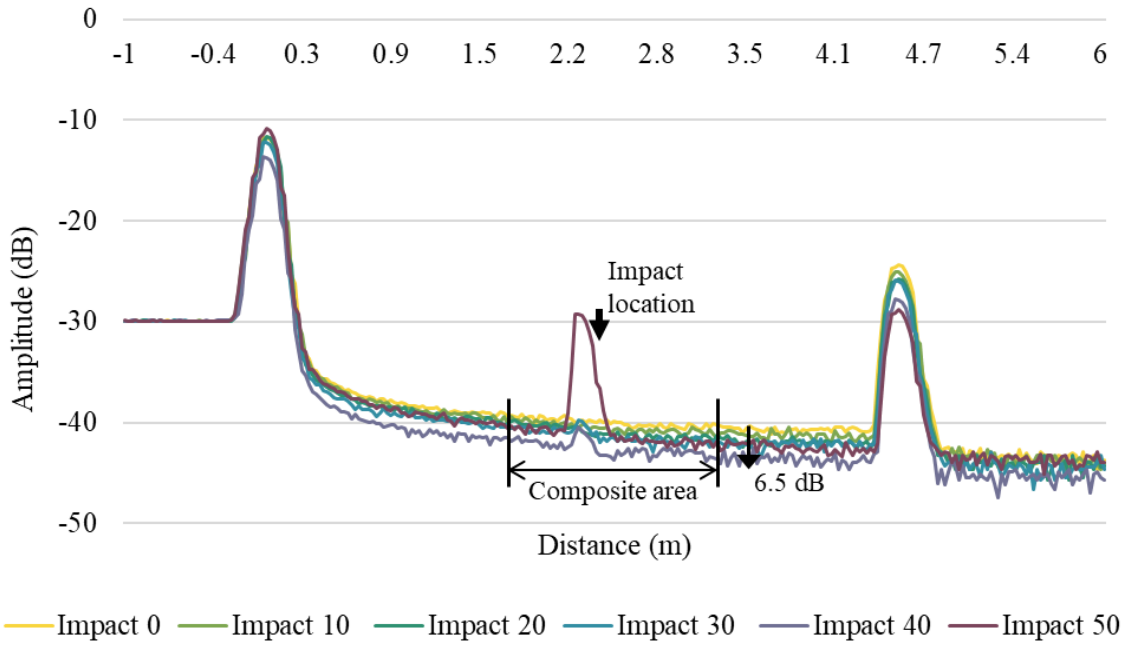

Figure 5.11. Signal of POF embedded in the bottom layer of the 4.72 picks/cm preform and impacted at 18 J energy level

In theory, the loss that occurs at 18 J should be higher than that at 9 J, but each POF must be treated individually due to the conditional nature of the test. The differences between the optical fiber signals obtained may have occurred because the impact was at a slightly different position in relation to the POF. During testing, the impact position was determined by manually judging the location of the optical fiber in the composite and then centering it under the tup. More accurate placement of the impact location and testing of multiple optical fibers under the same conditions would produce more consistent results.

27 J impact energy

Specimens with POF located in the top and bottom layers were damaged at 27 impact energy. A POF embedded in the top layer of the composite impacted at 27 J, Figure 5.12, shows more damage to the POF than previous tests at 9 J and 18 J. The attenuation drops 3.5 dB after being impacted only 3 times. The attenuation then increases by 2.5 dB after impacts 4 and 5. The POF remained connected to the OTDR during the duration of the impact events, therefore, a reconnection did not cause this increase, as explained in Appendix D. The POF, however, may have shifted in the connector, causing the change in signal. There is also a large peak at the impact location, which increases between 3 and 4 impacts. Interestingly, the actual impact

location and center of the damage always appear to the right of the peak, not in the center. The distance of the offset is not consistent between specimens. This shift could be due to the amount of reflection encountered by the detector, human error in measuring, error in the software, etc. It is also unclear if the peak occurs at the edge of the damaged area or the center of the damaged area. Further testing and analysis are needed to determine the cause of this shift so that an accurate distance is measured. This is especially important if the impact location is unknown.

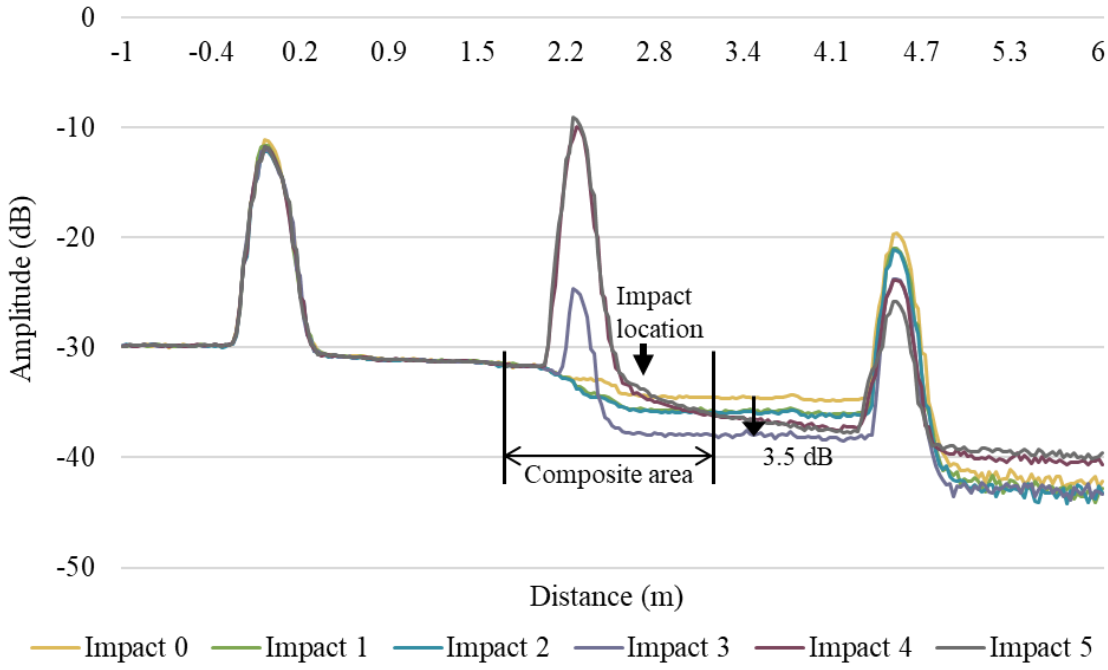

Figure 5.12. Signal of POF embedded in the top layer of the 4.72 picks/cm preform and impacted at a 27 J energy level

At 27 J impact energy a POF in the bottom layer was also tested. Again, the POF sensor is less sensitive to the impact event, but the POF does become damaged after 15 impacts, shown in Figure 5.13a. The attenuation drops 2.1 dB after 15 impacts. Taking a closer look at the peak between 2 and 3 m, Figure 5.14b, and signal for impacts 11-15, Figure 5.13a, there is an increase in the size of the peak that relates to the impact number. After impact 13, the peak increases to 3.1 dB compared to the baseline, after impact 14 the peak increases to 12 dB, and then the peak decreases from impact 14 to impact 15 to a peak size of 9 dB. This signal also has a high signal to noise ratio, which shows that even with a less than ideal signal, information about a damage event can still be obtained.

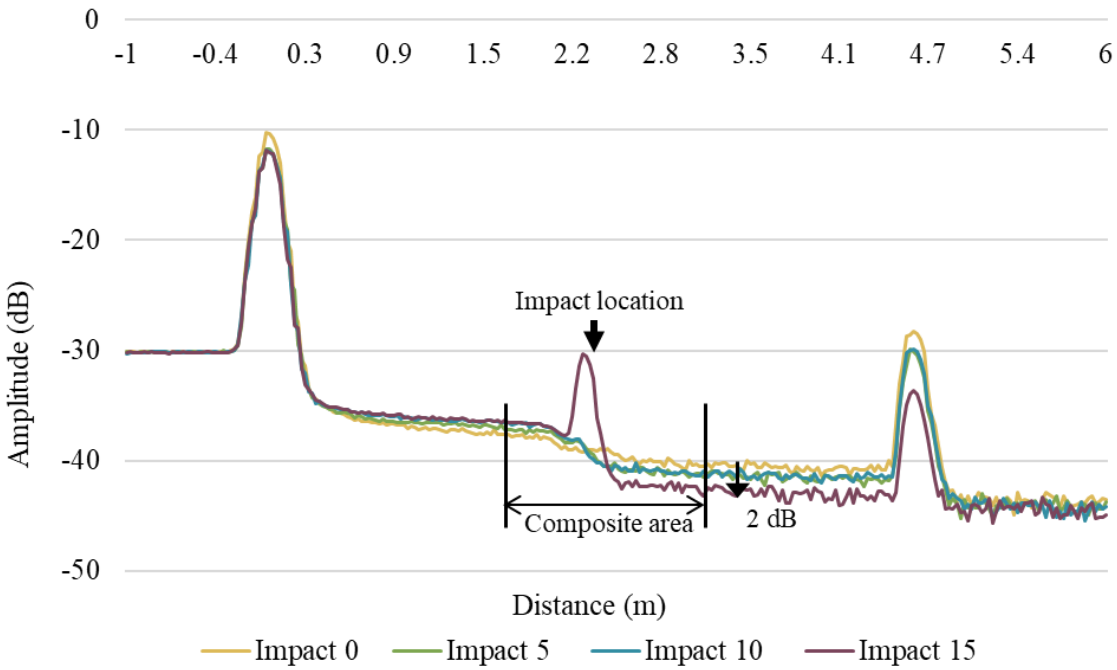

Figure 5.13. Signal of POF embedded in the bottom layer of the 4.72 picks/cm preform and impacted at a 27 J energy level

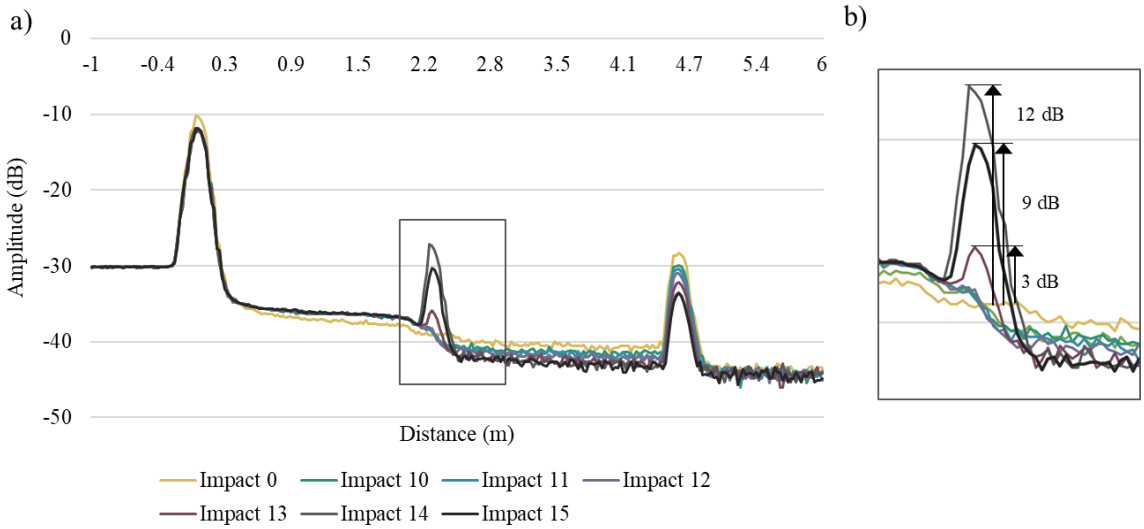

Figure 5.14. a) Signal of POF embedded in the bottom layer of the 4.72 picks/cm preform and impacted at 27 J energy level b) Expansion of damage peak from 2-3 m

Impact away from POF location

Another experiment was conducted to test the sensitivity of the optical fibers in regard to their location from the damage event. A POF embedded in the top layer of the composite was impacted at a 9 J energy level but at a location, 2 cm away from the POF, Figure 5.15a. After 30 impacts the signal does not show a significant drop in attenuation, Figure 5.15b. When impacted directly over the POF, the attenuation dropped 10 dB at 20 impacts. This leads to the conclusion, that a sensor located this far from the damage event is not able to detect the damage incurred by the composite.

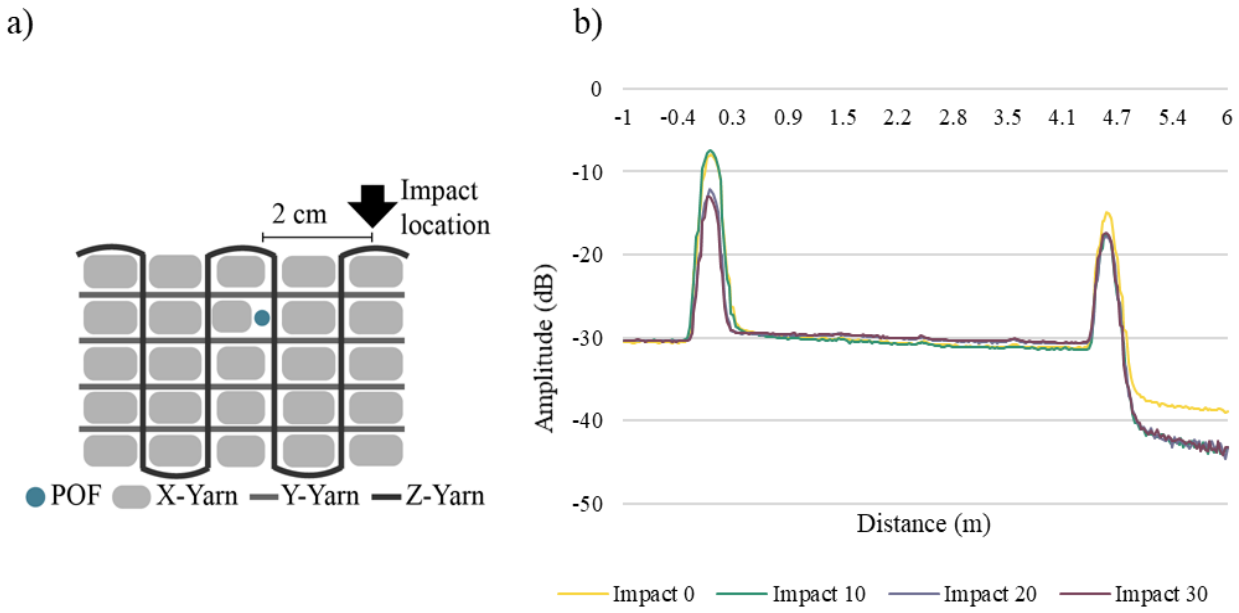

Figure 5.15. a) Side view of a POF embedded in the top layer of the 4.72 picks/cm preform and impacted at 9 J energy level, 2 cm away from the POF location b) OTDR measurement of the specimen

This same experiment was also conducted, but the impact location was changed to be 1 cm away from the POF. Figure 5.16b shows that with each consecutive impact, the damaged area grows closer to the POF location. The impact diameter for each impact is listed in Table 5.4. This growth is represented in the POF spectra as well, Figure 5.16a. At impact 1, the damage area is 2.79 cm^2 and has not reached the POF location. There is also not a significant change in attenuation. At impacts 5 and 10, the edge of the damaged area increases to 5.22 cm^2 and 5.98 cm^2 and reaches the POF location. At this point the POF signal experiences a drop of about 4 dB.

At impact 15, the damage area is 6.65 cm^2 and the dynamic range has reached 0 dB. This demonstrates that the POF must be fairly close, within 1 cm of the damage event in order to sense it. In practice, a damage event is unlikely to occur directly on top of the POF location.

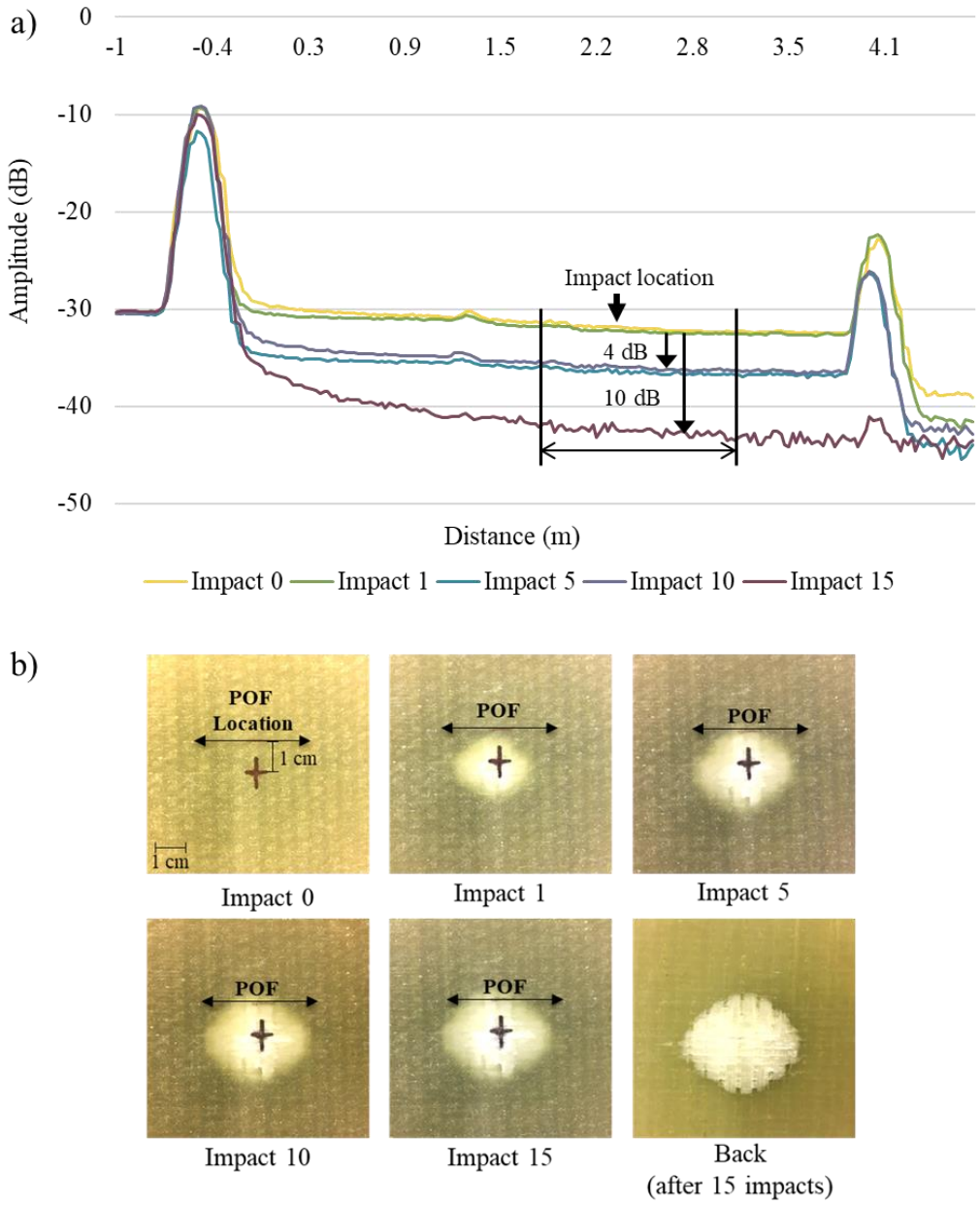

Figure 5.16. a) Signal of POF embedded in the top layer of the 4.72 picks/cm preform and impacted at 9 J energy level, 1 cm away from the POF location b) Progression of damage in relation to the POF location of this specimen

Table 5.4. Impact damage area (impact energy: 9 J, 1cm away from POF)

Impact number	**Area (cm^2)**
1	2.79
5	5.22
10	5.98
15	6.65
Back (15 impacts)	7.20

5.2.2. Tensile test results- high density

Tensile properties are a parameter to consider when characterizing the progression of damage. A tensile test was conducted in the weft direction after samples had been impacted at energy levels of 9 J and 18 J to determine the residual strength of the composite. Figure 5.17a shows the peak load of the high-density composites after being impacted. Stress-strain curves for these specimens can be found in Appendix H. There is a slight downward trend in the peak load of the specimens as the impact number increases. A strength loss of about 10% occurred between the specimen which was not impacted and the specimen which was impacted 30 times. Figure 5.17b shows more of a loss of .1-.2% strain at peak load as the impact number increases by 10.

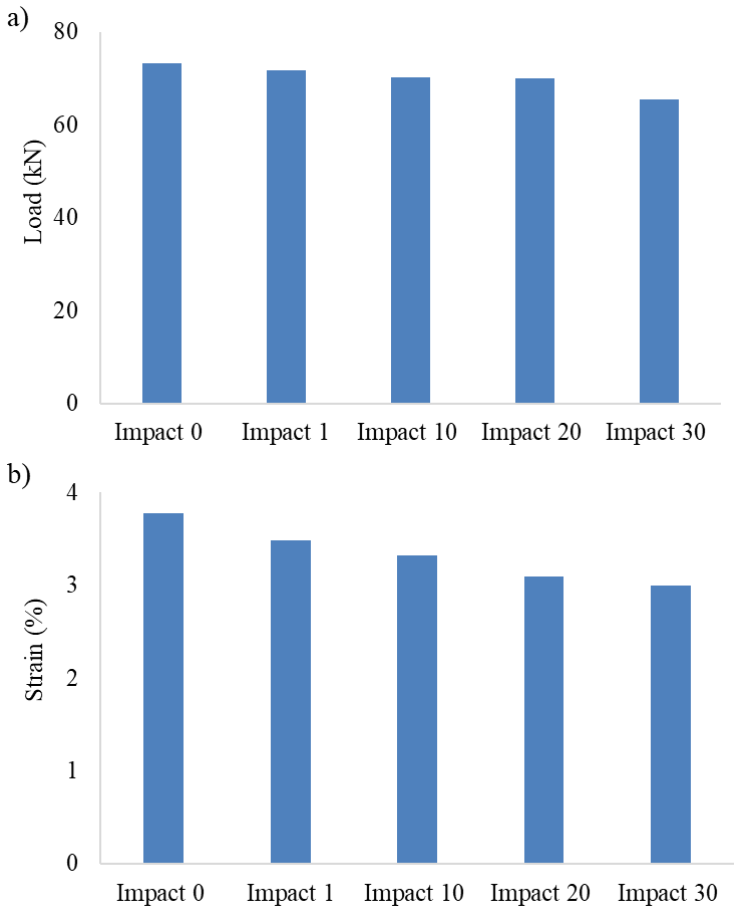

Figure 5.17. a) Peak load and b) % strain at peak load of high-density specimens tested in the weft direction after being impacted at 9 J

Tensile after impact was also conducted on specimens which had been impacted at 18 J impact energy. With this specimen, there is a larger decrease in the peak load of the specimens as the impact number increases, Figure 5.18a. Stress-strain curves for these specimens can be found in Appendix H. There was strength loss of almost 30%, 3 times higher than specimens impacted at 9 J, over the 30 impacts range. The strain at peak load, Figure 5.18b, also shows a similar trend and a sharper decrease than the specimens test at 9 J.

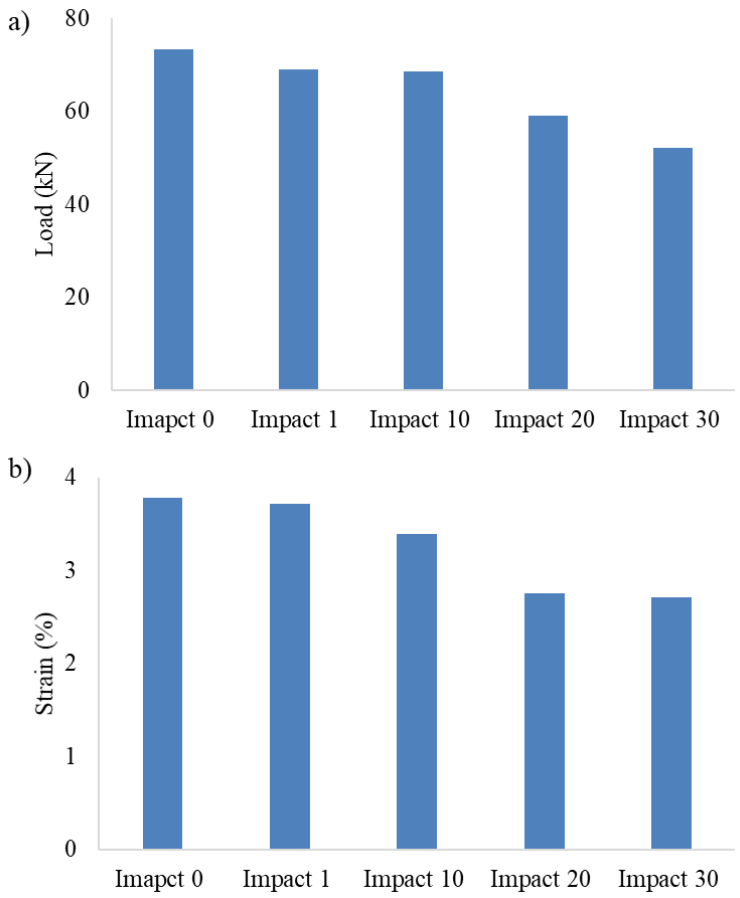

Figure 5.18. a) Peak load and b) % strain at peak load of high-density specimens tested in the weft direction after being impacted at 18 J

Specimens were also tested in the warp direction for 9 J impact energy. The specimens are not as strong in the warp direction. The peak load for specimens which had not been impacted, measured in the weft direction was on average 73 kN, while the peak load for the specimens which had not been impacted measured in the warp direction was 45 kN. This is due to the structure of the preform, which leads to more yarns in the weft direction to contribute to the strength. The specimens react similarly as when tested in the weft direction with an overall downward trend in both peak load, Figure 5.19a, and strain at peak load, Figure 5.19b, from 0 to 30 impacts. Stress-strain curves for these specimens can be found in Appendix H. Interestingly, the damage does not seem to affect the strength of the composite until 20 impacts. At 10 impacts there is a reduction of only 1% in strength compared to the undamaged specimen, which at 20 impacts there is a reduction of almost 30%.

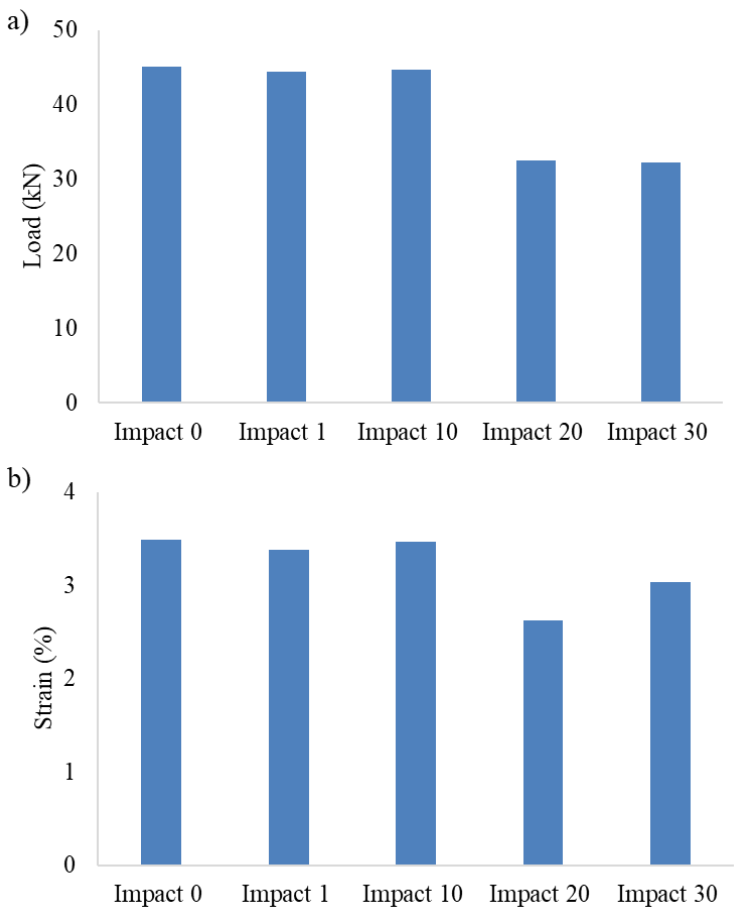

Figure 5.19. a) Peak load and b) % strain at peak load of high-density specimens tested in the warp direction after being impacted at 9 J

In the tensile after impact tests, the damaged area was often as large as or larger than the width of the test specimen. Therefore, these tests may be less accurate than the compression after impact tests in the next section at predicting residual strength. Also, the specimens used for the tensile tests were manufactured using the same parameters as OTDR, but there may be inherent differences which cause the variability. The small sample size also does not help to draw strong conclusions about the data. Ideally, the repetition of these samples would produce more conclusive results. Regardless, there are clear trends apparent in the data.

5.2.3. Compression test results- high density

The severity of the damage was determined by evaluating the residual compressive strength after exposure to the impact event. Compression after impact tests did not produce a good baseline

(impact 0) strength because they failed in an unacceptable manner. A combined loading compression test was therefore used to determine the baseline for composite specimens, Figure 5.20. Stress-strain curves for these specimens can be found in Appendix H. Compared to the compressive strength of 406 MPa determined by the CLC test, the specimens exhibit a loss of about 45% in strength after being impacted 10 times at 9 J, a loss of almost 50% in strength after being impacted 10 times at 18 J, and a loss of 55% in strength after being impacted 10 times at 27 J. Specimen size differs in the CLC (140 mm x 13 mm) and CAI (150 mm by 100 mm). This difference in width may account for part of the strength differences observed between these tests. There is, however, a clear downward trend in strength as the impact number increases from 0 to 30, Figure 5.21. The earliest impact events appear to have the most influence on the structural integrity of the composite structure, as the decrease in strength becomes less severe with an increase in the number of impacts. At 9 J impact energy, the decrease from impact 1 to impact 10 is 13%, while the decrease from impact 10 to impact 20 is only 0.6%. There also appears to be not much difference between 9 J and 18 J impact energy related to the residual compressive strength. The impact energy of 27 J, however, causes more damage to the composite, resulting in less compressive strength.

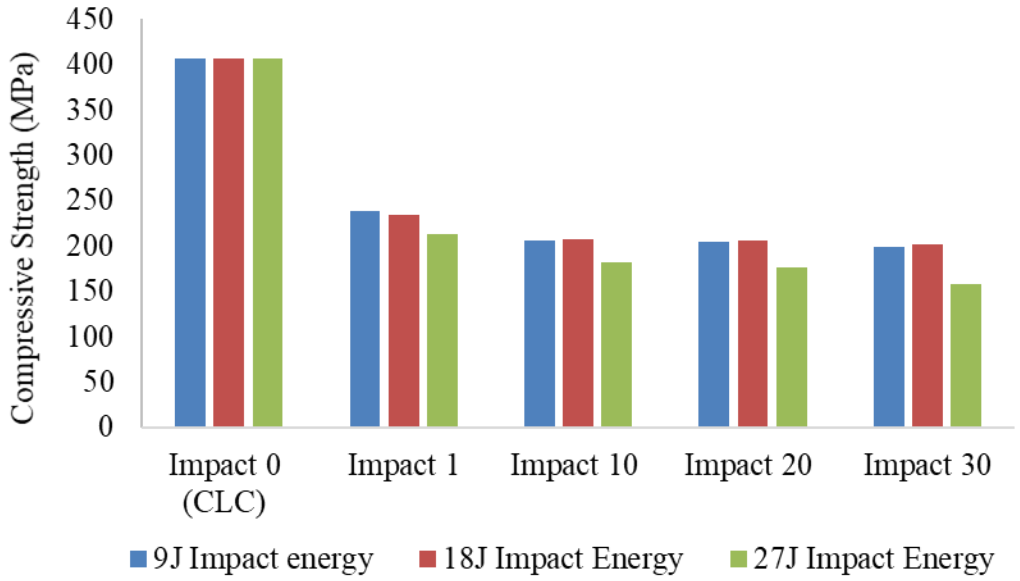

Figure 5.20. Residual compressive strength of high-density composite specimens using CLC test as a baseline

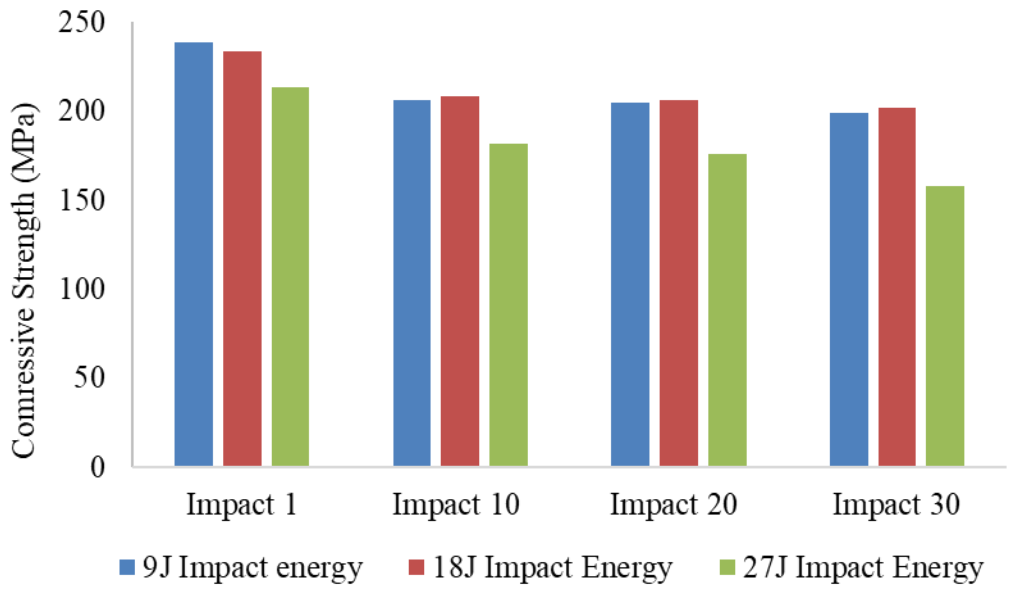

Figure 5.21. Residual compressive strength of high-density specimens

To understand how well the sensor relates to the severity of the damage, the percent loss of compressive strength in the composite was correlated with the percent loss observed in the POF signal for 9 J impact energy Figures 5.22 a, 18 J impact energy Figure 5.22b, and 27 J impact energy Figure 5.22c. There is not a point for 30 impacts on the graph for the POF embedded in the top layer, because the dynamic range in the POF signal reaches zero before 30 impacts are complete. The optical fibers in the top layer of the composite appear to be more sensitive to the small changes in compressive strength associated with a higher number of impacts. Given that there is such a large reduction in strength, almost 50% after the initial impacts at each energy level, a system that is more sensitive to damage may be more advantageous. Further testing, however, is needed to draw strong conclusions about the accuracy of the POF at predicting damage. The POF located in the top layer, approximately 2 mm from the surface, is the most sensitive to the damage event and correlates best with the strength loss observed. This is best position for damage testing, for other test parameters such as temperature or vibration monitoring however, the bottom layer may be the best location for the optical fiber so that it is best protected from environmental elements.

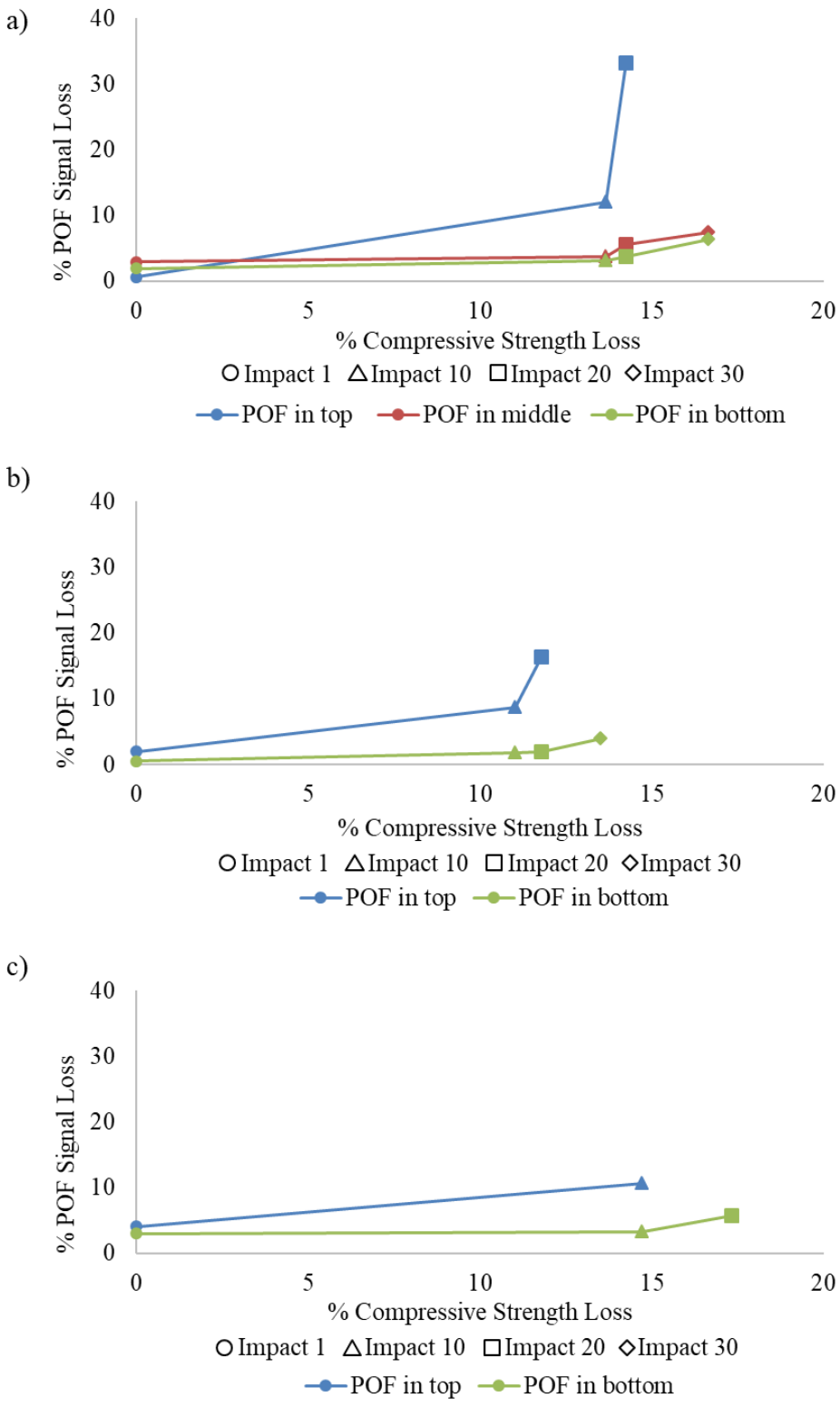

Figure 5.22. Percent loss observed in the POF signal as a function of the percent loss of compressive strength in the composite for impact energy a) 9 J b) 18 J c) 27 J

5.3. Comparison of pick density

Sample groups I and II were compared to determine the relationship between pick density of the composite and POF sensor sensitivity. In both groups, the POF is placed in the middle layer. Group I specimens were woven with a low pick density of 1.57 picks/cm and group II specimens were woven with a high pick density of 4.72 picks/cm. An analysis of high pick density specimens was covered in section 5.2. For impact testing of low-density specimens, energy levels of 9 J and 18 J were used.

5.3.1. POF signal results

This section investigates the effect of composite pick density on POF's ability to sense damage by comparing POF spectra after a damage event in Groups I and II. Figure 5.23 shows how damage progresses in a low pick density specimen after being impacted at 9 J impact energy. The impact damage area grew from an area of 1.97 cm^2 after 1 impact to an area of 3.82 cm^2 after 30 impacts, this is an increase in damage size of 94%. The impact damage area for each impact is listed in Table 5.5. A specimen in group I, impacted at 9 J shows a drop in attenuation of about 4 dB over 20 impacts, Figure 5.24. There is a large reflected signal at around 2.7 m in the spectra, just before the measured impact location, that indicates damage to the POF or bending of the POF. This drop first appears at impact 15 and continues to decrease at 20 impacts, where the dynamic range becomes 0 dB. A specimen with the POF in the middle location, but woven at a high pick density (group II), Figure 5.7, experienced a greater attenuation drop of 10 dB over 20 impacts, but the sharp drop in the signal does not appear, and the dynamic range at 20 impacts is still about 4 dB. The tighter weave structure appears to protect the POF so that it senses the damage but is not damaged itself.

Figure 5.23. Progression of impact damage at 9 J on a specimen with pick density 1.57 picks/cm

Table 5.5. Impact damage area (impact energy: 9 J, pick density: 1.57 picks/cm)

Impact number	Damage area (cm^2)
1	1.97
5	2.68
10	3.17
15	3.82

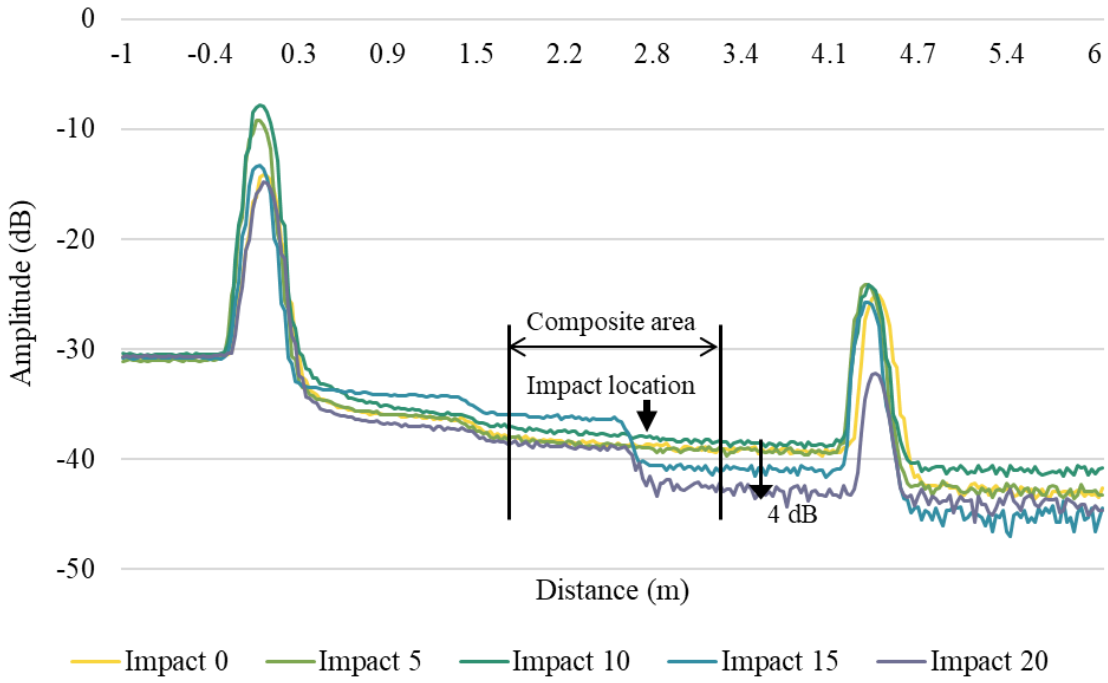

Figure 5.24. Signal of POF embedded in the middle layer of the 1.57 picks/cm preform and impacted at a 9 J energy level

Figure 5.25 shows the results of a specimen in group I, impacted repeatedly at 18 J for which the POF appears to become damaged after impact 1. After impact 1, a signal peak near the damage

location appears and the attenuation drops 5.5 dB, at which point the dynamic range becomes 0 dB. Although the sensor identifies the damage to the composite, it cannot be determined at this time if the POF is also damaged itself.

A specimen impacted at 18 J energy level, but 1 cm away from the POF, show in Figure 5.26 displayed no sensitivity to the damage event at all. Even after 15 impacts, at which time the composite was completely penetrated, the spectra showed no decrease in attenuation. In the higher density composites, the POF in the top layer was sensitive to the damage even at 1 cm away. Lower pick density composites were only made with the POF in the middle layer. The inability to sense damage at 1 cm away may be related to the sensor being in the middle layer rather than the top layer.

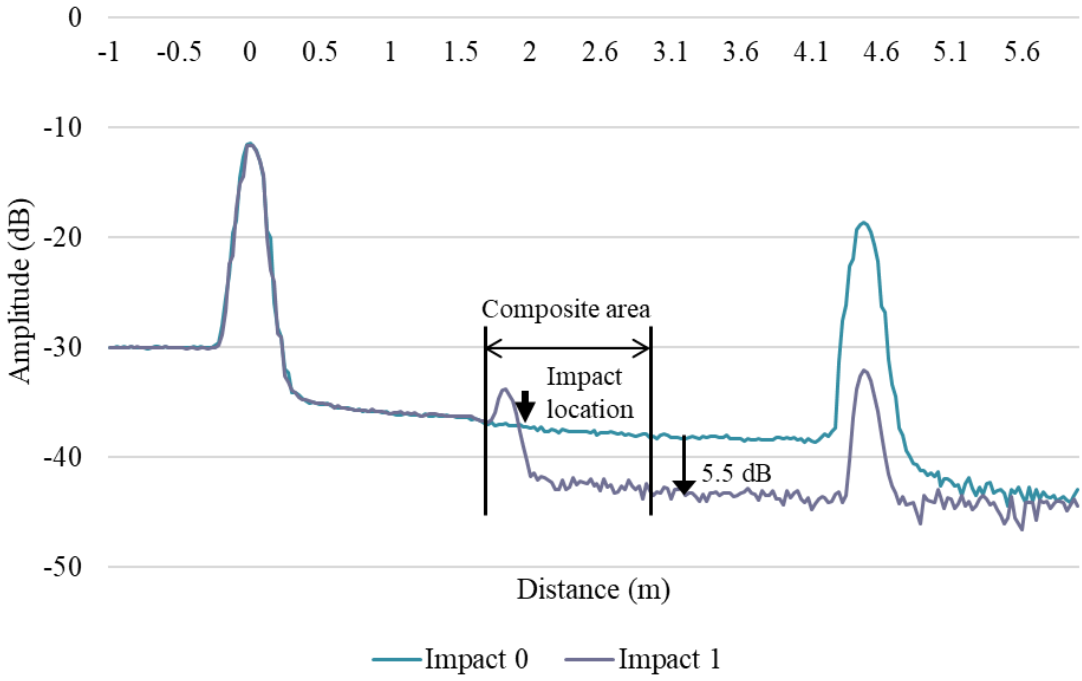

Figure 5.25. Signal of POF embedded in the middle layer of the 1.57 picks/cm preform and impacted at 18 J energy level

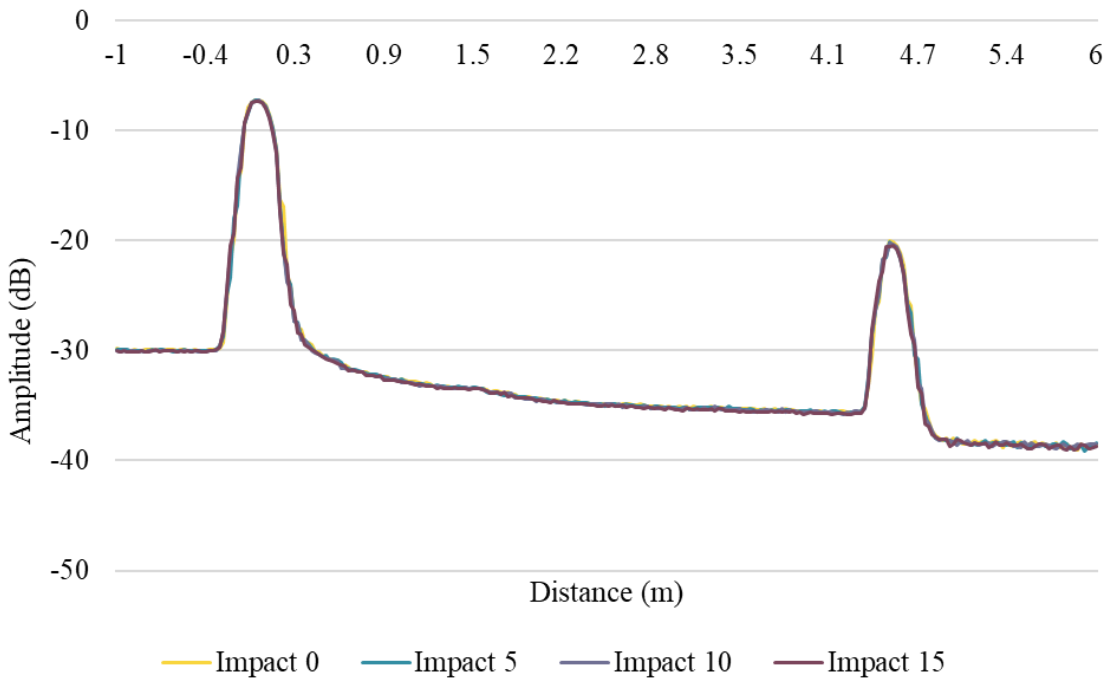

Figure 5.26. Signal of POF embedded in the middle layer of the 1.57 picks/cm preform and impacted at an 18 J energy level, impacted 1 cm from POF location

5.3.2. Tensile test results- low density

A tensile test was conducted in the weft direction of low pick density specimens after samples had been impacted at an energy level of 9 J. The results for peak load, Figure 5.27a and strain at peak load, Figure 5.27b show that there was only a 5% reduction in strength and in strain from 1 to 10 impacts, but a 30% reduction in strength and in strain from 1 to 20 impacts. Stress-strain curves for these specimens can be found in Appendix H.

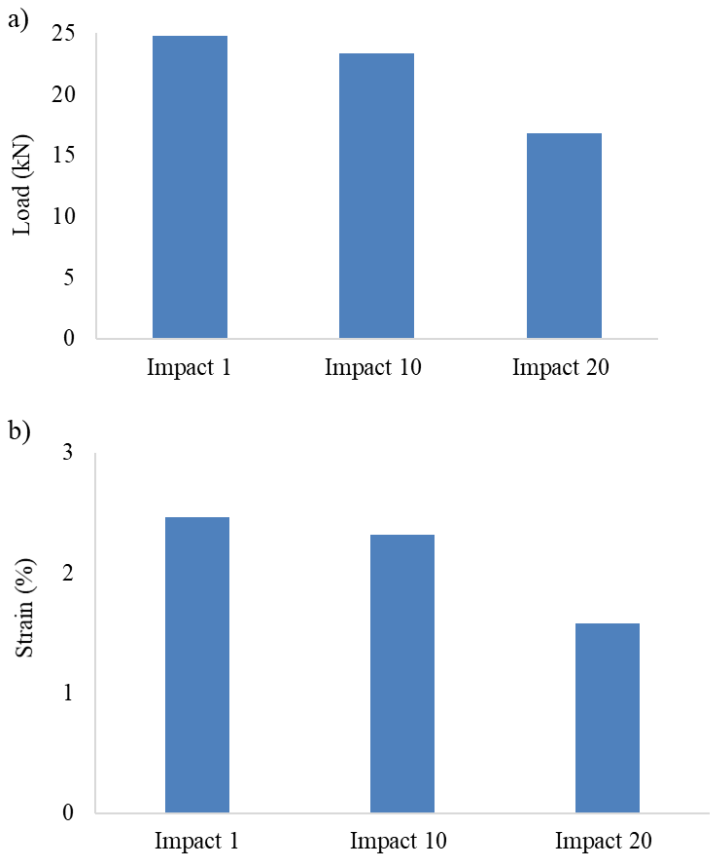

Figure 5.27. a) Peak load and b) % strain at break of low-density specimens tested in the weft direction after being impacted at 9 J

5.3.3. Compression test results- low density

The severity of the damage for the low pick density composites was also determined by evaluating the residual compressive strength after exposure to an impact event. Residual compressive strength for 9 J and 18 J impact energy of the low-density and of the high-density composites for impact 1, 10, 20, and 30 are compared in Figure 5.28. Stress-strain curves for these specimens can be found in Appendix H. Low-density specimens impacted at 18 J do not have data for 20 and 30 impacts, because the composite was completely penetrated around 15 impacts. Compared to the compressive strength determined by the CLC test to be 246 MPa, the low-density specimens exhibit a loss of about 40% in strength after being impacted 10 times at 9 J and 55% in strength after being impacted 10 times at 18 J.

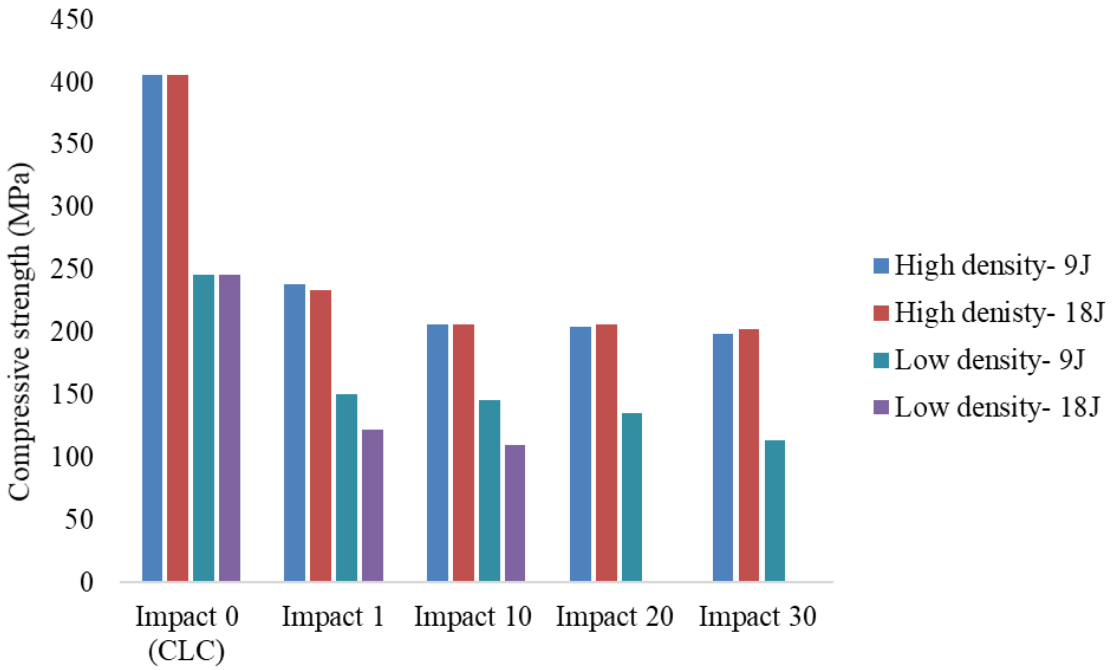

Figure 5.28. Residual compressive strength comparison between low-density and high-density specimens after 9 J and 18 J impact, where a CLC test is used as a baseline

To understand how well the sensor relates to the severity of the damage, the percent loss of compressive strength in the low-density composite was correlated with the percent loss observed in the POF signal for 9 J impact energy, Figure 5.29. This is compared with data from group II. The optical fiber in the low-density specimen is more sensitive to the changes in compressive strength associated with a higher number of impacts. This is probably because the POF is less protected in this type of structure.

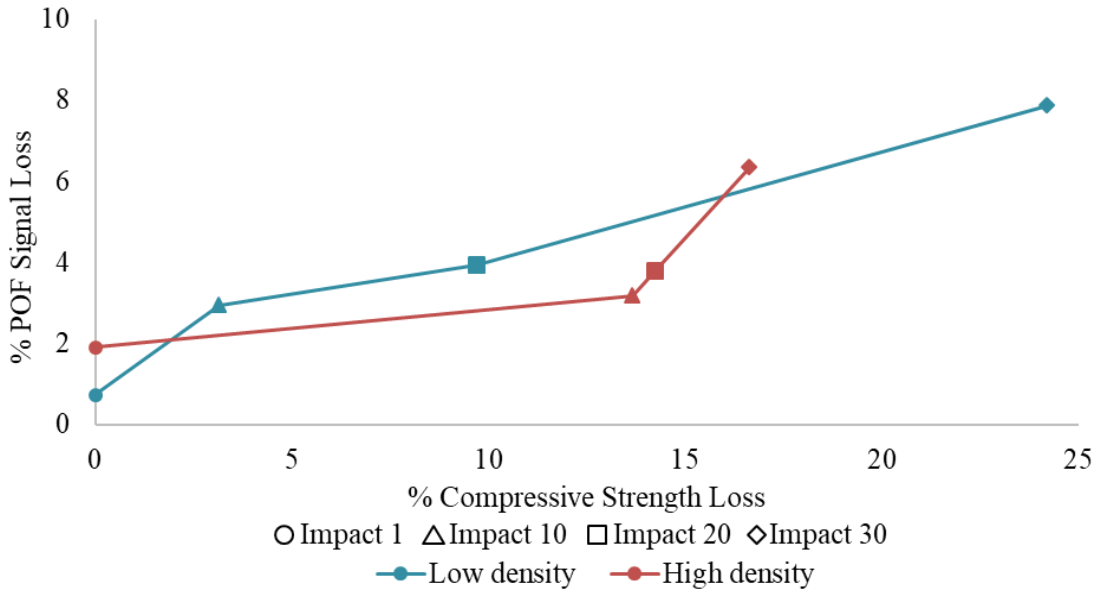

Figure 5.29. Percent loss observed in the POF signal as a function of the percent loss of compressive strength in the low-density specimen for 9 J impact energy

5.4. Conclusions

5.4.1. Summary of results

Due to the destructive nature of the testing and the fragility of the POF, all tests were conducted on individual specimens, which have inherent variation from one sample to another. This variation and the small sample size that resulted from the low success rate of the POF signal retention made it challenging to draw strong conclusions about the data. Slight changes in the connection of optical fiber to the OTDR also produced shifts in the signal obtained which resulted in some of the analysis being more qualitative (visually comparing aspects of the spectra) instead of quantitative. Nevertheless, there are clear trends in the data. The POF embedded in the composite is sensitive to impact damage. The POF in the top layer is the most sensitive in its reaction to the damage event, but does not provide a strong correlation with the damage experienced by the composite. In the top layer, the POF fails after 5 impacts at a higher impact energy (27 J), but the composite does not show this type of failure. The POF located in the middle and bottom layers exhibit a better correlation with composite damage. The POF in the middle layer was only tested at 9 J impact energy. At this low impact energy, it does show some changes in the signal, but not as drastic a decrease in attenuation as the POF in the top layer. The

POF in the bottom layer is the least sensitive, but it does show a sensitivity after many impacts and at higher impact energies. The POF in the bottom layer is also protected from higher impact energies and survived 3 times as many impacts as the POF in the top layer. The POF in the low-density composite is sensitive to the damage event, but is also easily damaged in the composite. The compressive and tensile tests both show an overall reduction in strength from impact 1 to impact 30 for all samples, however, the reduction in strength is minimal for low impact energies leading to the conclusion the most sensitive sensor may be the best in practice. More accurate placement of the impact location, improvement to the optical fiber/ OTDR connection, and testing of multiple optical fibers under the same conditions would produce more consistent results.

5.4.2. Design of SHM system

A relationship between the sensor's location, composite damage, and the resulting POF signal was used to determine the best location for optical fiber sensors to be placed within the composite so that they can predict structural damage. It was determined that the location of the POF must be close, within 1 cm, to the damage event in order to sense it. The POF positioned in the middle and bottom layers correlated the best with the composite damage caused by repeated impact. Figures 5.30 and 5.31 are examples of how an SHM system might be designed using these parameters. Figure 5.30 demonstrates an SHM system with multiple POF sensors spaced 1 cm apart. In practice, it is better to have multiple sensors so that if one becomes damaged, the others would be able to continue sensing. This type of design also minimizes bending, which can cause added defects in optical fibers. The downside, however, is that each optical fiber would require its own OTDR for sensing which would be costly. Figure 5.31 demonstrates an SHM system with 2 POF sensors which are woven so that they are only 1 cm apart from each other. They are woven such that one fiber is not bent past the critical bending radius. In this system, the required number of optical fiber sensors is less than the previous system, thus the number of required OTDRs and the cost will also be less.

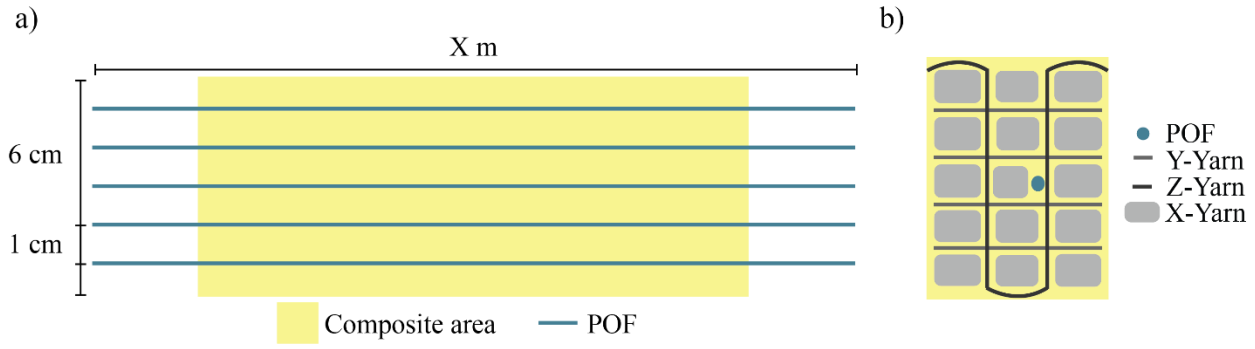

Figure 5.30. Example of SHM system design with a) multiple POF sensors embedded in straight paths b) POF located in the middle layer of the 3DOW composite

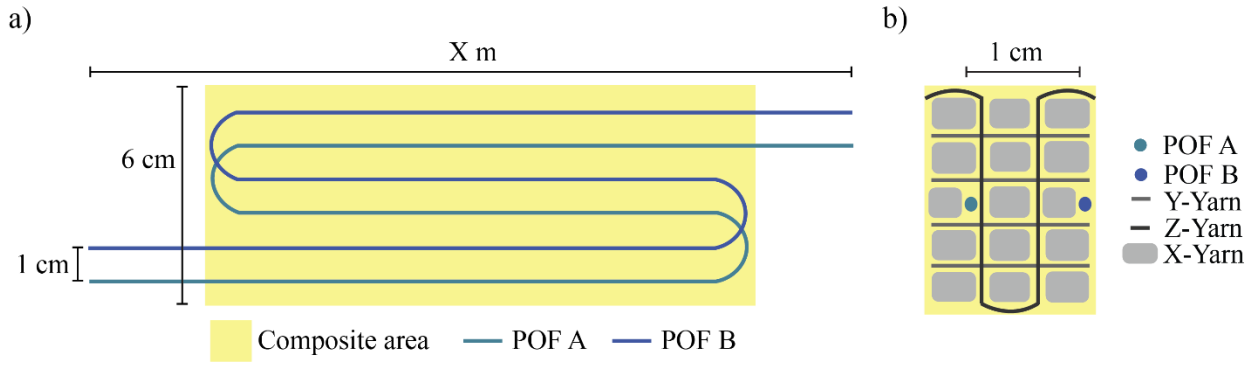

Figure 5.31. Example of SHM system design with a) 2 POF sensors weaving through the structure to accommodate the critical bending radius b) POF located in the middle layer of the 3DOW composite

Chapter 6: Technological Analysis

6.1. Introduction

6.1.1. Overview of the optical fiber market

Optical fiber sensors, specifically POF, are an area where technology has been slow to adapt in favor of more traditional approaches. As mentioned in the literature review there are several key emerging applications for which OF sensors may be beneficial. Lopez-Higuera et al. touches on the topic and points out that the key emerging application markets for distributed optical fiber sensors are wells, security, smart structures, and seismic detection [75]. Liehr et al. predict that the biggest market for POF strain sensors is expected to be the monitoring of civil engineering structures and earth works [20]. A study conducted by BBC research on the global market for optical fiber sensors concluded that the key application areas are telecommunication, oil and gas exploration and drilling, medical, and industrial market [124]. The applications mentioned in these optical fiber studies are very diverse and not necessarily specific to SHM, and therefore include industries such as medical which is a large industry for optical fibers but has little application regarding SHM. There are several SHM markets, however, that overlap with the key applications mentioned by the marketing studies. Within SHM there are also other large industries where optical fiber technology is applicable that may not have quite as large an impact on the comprehensive global market such as with the aerospace industry and wind turbines. In order to get a feel for the fiber optical market with respect to SHM applications, a deeper look into the industry is needed.

Although OF sensors have many application areas there are significant technical hurdles and market barriers that may hinder their implementation. One hurdle is that potential customers come from a wide range of industry and technical backgrounds, so there is a lack of understanding about the operation and benefits of using optical fiber sensors. Another hurdle, as mentioned in the literature review, is that optical fibers are fragile, and this can pose a problem for their widespread use and reliability. There is also the requirement of acquisition systems, software, and data processing algorithms that may hinder the market [125]. Regardless, the market of optical fibers is expected to grow. A summary of two marketing studies of OF was explored in order to gain better insight into this market. Markets and Markets conducted a study

in 2017 which forecasted the market through 2021 [126]. This study provided a definition of the market by cable type (single mode, multi-mode), optical fiber type (glass and plastics), and application (telecom, premises, utility, CATV, military, industrial, sensors, lighting, and metropolitan). Grand View Research Inc., conducted a study in 2017 which projected the market until 2025 [127]. In this study, the market is divided by type (single mode, multimode, and plastic optical fiber) and by application (telecom, oil and gas, military, aerospace, BFSI, medical, railway, and others). The fact that polymeric optical fibers are included as a subcategory in these reports shows the important role that they are beginning to play in the industry. Even though they still fall second to GOF, the POF segment is anticipated to experience the highest growth over the forecast period, especially as they become more cost effective [126].

Both studies suggest that the global optical fiber market will witness substantial growth over the forecasted period and the Asia-Pacific market is estimated to be the largest OF market. The market in North America is also expected to experience growth due to the growing premises and industrial application. It is also mentioned that optical fiber based sensors will gain importance in North America with recent discoveries of shale gas, which would drive the market in sensors application [126]. Many of the key players are based in North America and include Corning Inc., AFL Global, Finisar, Optical Cable Corporation, and OFS Fitel, LLC [126, 127]. Other key players mentioned are Prysmian Group (Italy) and Sterlite Technologies Limited (India) [126, 127]. Several new products that offer enhanced characteristics are being launched by manufacturers which are expected to drive the market. AFL Global and Corning Inc. have launched various products that were designed to withstand high tensile load, extreme temperatures, and repeated impacts [124].

6.1.2. Introduction to quantitative text analysis

One way to obtain a quick overview of a large amount of data is by a technique called quantitative text analysis. Text mining is one of the most popular forms of quantitative text analysis and is a knowledge-based process that uses analytical tools to derive meaningful information from a natural language text [128, 129]. It originated in social sciences as a form of content analysis and due to advances in natural language processing, text mining methods and tools have become increasingly available in several different research fields, including the hard

sciences [129]. The overarching goal is to turn text into data for analysis via analytical methods. It involves subjecting the chosen text to a series of actions which breaks the large body of information into smaller data pieces in order to add a layer of meaning to raw context. Researchers in academia have made significant progress in the area of applying text mining for keyword extraction and pattern recognition from unstructured data to reveal new ideas. By incorporating text mining approaches, researchers can organize large sets of text data and quickly identify associations, determine ideas communicated through text, and determine patterns. The analysis of articles, reports, patents, and academic literature to identify trends is useful in determining the market for OF because it can quickly illuminate the industries where OF technology is currently most relevant. Tech analysis also utilizes the large volumes of digital information available for OF to recognize possible development trends. This helps to determine what needs are currently being met in relation to SHM and holes where further products could penetrate.

Common techniques for quantitative text analysis can be classified into text mining and visualization techniques. Text mining involves natural language process-based approaches, semantic analysis, rules-based approaches, property function-based approaches, and neural network-based approaches. Visualization techniques involve a visual output such as patent networks, patent maps, and data clusters that emerge as a consequence of applying a particular algorithm [130]. When text mining techniques are applied to technical documents it is often referred to as technology or tech mining, and for patent analysis, it is named patent mining [129]. Text mining methods and tools have become increasing available in technology management where scholars try to extract useful information and textual patterns from technical documents. Porter is one of the pioneers in technology mining (TM) and defines it as the application of text mining tools to science and technology information, informed by an understanding of technological innovation processes [128].

Tech mining offers a critical competitive advantage to a wide range of institutions since a researcher can quickly identify key themes and trends in a large body of text [128]. Most TM outputs can be reduced to fours items; lists, breakouts from lists, maps, and trends [128]. Lists consist of simple activity counts that tell you how much of something is taking place. Breakouts

from lists can tell you about what each of the leaders in a field is doing. Two lists can be combined to make a matrix or a depiction. A map shows relationships among a chosen type of data. Trends show what is most popular among the dataset. Corpus analysis is a form of text analysis which allows the user to make comparison between objects at a large scale.

6.2. Objective

As shown in the literature review OF sensors are an established technology, but it does not yet have widespread industrial use. There are many potential applications of optical fibers sensors and these applications must be investigated to determine where OF trends are occurring to anticipate the future market. The purpose of this analysis is to determine applications where OF sensor technology will prove beneficial and to determine characteristics of the OF sensor needed for each application. This study looks at the current trends in optical fiber sensor technology, including applications, materials, and sensor type. Although this analysis is not a full tech mining approach or tech analysis, many of the techniques presented will be used to identify trends in the data.

6.3. Method

6.3.1. Search strategy

During a tech analysis, it is important to ensure that the text you analysis will yield the most complete coverage as possible. In order to meet the objectives of this study, specific technical information in digital format was needed for processing, analyzing, and interpreting. Information retrieval via database search engines was chosen to obtain the raw text data. Although online information searching has become a prevalent activity in daily life, not all online search results are relevant and useful to the topic of interest. For an effective database search, Porter and Cunningham suggest that a search strategy should be implemented which is aligned with the search purpose and with the available resources [128]. Science and technology literature searches are typically conducted via a keyword/term search [128]. The same approach can be applied to companies and business data retrieval. Thus, search queries containing keywords/terms can be formulated to retrieve information from the chosen database to ensure the search result quality in this study. In the present study, the focus was not on the search algorithms, but on how to come

up with an appropriate search strategy to collect relevant information to solve the research questions as effectively as possible.

The search strategy for this study was as follows:

1. Identification of the keywords
2. Identification the time span
3. Selection of the database

The keywords chosen for this search were optic* fiber sensor. The use of optic* covers all endings of the word such as optic, optical, optics, etc. This phrase was used to search in the all subjects and indexing category to make sure that optical fiber sensors was the subject of the articles retrieved. The last 5 years (2014-2019) were chosen for the timespan of the search to obtain only the most recent information.

In this study, database analysis was used to identify current trends in the market. Porter and Cunningham suggest that when choosing a database for data collection, characteristics of the database should be considered, such as suitable coverage, comprehensiveness of coverage, biases, content quality, record structure, and keyword availability. Science and technology (S&T) publications, patents, and trade journals are the primary and most accessible sources of technology information. Several databases available through NC State University are shown in Figure 6.1, listed in order of the stage of technological development that is most common within the database.

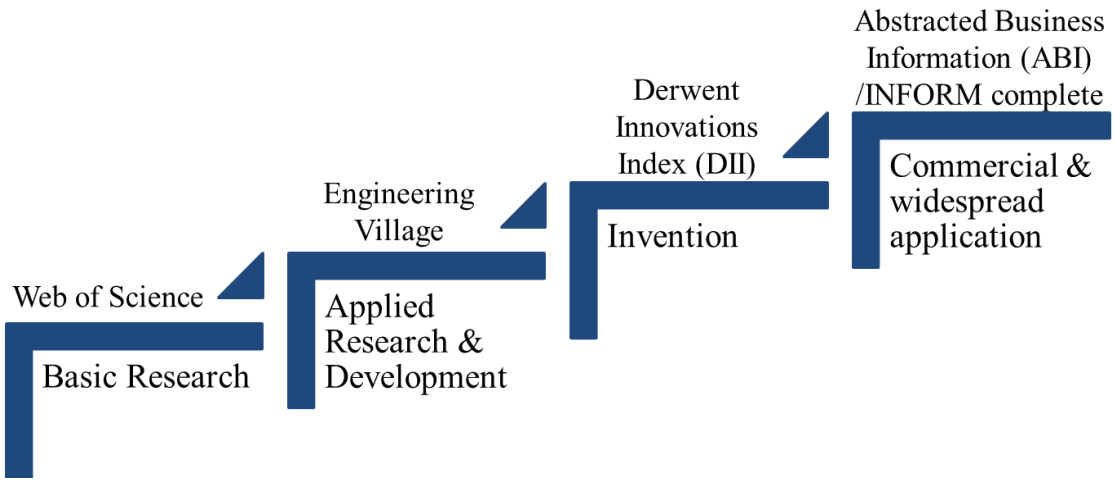

Figure 6.1. Demonstrates which databases correspond to the stage of technological development

Web of Science is a database which includes multidisciplinary coverage of over 10,000 high impact journals as well as international proceedings coverage for over 120,000 conferences. This database is good for providing information on fundamental or basic research.

Engineering focused databases Ei compendex and Inspec are part of Engineering Village, which is an engineering literature and patents database with largescale breadth and depth of content. Engineering Village contains various sources including news articles, trade journals, S&T journals, conference proceedings, government reports, patents, and other engineering information. This database is good for examining the applied science research areas.

The Derwent Innovation Index (DII) is a database with a comprehensive and international overview of patent information worldwide. The resource provides access to more than 14,800,000 patents and is linked to cited and citing patents, cited articles, and full-text patent data sources. The titles and content of the patents are rewritten to make it easier for the audience to understand. This feature provides more complete search results than using only classification codes. This database can be useful for understanding which patents are being used to create products, what companies are producing the most related patents, etc.

Abstracted Business information (ABI)/ INFORM has a wide collection of companies and business-related data globally, such as business and economics periodicals, country-and industry-

focused reports, full-text scholarly and trade journals articles, dissertations, market reports, and industry reports. This database is useful for determining who the key players are in the commercial development of the technology.

Due to the time limit in this analysis, Abstracted Business information/ INFORM complete was chosen to provide an overview of the current optic fiber technology and market. Given more time, this database could be used in conjunction with DII to gain a larger representation of the market.

6.3.2. Text reading and analysis

Once the keyword search in the ABI/ INFROM database was complete for each year, PDF format files of the relevant information was downloaded. Duplicate articles resulting from the search were removed before the text was download. The files were then uploaded in a web-based text reading and analysis environment called Voyant Tools [131]. Voyant Tools is an open source scholarly project that is designed to facilitate reading and interpretive practices for digital humanities students and scholars as well as for the general public. It was chosen for its ease of use and accessibility. Voyant Tools provides a number of visualization tools such as word clouds and trend graph which can be used to analyze data. Each corpus, or collection of texts, was divided by year so that trends could be established over time. A list of stop words was used to filter out common, but less relevant words. A standard list of stop words provided in Voyant Tools was used along with additional words related to the subject matter, listed in Appendix G. Lastly, the trends were analyzed.

Method for obtaining corpus data:

1. An advanced search in Proquest ABI/ INFORM collections database was preformed
    a. su(optic* fiber sensors)
    b. search selected time range (ex: January 2018-December 2018)
2. Duplicate articles were filtered out by identifying similar titles
3. The database was exported as a text only file
    a. Information exported: author, company/ organization, full-text, title, publication year, source type

6.3.3. Limitations to the search and analysis method

One limitation to this method is that the articles, patents, and records are only in English. The problem with this is that a portion of the SHM academic literature comes from Asia. Monitoring systems have been implemented on bridges in several countries including Europe, the United States, Canada, India, Japan, Korea, China [3, 72]. The Asia-Pacific market was also identified as the largest market for optical fiber sensors and the current use of optical fiber sensors is global. The chosen database has global coverage, but some key materials may have been missed since only English articles were downloaded. This could alter the results or skew them to show that English speaking countries have a higher contribution to OF technology and markets.

A limit to using the selected data analysis method is that PDF articles must be obtained manually, when reduces the size of data that is able to be obtained in a given time period. When trying the tease out a specific theme, the articles may be relevant, but not mention a specific theme or industry. Articles may also list multiple themes without specifics to the sensor requirements. Words found in an article may not necessarily relate to the theme or industry. A more in-depth analysis of the data, such as investigating the context of the words is needed in order to fully understand the meaning of this information. Another limitation is that since this analysis is being performed as part of a doctoral study, only one student conducted the analysis. A second analyzer may have another approach to retrieve and analyze the data and would therefore potentially obtain differing results.

6.4. Results and Discussion

During the keyword search, the ABI/ INFORM database provided information about the source from which the articles are obtained. Figure 6.2 shows the frequency of the various source types from the ABI/ INFORM database for each set of data downloaded by year. There is an overall increase in the number of total articles from 2014-2018. The search was conducted in May 2019, so articles from the year 2019 are only representative of the months January- April. It is expected that the total number of articles (January- December) for 2019 will also follow this trend and show an increase from 2018 to 2019. The highest increase observed, is in articles identified as wire feeds, which increased over 300% from 2014-2018. Wire feeds are a result of news

agencies creating news content and selling it to other organizations. An increase in this type of news content suggests that public interest in optical fiber sensors is becoming more frequent.

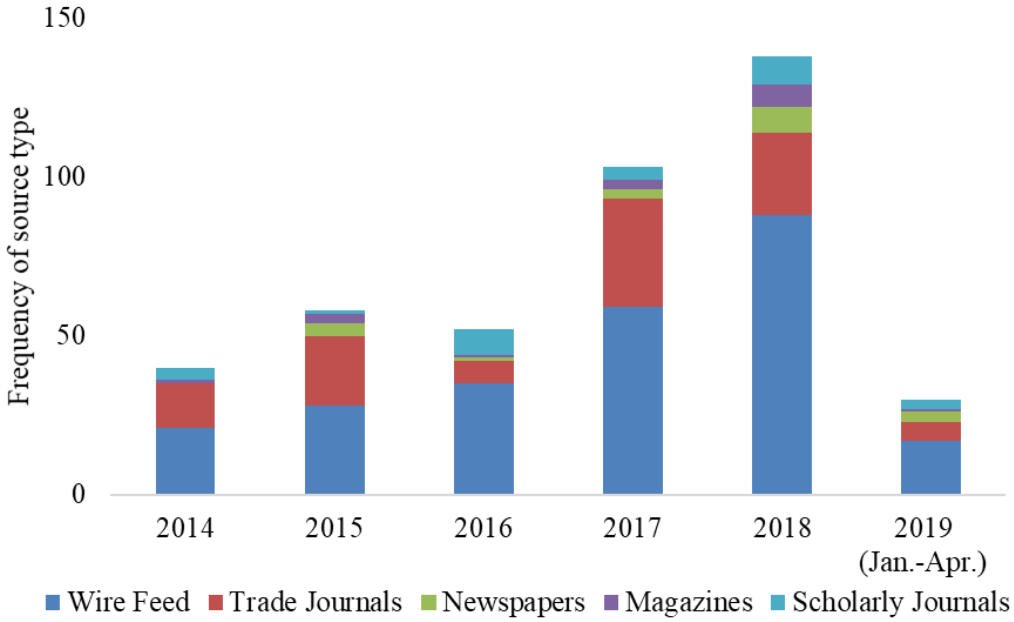

Figure 6.2. Frequency of source type per year for ABI/ INFORM database

A series of word frequencies were used to understand how common words in each corpus related to each other and to optical fiber sensors. One method of visualizing word frequencies is with a word cloud. In the word cloud, the terms which occur most frequently are sized the largest and positioned closer to the center. A word cloud of the most common terms before stop words had been removed is shown in Figure 6.3. Understandably words like fiber, optical, and sensor appear more frequently because they were the searched words. Other frequent words include patent and market, which indicates the text downloaded most likely contains several patents and market studies. These words may be the most common, but they did not provide a significant amount of information about the content of the document.

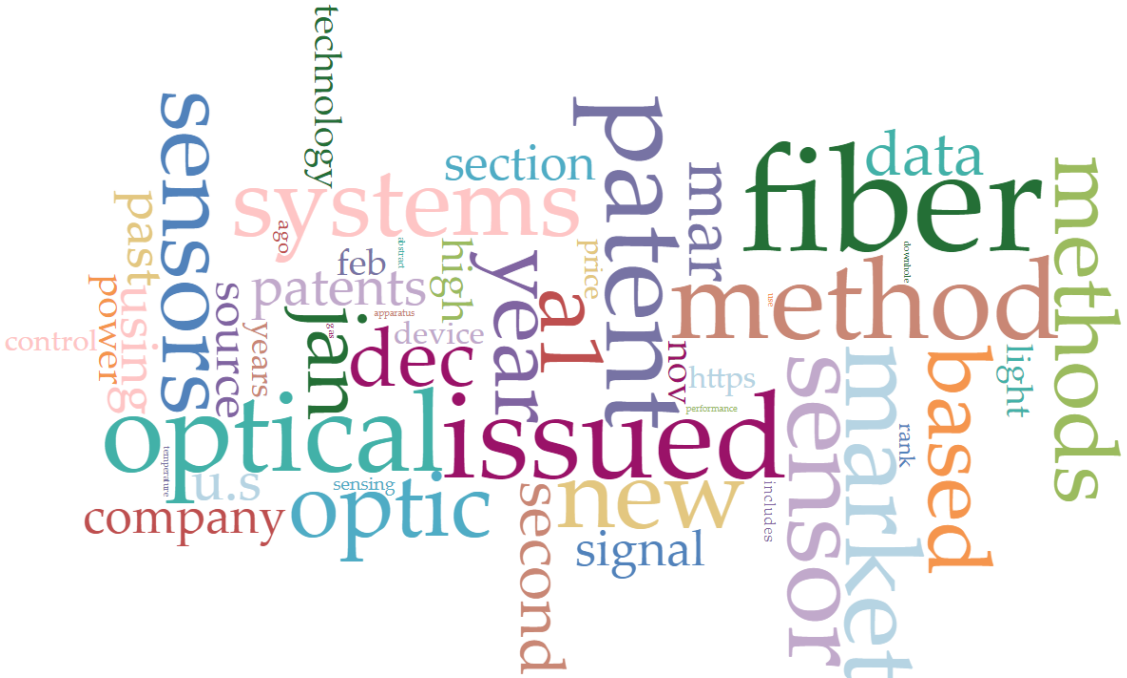

Figure 6.3. Word cloud of word frequencies before addition of stop words [131]

A list of stop words, provided in Appendix G, was added to refine the results and produce more meaningful data for analysis. The resulting word cloud is shown in Figure 6.4. This along with a list of the most common words found in the corpus was used to gain an idea of the themes present in the data. The 25 most common words and their frequency are listed in Table 6.1. There are several words that stick out related to parameters that optical fiber sensors may sense such as pressure, temperature, and fluid. Related to potential industries are the words gas, energy, turbine, electric, and drilling. Related to materials are the words glass, silica, and polymer. Word clouds are effective at quickly drawing attention to high frequency terms. They, however, have also been criticized as being reductive and misleading and are best used in conjunction with other more exploratory and nuanced tools. Since word clouds only provide single words, the meaning and context of the word may not be represented as intended. A word such as turbine for example can be related to wind, gas, engine, etc. This indicates that words of significance should be looked at more in depth using other text mining tools.

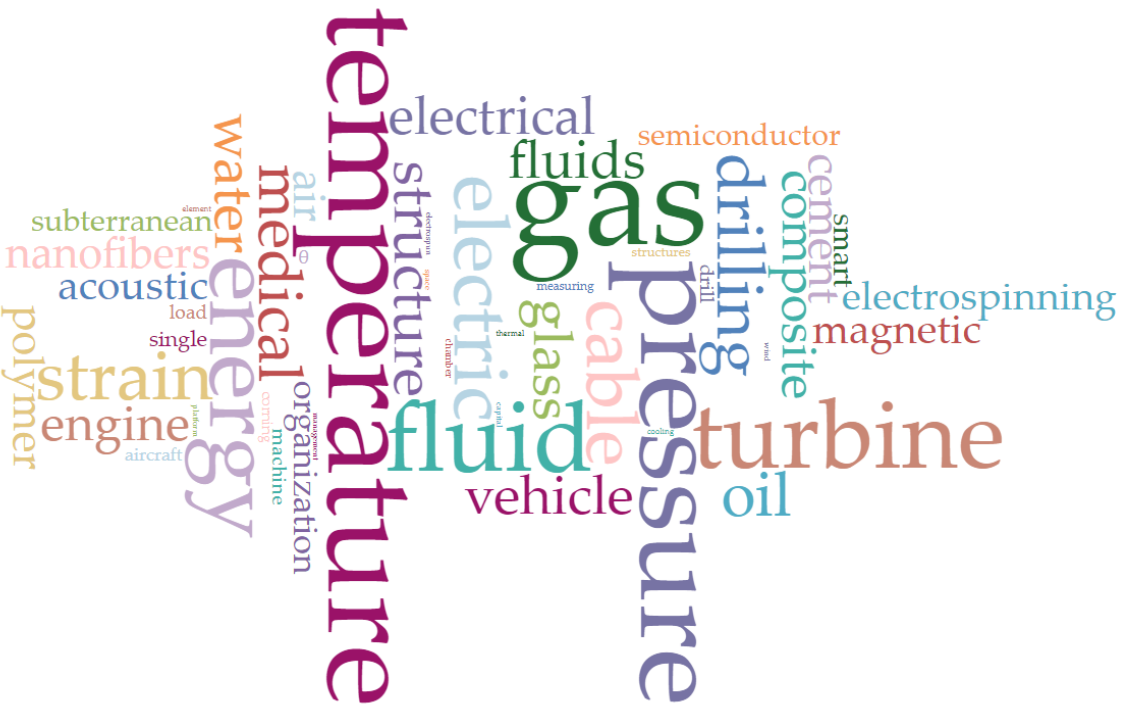

Figure 6.4. Word cloud of most frequently occurring words in the database [131]

Table 6.1. List of top 25 most frequent words

	Term	Count
1	gas	597
2	temperature	596
3	pressure	525
4	fluid	461
5	turbine	430
6	energy	379
7	european	340
8	electric	339
9	strain	308
10	drilling	304
11	cable	301
12	oil	284
13	structure	261
14	medical	258
15	fluids	247
16	electrical	242
17	glass	240
18	vehicle	240
19	water	240
20	engine	224
21	composite	223
22	air	220
23	cement	211
24	nanofibers	211
25	polymer	207

Collocates are terms which appear frequently in proximity to key words across the corpus. A collocate study was conducted on the corpus to discover words frequently found within a proximity of 5 words to the keyword market. The collocates tool within Voyant Tools provided a table view of the term (keyword being searched), the collocate (word found in proximity of the keyword), and the count (frequency of the collocate occurring in proximity to the keyword). Table 6.2 displays the results of this search. Words which are often associated with the word market, but which were not of interest for this search such as segmented, forecast, players, etc. were removed from the list. The words were then categorized, and color coated based on what type of market they represent industrial (green), testing parameter (blue), and location (red).

Table 6.2. Collocates with the word market

	Term	Collocate	Count (context)
1	Market	temperature	66
2	Market	photoelectric	47
3	Market	medical	26
4	Market	submarine	18
5	Market	america	18
6	Market	pressure	16
7	Market	oil	16
8	Market	semiconductor	13
9	Market	acoustic	13
10	Market	iot	12
11	Market	gas	12
12	Market	china	12
13	Market	europe	11
14	Market	japan	10
15	Market	asia	10

Word trends were used to look at how the frequency of the chosen word changed over the corpus, which in this case were all the articles downloaded for the given year (2014-2019). Each frequency is displayed as the number of times a word appears relative to the number of words for all articles within that year. Words were chosen from a list of the most commonly occurring words in the corpus and placed into themes to explore. This was also correlated with the words found using the collocates tool. A word trend graph is provided in Figure 6.5 to show the frequency of regional words (Asia, Europe, America) appearing in proximity to the keyword market found by the collocate tool. All of the three regions observed have the highest frequency in 2015 and decrease after this. The articles selected for 2015 may be more market focused than the ones for other years, causing this effect. From this graph, it is observed that Europe was mentioned more frequently in than American and Asia, until 2017, when it becomes the least frequently mentioned. In section 6.1.1 it was mentioned that the Asia-Pacific market is estimated to be the largest OF market and that the North American market is also expected to experience growth. These things may be correlated, but further investigation is needed to determine if this relationship is accurate.

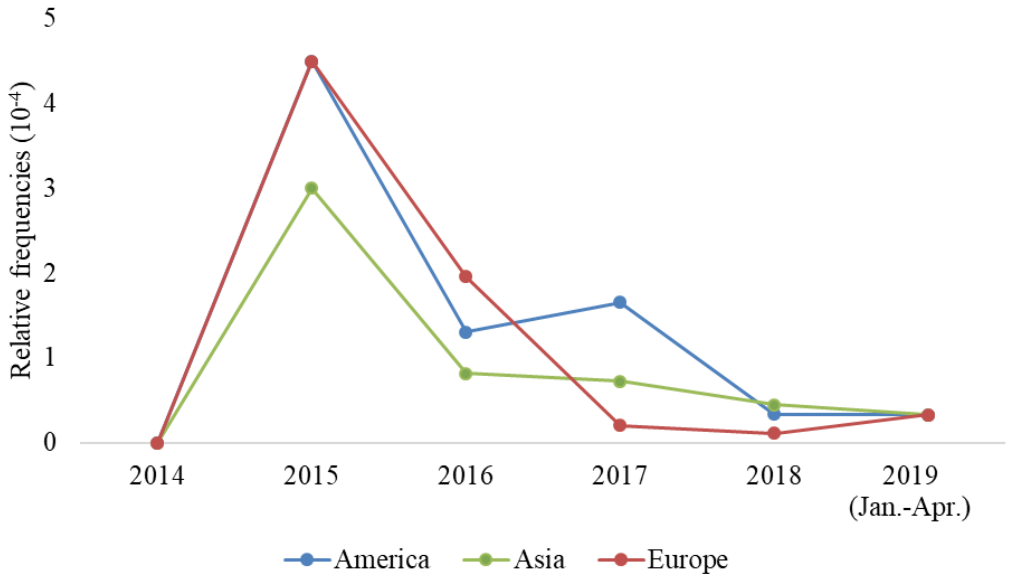

Figure 6.5. Word frequency of regions appearing within proximity to the keyword market

A collocates graph represents keywords and terms that occur in close proximity as a force directed network graph. The keyword is shown in blue and the collocates are shown in orange. This tool was used to identify words related to the keyword measure with the objective of identifying words associated with parameters that an optical fiber sensor may measure. Four words were identified as being related to the keyword, shown in Figure 6.6a. A word frequency graph was implemented, Figure 6.6b, to show the frequency of these three common sensing parameters. Strain is the most consistent over the timespan of the corpus, while temperature and pressure fluctuate.

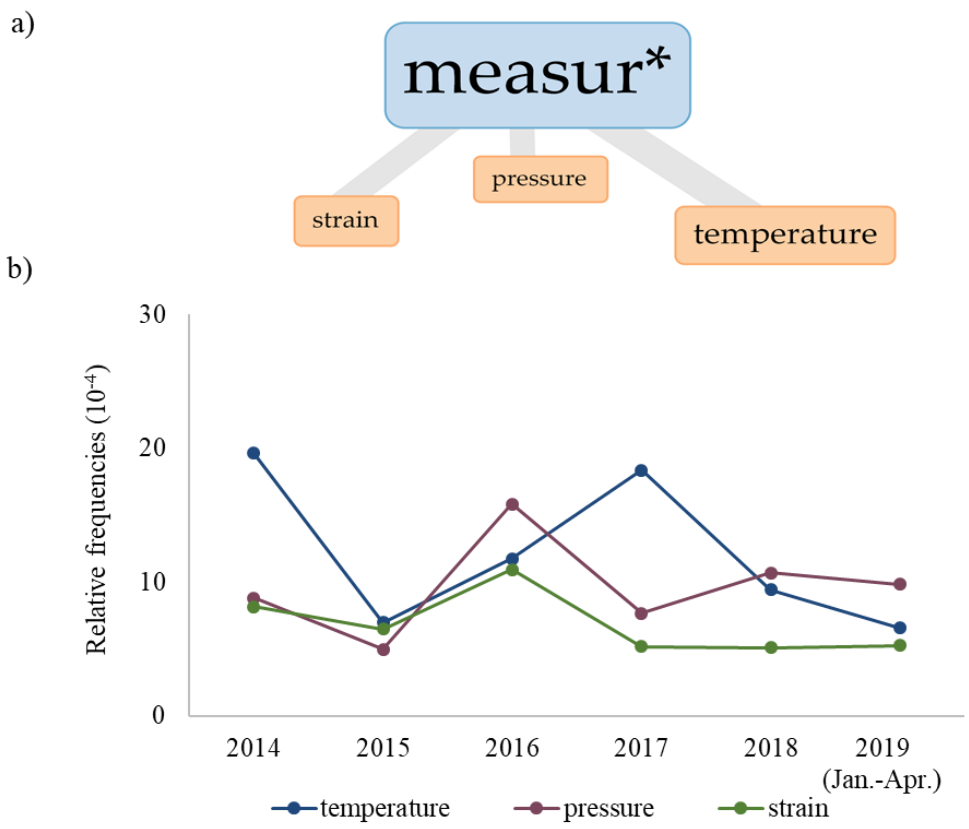

Figure 6.6. a) Words that appear in proximity to the keyword measure b) word frequency of these parameters [131]

To perceive the activity of optical fibers in industries, the collocates tool was used to determine words located in proximity to the keyword industry. Figure 6.7a show words that occur frequently with the word industry, and represent several of the industries where optical fiber sensors are advancing including medical, aerospace, and oil and gas. The word frequency of these industries was observed, shown in Figure 6.7b. The three industries show similar trends in word frequency, being the most frequent in 2015.

A quick context search of a word helps gain more meaning and obtain more information about the subject matter. Medical is an industry which stood out in this search. After conducting a quick context search, it was learned that optical fiber sensors are expected to lead innovation in the medical sector due to their lack of wires, non- conducting nature, and ability to be inserted into a human body. They are being used to implement miniature microscopy, measure intravascular blood pressure, conduct minimally invasive surgery, and as imaging rods to

determine presence of tumors [132]. There was also a recent breakthrough which allows the mapping of liquid outside the boundary of the glass optical fiber, allowing the one to probe the surroundings of the optical fiber, a function similar to ultrasonic imaging [133].

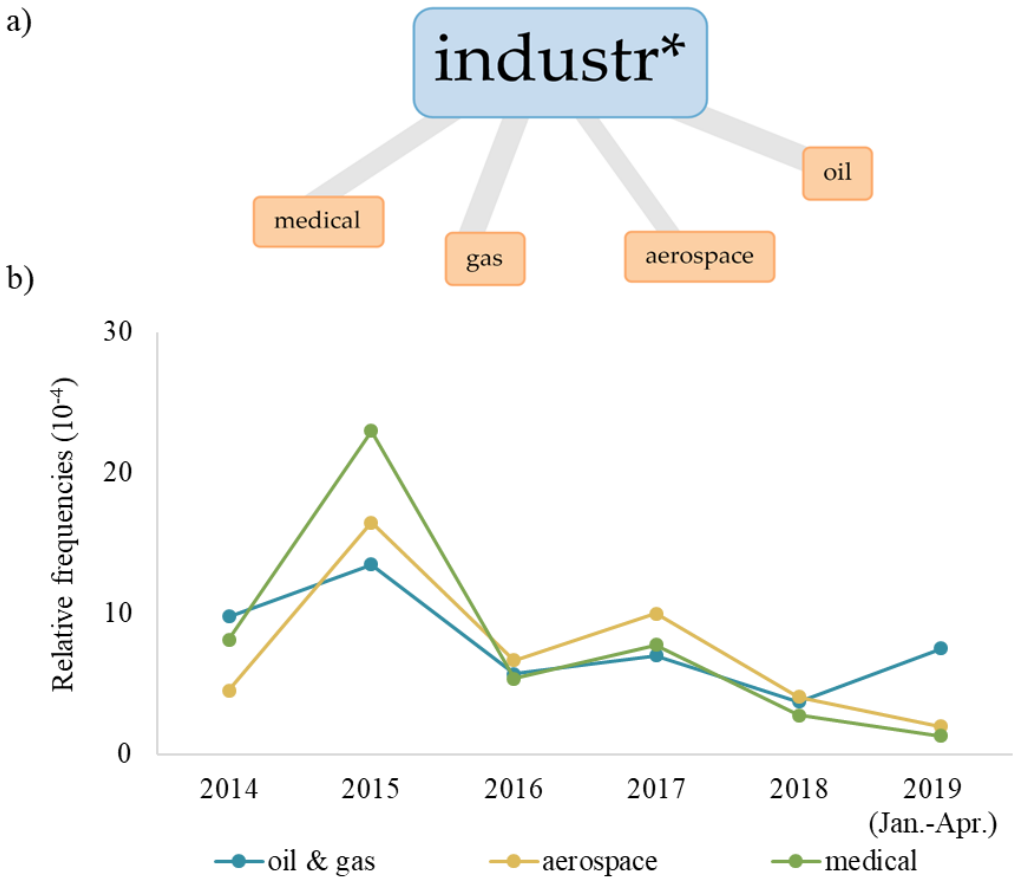

Figure 6.7. a) Words that appear in proximity to industry b) word frequency of end-use industry

Relative patent frequency was also evaluated, shown in Figure 6.8. The trend for the word patent increases over time. Although this does not represent the actual number of patents obtained, it does suggest patents related to optical fiber sensors are appearing more frequently over time. A context search was used to identify companies related to these patents from 2017-2019, provided in the list below. A couple of the companies listed (Corning and Finisar) align with the key players mentioned by a market studies in section 6.1.1. Several other companies were also identified, providing more information about optical fiber sensor development.

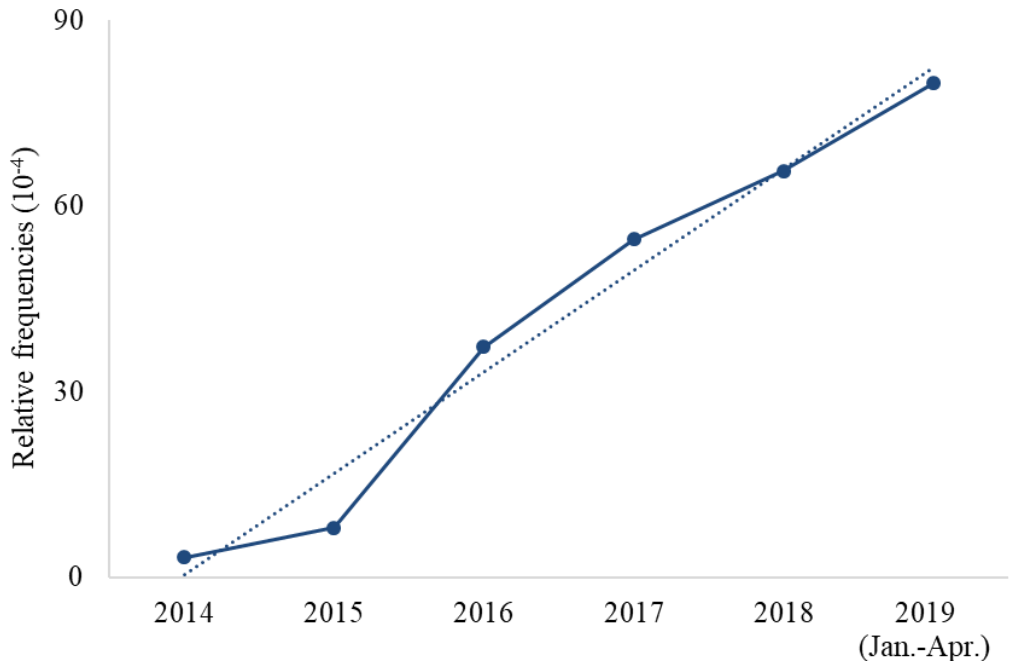

Figure 6.8. Frequency of the word patent

List of companies obtained from a context search on the word patent:

- 3M
- Aker Solutions
- Apple
- Boeing
- Corning
- Finisar
- Fujitsu
- General electric
- Halliburton
- Lockheed Martin
- Mitsubishi
- Sanmina
- Schlumberger
- Sensobright industries
- Siemens

6.5. Conclusion

A text analysis was conducted on textual data obtained from the ABI/ INFORM database using a keyword search for optical fiber sensors. This analysis provided information on the optical fiber

sensor market, measurement parameters, industrial applications, and patents. The main advantage of this data was that it provided a comprehensive overview of the information in industry related to optical fiber sensing technologies and that these trends can be analyzed by year. Although this was not an in-depth search, conclusions can be drawn about themes and trends in the current optical fiber sensor market.

Chapter 7: Overall Conclusions and Suggestions for Future Work

7.1. Overall conclusions

Combining a composite structure with optical fiber sensors results in a smart composite that offers advantages over traditional sensors. Advantages such as the ability to tailor materials to specific uses, the ability to embed the sensor in the material, and the ability of a structure to interact with its environment. The proposed smart composite system, composed of a POF embedded in a 3DOW composite, proves to be a viable SHM system and will continue to improve with further characterization and testing. This multi-disciplinary system brings together several advanced technological components to create a system that utilizes the advantages of each. The POF chosen is more flexible than more common glass optical fiber sensors. Composites are strong and lightweight compared to conventional building materials. It was shown that 3DOW preforms make an excellent host for optical fibers because the yarns are arranged in straight paths, providing minimum crimp and less damage to the optical fibers.

Establishing relationships between signal loss and compressive strength loss enables better monitoring of structural health. The POF positioned in the top layer is the most sensitive in its reaction to the damage event but fails easily and does not provide a strong correlation with the damage experienced by the composite. A system that correlates well with composite damage is the most advantageous. The POF located in the middle and bottom layers correlated better with the composite damage. Further testing, however, is needed to draw strong conclusions about the accuracy of the POF at predicting damage due to the variation between samples and small sample size. More accurate placement of the impact location, improvement to the optical fiber/ OTDR connection, and testing of multiple optical fibers under the same conditions would produce more consistent results.

As with any technology, improvements to the optical fiber sensor, especially to the flexibility, attenuation, and reliably will greatly improve the viability of the system. The market for optical fiber sensors is rapidly growing and research is actively being conducted to meet these improvement goals. OF sensors are most often implemented for temperature, pressure and strain monitoring. They appear to be prominent for use in the oil and gas industry, aerospace, and for

use in bridges. Overall the outlook for optical fibers as part of a structural health monitoring system is positive and is sure to play an integral part in ensuring infrastructure remains resilient and safe for the future.

7.2. Suggestions for Future work

As mentioned, the goals of SHM are to increase the safety of the structure and people using it, increase the longevity of the structure, reduce the cost of preparation and maintenance, and to be reliable and accurate at predicting failure within the structure. Completion of these goals comes with extra benefits for industry application. An increase in safety results in earlier warning signs of hazards, fewer accidents, and less cost associated with damage. Increasing the life of the structure means that new structures don't have to be built as often, and buildings can be preserved longer. SHM can monitor a structure from its construction to its final days. Being able to monitor a structure while it is being constructed will confirm that the parts are being put together correctly and constant monitoring of a structure will lead to need based maintenance which requires less cost than scheduled inspections and maintenance. The ability to be reliable and accurate will advance as research continues for these systems. The advances in sensor and data processing and usability will only result in further growth and increased application of these technologies. This section provides some suggestions for future works to further this goal.

When manufacturing future composites extra care should be taken in the handling of the OF sensors. Support should be added to minimize the risk of damage at the ingress points of the OF and the composite. The edges where the fiber bends and is exposed before being reinserted in the fabric should also be supported, either by keeping the bend within the selvage, so that it is protected by the composite or by external support.

There are unanswered questions which remain about the POF spectra. There is a shift that occurs between a reflection peak and the actual damage location. This shift could be due to the amount of reflection encountered by the detector, human error in measuring, error in the software, etc. Further testing and analysis are needed to determine the cause of this shift so that an accurate distance is measured. This is especially important if the impact location is unknown beforehand. It is also unknown why sometimes a peak appears at the damage location, and sometimes there is

only a decrease in attenuation. Future testing and analysis should be conducted to determine the cause of these anomalies. A C-scan for nondestructive qualitative examination of void distribution and delamination faults in composite materials may also help to correlate the spectra with the type of damage incurred. Once the reason for these spectra items is determined a better baseline from which to evaluate damage can be achieved. This will aid in the use of algorithms to process the spectral data as well.

A distributed, POF sensor may not be the best option for the future of SHM. Research and development are being conducted on optical fiber sensors. These new fibers which promise to be more flexible, more resistant to attenuation, and more reliable should be investigated for embedding in the composite. For example, Corning recently began producing highly flexible, glass, multimode optical fibers which are designed to withstand tight bends with substantially less signal loss than conventional multimode fiber. A preliminary OTDR test was conducted, provided in Appendix F, and they were found to have minimal attenuation loss and to be suitable candidates for future projects. In the literature review FBG sensors were mentioned as one of the most mature sensors for SHM, but they are predominately made of glass. As more flexible FBG sensors available this may be another viable option for future studies.

3DOW structures are not the only viable textile structure in which optical fibers can be embedded. There are many woven, knitted, and nonwoven structures that can and should be explored. There are numbers of designs, patterns, and constructions that may be more suitable for a given application.

The literature review mentioned several types of optical fiber sensors. Given that the embedded POF is not disruptive to the overall structure or integrity of the 3DOW composite. A proposal for a system that contains multiple types of optical fibers position in different layers of the structure, depicted in Figure 7.1, could be implemented. Each fiber could be used to measure a different parameter. For example, OF A and B positioned in the top layer, may be used to detect impact damage. OF C could be placed in the bottom layer where it is better protected and measure a different parameter such as vibration, where it may not be required to be near the surface.

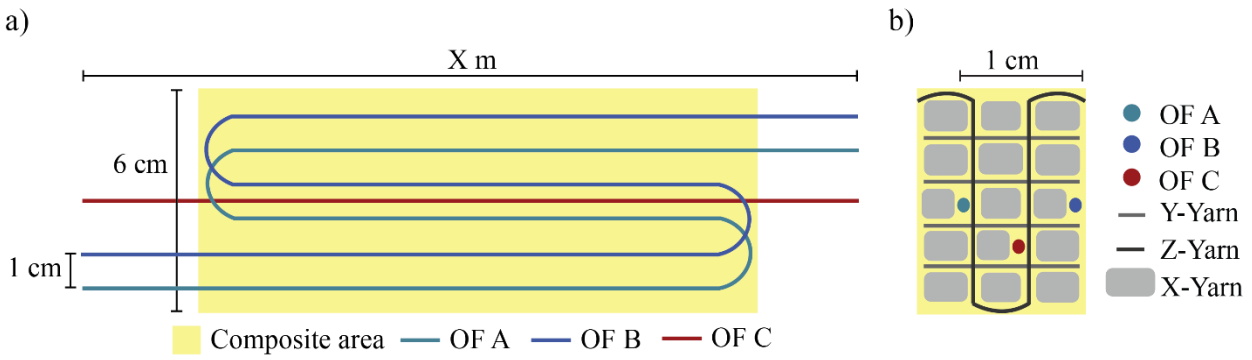

Figure 7.1. Example of SHM system design with a) multiple OF sensors embedded in a composite to monitor several parameters b) OF A and B are located in the middle layer of the 3DOW composite to monitor composite damage and OF C is located in the bottom layer of the composite to be better protected

REFERENCES

[1] C. K. Leung, K. T. Wan, D. Inaudi, X. Bao, W. Habel, Z. Zhou, J. Ou, M. Ghandehari, H. C. Wu and M. Imai, "Review: optical fiber sensors for civil engineering applications," *Mater. Struct.*, vol. 48, *(4)*, pp. 871-906, 2015.

[2] M. Majumder, T. K. Gangopadhyay, A. K. Chakraborty, K. Dasgupta and D. K. Bhattacharya, "Fibre Bragg gratings in structural health monitoring—Present status and applications," *Sensors and Actuators A: Physical*, vol. 147, *(1)*, pp. 150-164, 2008.

[3] H. Li, D. Li and G. Song, "Recent applications of fiber optic sensors to health monitoring in civil engineering," *Engineering Structures*, vol. 26, *(11)*, pp. 1647-1657, 2004. Available: internal-pdf://Recent applications of fiber optic sensors to health monitoring in civil engineering-2047369477/Recent applications of fiber optic sensors to health monitoring in civil engineering.pdf. DOI: 10.1016/j.engstruct.2004.05.018.

[4] D. Balageas, C. Fritzen and A. Güemes, *Structural Health Monitoring.* Wiley Online Library, 2006*493*.

[5] J. Sebastian, N. Schehl, M. Bouchard, M. Boehle, L. Li, A. Lagounov and K. Lafdi, "Health monitoring of structural composites with embedded carbon nanotube coated glass fiber sensors," *Carbon*, vol. 66, pp. 191-200, 2014. Available: internal-pdf://Health monitoring of structural composites with embedded carbon nanotube coated glass fi-0520619013/Health monitoring of structural composites with embedded carbon nanotube coated glass fiber sensors.pdf. DOI: 10.1016/j.carbon.2013.08.058.

[6] R. Di Sante, "Fibre optic sensors for structural health monitoring of aircraft composite structures: Recent advances and applications," *Sensors*, vol. 15, *(8)*, pp. 18666-18713, 2015.

[7] H. Guo, G. Xiao, N. Mrad and J. Yao, "Fiber optic sensors for structural health monitoring of air platforms," *Sensors (Basel)*, vol. 11, *(4)*, pp. 3687-705, 2011. Available: internal-pdf://Fiber Optic Sensors for Structural Health Monitoring of Air Platforms-2550658565/Fiber Optic Sensors for Structural Health Monitoring of Air Platforms.pdf. DOI: 10.3390/s110403687.

[8] G. Luyckx, E. Voet, N. Lammens and J. Degrieck, "Strain measurements of composite laminates with embedded fibre Bragg gratings: Criticism and opportunities for research," *Sensors*, vol. 11, *(1)*, pp. 384-408, 2011.

[9] O. Ziemann, J. Krauser, P. E. Zamzow and W. Daum, *POF Handbook: Optical Short Range Transmission Systems.* Springer Science & Business Media, 2008.

[10] W. R. Habel and K. Krebber, "Fiber-optic sensor applications in civil and geotechnical engineering," *Photonic Sensors*, vol. 1, *(3)*, pp. 268-280, 2011. Available: internal-pdf://Fiber Optic Sensor Applications in Civil and Geotechnical Engineering-0973594629/Fiber Optic Sensor Applications in Civil and Geotechnical Engineering.pdf. DOI: 10.1007/s13320-011-0011-x.

[11] K. Peters, "Polymer optical fiber sensors—a review," *Smart Materials and Structures*, vol. 20, *(1)*, pp. 013002, 2011. Available: internal-pdf://Polymer optical fiber sensors a review-

1812485893/Polymer optical fiber sensors a review.pdf. DOI: 10.1088/0964-1726/20/1/013002.

[12] J. R. Casas and P. J. Cruz, "Fiber optic sensors for bridge monitoring," *J. Bridge Eng.*, vol. 8, *(6)*, pp. 362-373, 2003.

[13] G. Zhou and L. Sim, "Damage detection and assessment in fibre-reinforced composite structures with embedded fibre optic sensors-review," *Smart Mater. Struct.*, vol. 11, *(6)*, pp. 925, 2002.

[14] Z. Wu, J. Zhang and M. Noori, *Fiber-Optic Sensors for Infastructure Health Monitoring, Volume 1*. (1st ed.) New York, NY: Momentum Press, LLC, 2019.

[15] J. Zubia and J. Arrue, "Plastic optical fibers: An introduction to their technological processes and applications," *Optical Fiber Technology*, vol. 7, *(2)*, pp. 101-140, 2001.

[16] C. Merzbacher, A. Kersey and E. Friebele, "Fiber optic sensors in concrete structures: a review," *Smart Mater. Struct.*, vol. 5, *(2)*, pp. 196, 1996.

[17] H. Li, T. Yi, L. Ren, D. Li and L. Huo, "Reviews on innovations and applications in structural health monitoring for infrastructures," *Structural Monitoring and Maintenance*, vol. 1, *(1)*, pp. 1-45, 2014.

[18] K. S. C. Kuang, S. T. Quek, C. G. Koh, W. J. Cantwell and P. J. Scully, "Plastic Optical Fibre Sensors for Structural Health Monitoring: A Review of Recent Progress," *Journal of Sensors*, vol. 2009, pp. 1-13, 2009. Available: internal-pdf://Plastic Optical Fibre Sensors for Structural Health Monitoring A Review of Recent Progress-0671629829/Plastic Optical Fibre Sensors for Structural Health Monitoring A Review of Recent Progress.pdf. DOI: 10.1155/2009/312053.

[19] K. Grattan and T. Sun, "Fiber optic sensor technology: an overview," *Sensors and Actuators A: Physical*, vol. 82, *(1)*, pp. 40-61, 2000.

[20] S. Liehr, P. Lenke, M. Wendt, K. Krebber, M. Seeger, E. Thiele, H. Metschies, B. Gebreselassie and J. Munich, "Polymer optical fiber sensors for distributed strain measurement and application in structural health monitoring," *Sensors Journal, IEEE*, vol. 9, *(11)*, pp. 1330-1338, 2009.

[21] M. G. Kuzyk, *Polymer Fiber Optics: Materials, Physics, and Applications.* CRC press, 2006.

[22] A. Appajaiah, *Climatic Stability of Polymer Optical Fibers (POF).* Wirtschaftsverl. NW, Verlag für neue Wiss., 2005.

[23] M. Koerdt, S. Kibben, O. Bendig, S. Chandrashekhar, J. Hesselbach, C. Brauner, A. S. Herrmann, F. Vollertsen and L. Kroll, "Fabrication and characterization of Bragg gratings in perfluorinated polymer optical fibers and their embedding in composites," *Mechatronics*, vol. 34, pp. 137-146, 2016.

[24] E. Arrospide, I. Bikandi, I. García, G. Durana, G. Aldabaldetreku and J. Zubia, "7 - mechanical properties of polymer-optical fibres," in *Polymer Optical Fibres*, C. Bunge, , T. Gries, , and M. Beckers, Eds. Woodhead Publishing, 2017, pp. 201-216. DOI: http://dx.doi.org/10.1016/B978-0-08-100039-7.00007-5.

[25] B. H. Lee, Y. H. Kim, K. S. Park, J. B. Eom, M. J. Kim, B. S. Rho and H. Y. Choi, "Interferometric fiber optic sensors," *Sensors,* vol. 12, *(3),* pp. 2467-2486, 2012.

[26] J. H. Lim, H. S. Jang, K. S. Lee, J. C. Kim and B. H. Lee, "Mach–Zehnder interferometer formed in a photonic crystal fiber based on a pair of long-period fiber gratings," *Opt. Lett.,* vol. 29, *(4),* pp. 346-348, 2004.

[27] Y. Kim, U. Paek and B. H. Lee, "Measurement of refractive-index variation with temperature by use of long-period fiber gratings," *Opt. Lett.,* vol. 27, *(15),* pp. 1297-1299, 2002.

[28] L. Yuan, L. Zhou and J. Wu, "Fiber optic temperature sensor with duplex Michleson interferometric technique," *Sensors and Actuators A: Physical,* vol. 86, *(1-2),* pp. 2-7, 2000.

[29] R. Di Sante and L. Scalise, "A novel fiber optic sensor for multiple and simultaneous measurement of vibration velocity," *Rev. Sci. Instrum.,* vol. 75, *(6),* pp. 1952-1958, 2004.

[30] G. A. Brown and A. Hartog, "Optical fiber sensors in upstream oil & gas," *J. Pet. Technol.,* vol. 54, *(11),* pp. 63-65, 2002.

[31] M. Barnoski, M. Rourke, S. Jensen and R. Melville, "Optical time domain reflectometer," *Appl. Opt.,* vol. 16, *(9),* pp. 2375-2379, 1977.

[32] B. L. Danielson, "Optical time-domain reflectometer specifications and performance testing," *Appl. Opt.,* vol. 24, *(15),* pp. 2313-2322, 1985.

[33] D. R. Anderson, L. M. Johnson and F. G. Bell, *Troubleshooting Optical Fiber Networks: Understanding and using Optical Time-Domain Reflectometers.* Academic Press, 2004.

[34] C. Saunders and P. Scully, "Sensing applications for POF and hybrid fibres using a photon counting OTDR," *Measurement Science and Technology,* vol. 18, *(3),* pp. 615, 2007.

[35] I. R. Husdi, K. Nakamura and S. Ueha, "Sensing characteristics of plastic optical fibres measured by optical time-domain reflectometry," *Measurement Science and Technology,* vol. 15, *(8),* pp. 1553-1559, 2004. Available: internal-pdf://Sensing characteristics of plastic optical fibres measured by optical time domain reflectome-2684913413/Sensing characteristics of plastic optical fibres measured by optical time domain reflectometry.pdf. DOI: 10.1088/0957-0233/15/8/022.

[36] T. M. Hamouda, *Smart Textiles: Evaluation of Fiber Optic Sensors Embedded in 3 D Orthogonal Woven Composites and their Impact on the Host Structure Integrity.* North Carolina State University, 2012.

[37] J. Gagnon, "The fundamentals of an OTDR," in *Optical Business Unit*. EXFO, 2008, .

[38] C. Saunders and P. Scully, "Distributed plastic optical fibre measurement of pH using a photon counting OTDR," in *Journal of Physics: Conference Series,* 2005, pp. 61.

[39] G. Rodriguez, J. R. Casas and S. Villalba, "SHM by DOFS in civil engineering: A review," *Struct.Monit.Maint,* vol. 2, *(4),* pp. 357-382, 2015.

[40] A. R. Bahrampour and F. Maasoumi, "Resolution enhancement in long pulse OTDR for application in structural health monitoring," *Optical Fiber Technology,* vol. 16, *(4),* pp. 240-249, 2010.

[41] Z. Ding, C. Wang, K. Liu, J. Jiang, D. Yang, G. Pan, Z. Pu and T. Liu, "Distributed optical fiber sensors based on optical frequency domain reflectometry: A review," *Sensors,* vol. 18, *(4),* pp. 1072, 2018.

[42] S. Liehr, N. Nöther and K. Krebber, "Incoherent optical frequency domain reflectometry and distributed strain detection in polymer optical fibers," *Measurement Science and Technology,* vol. 21, *(1),* pp. 017001, 2009.

[43] *Composites in the Airframe and Primary Structure*.

[44] D. Hull and T. W. Clyne, *An Introduction to Composite Materials.* (2nd ed.) Cambridge ; New York: Cambridge University Press, 1996Available: http://www.loc.gov/catdir/description/cam027/96005701.html; http://www.loc.gov/catdir/toc/cam022/96005701.html.

[45] R. Verdejo, M. M. Bernal, L. J. Romasanta and M. A. Lopez-Manchado, "Graphene filled polymer nanocomposites," *Journal of Materials Chemistry,* vol. 21, *(10),* pp. 3301-3310, 2011.

[46] J. R. Fried, *Polymer Science and Technology.* (2nd ed.) Upper Saddle River, NJ: Prentice Hall PTR, 2003.

[47] N. G. McCrum, C. P. Buckley and C. B. Bucknall, *Principles of Polymer Engineering.* (2nd ed.) Oxford ; New York: Oxford University Press, 1997.

[48] L. H. Sperling, *Introduction to Physical Polymer Science.* (4th ed.) Hoboken, N.J.: Wiley-Interscience, 2006.

[49] D. R. Askeland and P. P. Phulé, *The Science and Engineering of Materials.* (5th ed.) Toronto; London: Nelson; Thomson, 2006.

[50] I. M. Daniel and O. Ishai, *Engineering Mechanics of Composite Materials.* (2nd ed.) New York: Oxford University Press, 2006.

[51] W. Cantwell and J. Morton, "The impact resistance of composite materials—a review," *Composites,* vol. 22, *(5),* pp. 347-362, 1991.

[52] E. Aoki, K. Fukuta, R. Miyashita, Y. Nagatsuka, M. Sasahara, J. Sekiguti and S. Tsuburaya, *Three-Dimensional Fabric, and Method and Loom Construction for the Production Thereof,* 1974.

[53] M. Bannister, "Challenges for composites into the next millennium—a reinforcement perspective," *Composites Part A: Applied Science and Manufacturing,* vol. 32, *(7),* pp. 901-910, 2001.

[54] X. Chen, L. W. Taylor and L. Tsai, "An overview on fabrication of three-dimensional woven textile preforms for composites," *Text. Res. J.,* vol. 81, *(9),* pp. 932-944, 2011.

[55] M. H. Mohamed, "Three-dimensional textiles," *Am. Sci.,* pp. 530-541, 1990.

[56] M. Mohamed and A. Bogdanovich, "Comparative analysis of different 3D weaving processes, machines and products," in *Proceedings of the 17th International Conference on Composite Materials (ICCM-17)*, 2009, .

[57] S. V. Lomov, A. E. Bogdanovich, D. S. Ivanov, D. Mungalov, M. Karahan and I. Verpoest, "A comparative study of tensile properties of non-crimp 3D orthogonal weave and multi-layer plain weave E-glass composites. Part 1: Materials, methods and principal results," *Composites Part A: Applied Science and Manufacturing*, vol. 40, *(8)*, pp. 1134-1143, 2009.

[58] M. E. Ince, *Performance of Composites from 3D Orthogonal Woven Preforms in Terms of Architecture and Sample Location during Resin Infusion.* 2013.

[59] K. Greenwood, *Loom*, 1974.

[60] M. H. Mohamed and Z. Zhang, *Method of Forming Variable Cross-Sectional Shaped Three-Dimensional Fabrics*, 1992.

[61] P. K. Banerjee, "Basic weaves and the process of drawing-in," in *Principles of Fabric Formation* Boca Raton, FL: Taylor & Francis Group, 2015, pp. 83.

[62] L. Tong, A. P. Mouritz and M. K. Bannister, "3D fibre reinforced polymer composites," 2002. Available: http://proxying.lib.ncsu.edu/index.php?url=http://www.sciencedirect.com/science/book/9780080439389; http://proxying.lib.ncsu.edu/index.php?url=http://site.ebrary.com/lib/ncsu/Top?id=10190896.

[63] A. Mouritz, M. Bannister, P. Falzon and K. Leong, "Review of applications for advanced three-dimensional fibre textile composites," *Composites Part A: Applied Science and Manufacturing*, vol. 30, *(12)*, pp. 1445-1461, 1999.

[64] T. Hamouda, A. M. Seyam and K. Peters, "Evaluation of the integrity of 3D orthogonal woven composites with embedded polymer optical fibers," *Composites Part B: Engineering*, vol. 78, pp. 79-85, 2015.

[65] K. Satori, K. Fukuchi, Y. Kurosawa, A. Hongo and N. Takeda, "Polyimide-coated small-diameter optical fiber sensors for embedding in composite laminate structures," in *Smart Structures and Materials 2001: Sensory Phenomena and Measurement Instrumentation for Smart Structures and Materials*, 2001, pp. 285-295.

[66] M. Schukar, B. Grzemba, K. Krebber and M. Luber, "Integration technology of POF sensors into composites for structural health monitoring," 2009.

[67] R. Di Sante and L. Donati, "Strain monitoring with embedded Fiber Bragg Gratings in advanced composite structures for nautical applications," *Measurement*, vol. 46, *(7)*, pp. 2118-2126, 2013.

[68] *2017 Infrastructure Report Card*. Available: https://www.infrastructurereportcard.org/cat-item/bridges/.

[69] "Global distributed fiber optic sensor market size, share, development, growth and demand forecast to 2023," Prescient & Strategic Intelligence Private Limited, June 2017.

[70] C. Yun and J. Min, "Smart sensing, monitoring, and damage detection for civil infrastructures," *KSCE Journal of Civil Engineering,* vol. 15, *(1),* pp. 1-14, 2010. Available: internal-pdf://Smart Sensing Monitoring and Damage Detection for Civil Infrastructures-2869464837/Smart Sensing Monitoring and Damage Detection for Civil Infrastructures.pdf. DOI: 10.1007/s12205-011-0001-y.

[71] *ASCE 2017 Infrastructure Report Card*.

[72] J. M. Ko and Y. Q. Ni, "Technology developments in structural health monitoring of large-scale bridges," *Engineering Structures,* vol. 27, *(12),* pp. 1715-1725, 2005. Available: internal-pdf://Technology developments in structural health monitoring of large-scale bridges-0336131845/Technology developments in structural health monitoring of large-scale bridges.pdf. DOI: 10.1016/j.engstruct.2005.02.021.

[73] K. Kuang, W. Cantwell and C. Thomas, "Crack detection and vertical deflection monitoring in concrete beams using plastic optical fibre sensors," *Measurement Science and Technology,* vol. 14, *(2),* pp. 205, 2003.

[74] N. Takeda, "Characterization of microscopic damage in composite laminates and real-time monitoring by embedded optical fiber sensors," *Int. J. Fatigue,* vol. 24, *(2),* pp. 281-289, 2002.

[75] J. M. Lopez-Higuera, L. Rodriguez Cobo, A. Quintela Incera and A. Cobo, "Fiber Optic Sensors in Structural Health Monitoring," *Lightwave Technology, Journal Of,* vol. 29, *(4),* pp. 587-608, 2011. . DOI: 10.1109/JLT.2011.2106479.

[76] A. Alavie, R. Maaskant, M. Ohn, S. Karr and S. Huang, "A structurally integrated Bragg grating laser sensing system for a carbon fiber prestressed concrete highway bridge," *Smart Mater. Struct.,* vol. 4, *(1),* pp. 20, 1995.

[77] K. Kuang and W. Cantwell, "The use of plastic optical fibres and shape memory alloys for damage assessment and damping control in composite materials," *Measurement Science and Technology,* vol. 14, *(8),* pp. 1305, 2003.

[78] K. Kuang and W. Cantwell, "The use of plastic optical fibre sensors for monitoring the dynamic response of fibre composite beams," *Measurement Science and Technology,* vol. 14, *(6),* pp. 736, 2003.

[79] "Global fiber optic sensors market size, market share, application analysis, regional outlook, growth trends, key players, competitive strategies and forecasts, 2018 to 2026," Acute Market Reports, January 2019.

[80] I. Kwon, G. Jin, D. Seo, C. Kim, N. Lee and C. Yun, "Feasibility study for monitoring of off-shore pipelines using BOTDA system," in *SPIE Defense, Security, and Sensing,* 2009, pp. 73170O-73170O-11.

[81] K. Diamanti and C. Soutis, "Structural health monitoring techniques for aircraft composite structures," *Progress in Aerospace Sciences*, vol. 46, *(8)*, pp. 342-352, 2010. Available: internal-pdf://Sturctural health monitoring techniques for aircraft composite sturctures-0151580421/Sturctural health monitoring techniques for aircraft composite sturctures.pdf. DOI: 10.1016/j.paerosci.2010.05.001.

[82] W. J. Staszewski, S. Mahzan and R. Traynor, "Health monitoring of aerospace composite structures – Active and passive approach," *Composites Science and Technology*, vol. 69, *(11-12)*, pp. 1678-1685, 2009. Available: internal-pdf://Health monitoring of aerospce composite sturctures-1376264965/Health monitoring of aerospce composite sturctures.pdf. DOI: 10.1016/j.compscitech.2008.09.034.

[83] H. Tsutsui, A. Kawamata, T. Sanda and N. Takeda, "Detection of impact damage of stiffened composite panels using embedded small-diameter optical fibers," *Smart Mater. Struct.*, vol. 13, *(6)*, pp. 1284, 2004.

[84] H. Tsutsui, A. Kawamata, J. Kimoto, A. Isoe, Y. Hirose, T. Sanda and N. Takeda, "Impact damage detection system using small-diameter optical-fiber sensors embedded in CFRP laminate structures," *Advanced Composite Materials*, vol. 13, *(1)*, pp. 43-55, 2004.

[85] H. Tsutsui, N. Hirano, J. Kimoto, T. Akatsuka, H. Sashikuma, N. Takeda and N. Tajima, "Research and development of impact damage detection system for airframe structures using optical fiber sensors," in *Smart Sensor Phenomena, Technology, Networks, and Systems 2008*, 2008, pp. 69330P.

[86] T. Vella, S. Chadderdon, R. Selfridge, S. Schultz, S. Webb, C. Park, K. Peters and M. Zikry, "Full-spectrum interrogation of fiber Bragg gratings at 100 kHz for detection of impact loading," *Measurement Science and Technology*, vol. 21, *(9)*, pp. 094009, 2010.

[87] A. Güemes, A. Fernández-López and B. Soller, "Optical fiber distributed sensing-physical principles and applications," *Structural Health Monitoring*, vol. 9, *(3)*, pp. 233-245, 2010.

[88] A. Güemes, A. Fernandez-Lopez and P. Fernandez, "Damage detection in composite structures from fibre optic distributed strain measurements," in *EWSHM-7th European Workshop on Structural Health Monitoring*, 2014, .

[89] I. Mckenzie and N. Karafolas, "Fiber optic sensing in space structures: The experience of the european space agency," in *17th International Conference on Optical Fibre Sensors*, 2005, pp. 262-270.

[90] A. Zagrai, N. Demidovich, B. Cooper, J. Schlavin, C. White, S. Kessler, J. MacGillivray, S. Chesebrough, L. Magnusion and L. Puckett, "Structural health monitoring during suborbital spaceflight," in *66th International Astronautical Congress, Jerusalem, Israel, Oct*, 2015, pp. 12-16.

[91] X. Chen, "Fracture of wind turbine blades in operation—Part I: A comprehensive forensic investigation," *Wind Energy*, vol. 21, *(11)*, pp. 1046-1063, 11/01; 2019/03, 2018. Available: https://doi.org/10.1002/we.2212. DOI: 10.1002/we.2212.

[92] A. Ghoshal, M. J. Sundaresan, M. J. Schulz and P. Frank Pai, "Structural health monitoring techniques for wind turbine blades," *J. Wind Eng. Ind. Aerodyn.,* vol. 85, *(3),* pp. 309-324, 2000.

[93] W. Liu, B. Tang and Y. Jiang, "Status and problems of wind turbine structural health monitoring techniques in China," *Renewable Energy,* vol. 35, *(7),* pp. 1414-1418, 2010. Available: internal-pdf://Status and problems of wind turbine structural health monitoring techiques in China-2131273477/Status and problems of wind turbine structural health monitoring techiques in China.pdf. DOI: 10.1016/j.renene.2010.01.006.

[94] S. Villalba and J. R. Casas, "Application of optical fiber distributed sensing to health monitoring of concrete structures," *Mechanical Systems and Signal Processing,* vol. 39, *(1-2),* pp. 441-451, 2013. Available: internal-pdf://Application of optical fiber distributed sensing to health monitoring of concrete structures-1678231045/Application of optical fiber distributed sensing to health monitoring of concrete structures.pdf. DOI: 10.1016/j.ymssp.2012.01.027.

[95] H. Pei, J. Teng, J. Yin and R. Chen, "A review of previous studies on the applications of optical fiber sensors in geotechnical health monitoring," *Measurement,* vol. 58, pp. 207-214, 2014. Available: internal-pdf://A review of previous studies on applictaions of optical fiber sensors in geotechnica-1812445957/A review of previous studies on applictaions of optical fiber sensors in geotechnical health monitoring.pdf. DOI: 10.1016/j.measurement.2014.08.013.

[96] Y. Wong, P. Scully, R. Bartlett, K. Kuang and W. Cantwell, "Plastic optical fibre sensors for environmental monitoring: biofouling and strain applications," *Strain,* vol. 39, *(3),* pp. 115-119, 2003.

[97] W. De Morais, S. Monteiro and J. d'Almeida, "Effect of the laminate thickness on the composite strength to repeated low energy impacts," *Composite Structures,* vol. 70, *(2),* pp. 223-228, 2005.

[98] T. Hamouda, A. M. Seyam and K. Peters, "Polymer optical fibers integrated directly into 3D orthogonal woven composites for sensing," *Smart Mater. Struct.,* vol. 24, *(2),* pp. 025027, 2015.

[99] T. Hamouda, K. Peters and A. M. Seyam, "Effect of resin type on the signal integrity of an embedded perfluorinated polymer optical fiber," *Smart Mater. Struct.,* vol. 21, *(5),* pp. 055023, 2012.

[100] A. M. Seyam and T. Hamouda, "Smart textiles: evaluation of optical fibres as embedded sensors for structure health monitoring of fibre reinforced composites," *Journal of the Textile Institute,* vol. 104, *(8),* pp. 892-899, 2013.

[101] *Product Data Sheet*.

[102] "ASTM D792 - 00 Standard Test Methods for Density and Specific Gravity (Relative Density) of Plastics by Displacement," *ASTM International, West Conshohocken, PA,* 2000.

[103] M. Richardson and M. Wisheart, "Review of low-velocity impact properties of composite materials," *Composites Part A: Applied Science and Manufacturing,* vol. 27, *(12),* pp. 1123-1131, 1996.

[104] M. V. Donadon, L. Iannucci, B. G. Falzon, J. M. Hodgkinson and S. F. M. de Almeida, "A progressive failure model for composite laminates subjected to low velocity impact damage," *Computers & Structures,* vol. 86, *(11),* pp. 1232-1252, June 2008, 2008. . DOI: https://doi.org/10.1016/j.compstruc.2007.11.004.

[105] T. Shyr and Y. Pan, "Impact resistance and damage characteristics of composite laminates," *Composite Structures,* vol. 62, *(2),* pp. 193-203, November 2003, 2003. . DOI: https://doi.org/10.1016/S0263-8223(03)00114-4.

[106] S. Wang, L. Wu and L. Ma, "Low-velocity impact and residual tensile strength analysis to carbon fiber composite laminates," *Materials & Design,* vol. 31, *(1),* pp. 118-125, January 2010, 2010. . DOI: https://doi.org/10.1016/j.matdes.2009.07.003.

[107] W. De Morais, S. Monteiro and J. d'Almeida, "Evaluation of repeated low energy impact damage in carbon–epoxy composite materials," *Composite Structures,* vol. 67, *(3),* pp. 307-315, 2005.

[108] D. Zhang, Y. Sun, L. Chen and N. Pan, "A comparative study on low-velocity impact response of fabric composite laminates," *Mater Des,* vol. 50, pp. 750-756, 2013.

[109] J. Baucom and M. Zikry, "Low-velocity impact damage progression in woven E-glass composite systems," *Composites Part A: Applied Science and Manufacturing,* vol. 36, *(5),* pp. 658-664, 2005.

[110] B. Jang, W. Kowbel and B. Jang, "Impact behavior and impact-fatigue testing of polymer composites," *Composites Sci. Technol.,* vol. 44, *(2),* pp. 107-118, 1992.

[111] M. Y. Tooski, R. Alderliesten, R. Ghajar and S. Khalili, "Experimental investigation on distance effects in repeated low velocity impact on fiber–metal laminates," *Composite Structures,* vol. 99, pp. 31-40, 2013.

[112] B. M. Icten, "Repeated impact behavior of glass/epoxy laminates," *Polymer Composites,* vol. 30, *(11),* pp. 1562-1569, 2009.

[113] E. Sevkat, B. Liaw, F. Delale and B. B. Raju, "Effect of repeated impacts on the response of plain-woven hybrid composites," *Composites Part B: Engineering,* vol. 41, *(5),* pp. 403-413, 2010.

[114] "ASTM D7136 / D7136M-15, Standard Test Method for Measuring the Damage Resistance of a Fiber-Reinforced Polymer Matrix Composite to a Drop-Weight Impact Event ," 2015.

[115] *High Resolution OTDR for Aviation, defense, transportation and Oil and Gas applications*.

[116] Irwan Rawal Husdi and Kentaro Nakamura and,Sadayuki Ueha, "Sensing characteristics of plastic optical fibres measured by optical time-domain reflectometry," *Measurement Science and Technology,* vol. 15, *(8),* pp. 1553, 2004. Available: http://stacks.iop.org/0957-0233/15/i=8/a=022.

[117] D. Cartie and P. Irving, "Effect of resin and fibre properties on impact and compression after impact performance of CFRP," *Composites Part A: Applied Science and Manufacturing,* vol. 33, *(4),* pp. 483-493, 2002.

[118] Y. Hirai, H. Hamada and J. Kim, "Impact response of woven glass-fabric composites—I.: Effect of fibre surface treatment," *Composites Sci. Technol.,* vol. 58, *(1),* pp. 91-104, 1998.

[119] H. Yan, C. Oskay, A. Krishnan and L. R. Xu, "Compression-after-impact response of woven fiber-reinforced composites," *Composites Sci. Technol.,* vol. 70, *(14),* pp. 2128-2136, 2010.

[120] "ASTM D7137 / D7137M-12, Standard Test Method for Compressive Residual Strength Properties of Damaged Polymer Matrix Composite Plates," 2012.

[121] "Standard Test Method for Compressive Properties of Polymer Matrix Composite Materials Using a Combined Loading Compression (CLC) Test Fixture," vol. Annual Book of ASTM Standards, 2000.

[122] G. Caprino, "Residual strength prediction of impacted CFRP laminates," *J. Composite Mater.,* vol. 18, *(6),* pp. 508-518, 1984.

[123] A. Standard, "Standard test method for tensile properties of polymer matrix composite materials," *Astm D3039/D 3039m,* 2008.

[124] "Fiber optic sensors: Global markets," BCC Research, Tech. Rep. PHO010A, 2014.

[125] A. Mendez, "Fiber bragg grating sensors: A market overview," in *Third European Workshop on Optical Fibre Sensors*, 2007, pp. 661905.

[126] Markets and Markets, "Fiber optics market- global forecasts to 2021," MarketsandMarkets, 2017.

[127] Grand View Reserach, "Fiber optics market," Grand View Research Inc, USA, 2017.

[128] A. L. Porter and S. W. Cunningham, *Tech Mining: Exploiting New Technologies for Competitive Advantage*. John Wiley & Sons, 2004*29*.

[129] F. Madani and C. Weber, "The evolution of patent mining: Applying bibliometrics analysis and keyword network analysis," *World Patent Information,* vol. 46, pp. 32-48, 2016.

[130] A. Abbas, L. Zhang and S. U. Khan, "A literature review on the state-of-the-art in patent analysis," *World Patent Information,* vol. 37, pp. 3-13, 2014.

[131] S. Sinclair and G. Rockwell, "Voyant Tools (web application)," 2012.

[132] K. Rauscher, "4 Exciting New Medical Applications for Fiber Optic Technology," *Fiberguide Industries,* 2017.

[133] H. H. Diamandi, Y. London, G. Bashan and A. Zadok, "Distributed opto-mechanical analysis of liquids outside standard fibers coated with polyimide," *APL Photonics,* vol. 4, *(1),* pp. 016105, 2019.

APPENDICES

Appendix A: List of Abbreviations

2D	Two-dimensional
3D	Three-dimensional
3DOW	Three Dimensional Orthogonal Woven
ABI	Abstracted Business information
BOTDR	OTDR based on Brillouin scattering
CAGR	Compound Annual Growth Rate
CAI	Compression after impact
CFRC	Carbon Fiber Reinforced Composite
CLC	Combined Loading Compression
CMC	Ceramic Matrix Composite
dB	Decibel
DII	Derwent Innovation Index
E-glass	Electrical glass
FBG	Fiber Bragg Grating
GFRC	Glass Fiber Reinforced Composite
GI	Graded Refractive Index Profile
GOF	Glass Optical Fiber
GPS	Global Positioning System
LED	Light Emitting Diode
MMC	Metal Matrix Composite
OFDR	Optical Frequency Domain Reflectometer
OTDR	Optical Time Domain Reflectometer
PC	Polycarbonate
PF	Fluorinated polymer
PMC	Polymeric Matrix Composite
PMMA	Polymethylmethacrylate
POF	Polymeric Optical Fiber
PS	Polystyrene

PTFE	Polytetrafluoroethylene
PVDF	Polyvinylidene Fluoride
ROTDR	OTDR based on Raman scattering
S&T	Science and Technology
SHM	Structural Health Monitoring
SI	Step Index Profile
SOFO	French acronym of “Surveillance d’Ouvrages par Fibres Optiques“
TM	Tech Mining
VARTM	Vacuum Assisted Resin Transfer Molding

Appendix B: OTDR Specifications

- Wavelength options: 670 nm, 850 nm
- Fiber Type: MMF 200 µm, 62.5 µm, or 50 µm
- Optical connector: Universal, PC Type, with FC, SC or ST adapter
- Optical pulse width: 1 ns
- Measurement range: 1.25, 2.5, 5, 10, 20, 40, 80, 160 km
- Dynamic range:
    - Return Loss: 100 dB
    - Rayleigh Backscattering: >20 dB
- Dead zones:
    - Event dead zone: 10 cm
    - Attenuation dead zone: 40 cm
- Distance accuracy: ± (10 mm + 5x10-5 x[fiber length])
- Reflectance accuracy: 1.5 dB
- Loss accuracy: ± 0.1 dB ± 0.02 dB/dB

Appendix C: Steps of Vacuum Assisted Resin Transfer Molding

1. Clean glass tabletop using a razor blade and adhesive remover
2. Prepare the 3D preform by cutting off the taped ends
3. Lay a layer of release film, the same size, or slightly larger than the sample on the glass tabletop
4. Lay the prepared 3D preform on top of the release film
5. Place the nylon woven peel ply layer on top of the 3D preform to ensure good and even resin distribution during the infusion process. This layer is at least an inch wider and an inch longer than the preform on all sides to make the removal easier.
6. Place the resin flow media on top of the peel ply layer to allow quick resin flow across the preform during infusion. This layer should be 2/3 the length of sample and the same width.
7. For the resin inlet and outlet, a 1.5 cm diameter spiral tube is placed on both edges of the preform. The tube is the width of sample + 1 inch. Use brown tape to tape opposite end of the spiral tube to prevent it from puncturing the vacuum bag.
8. Cut the connector tube (about 5cm) and attach it to outside of the spiral tube by rotating anticlockwise
9. Both the inlet and outlet spiral tubes are connected, via the connector tube, to a 1.5 cm diameter flexible polyethylene tube, inlet tube will be connected to resin supply and outlet tube will be connected to the vacuum pump. The inlet tube is about 1 meter in length. The outlet tube should be long enough to reach the vacuum pump.
10. Seal the connections with sticky tape
11. Place a spiral tube along the 3D preform sides, this should be the side without selvage if optic fiber is uses. Us sticky tape to secure the end with brown tape to the table.
12. Place the sealant sticky tape around the preform so that the tape is positioned next to the fabric, and about 1 inch away on side with taped spiral tube because of wrinkling
13. Tape down the connector tube in the middle of the sticky tape.
14. Place POF ends threaded through furcation tubes carefully on top of the sticky tape and add an additional small piece of sticky tape on top of the furcation tube to ensure that no air gap that may cause air leak during the vacuum process
15. Secure all connections with sticky tape. At the inlet and outlet use rolled pieces of sticky tape to fill in the gaps on the side and place a slightly bigger piece of sticky tape over the top of the connector tube. Make sure and squish down these areas so that there are no gaps between the tape
16. Cover the preform with the nylon bagging film and seal with sealant tape. Start at corners and press down while applying tension on both sides of the bag. Next, press down edges along the edges. Use a flat stick to press along outer edge and to secure the corners.
17. Connect the vacuum pump to the resin outlet tube and connect resin inlet to an absolute pressure gage.
18. Apply 100 kPa negative pressure to the prepared preform.
19. Switch off the vacuum pump for 1 hour with observation to the vacuum gage to ensure that there is no air leak and that the prepared sample is keeping the vacuum pressure.
20. Disconnect the pressure gage and clamp the resin inlet until the resin is prepared.

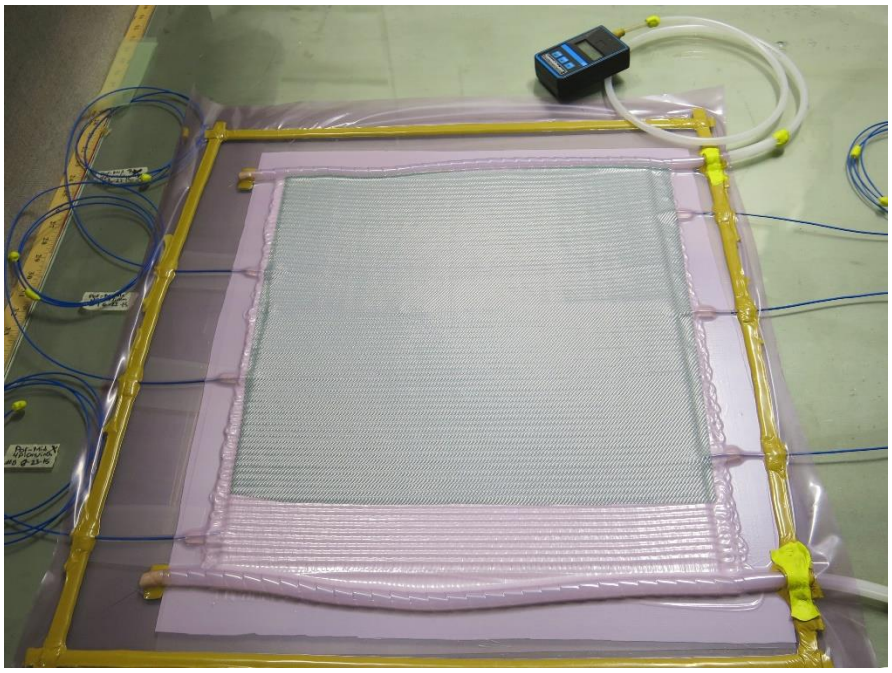

Figure C1. Vacuum bag set-up

Preparing Epoxy Resin

1. Epoxy resin is mixed in a bucket at a 100:27 weight ratio of epoxy to hardener. The resin is hand mixed using a wooden stirring stick.
2. Place the mixed resin in a vacuum desiccator for degassing to removes all air bubbles that were created during stirring the mixture.
3. After 30 minutes, remove the resin mixture from the vacuum desiccator and carry to infusion table.
4. Place the resin inlet tube on the resin mixture bucket, then, switch the vacuum pump on
5. Unclamp the resin inlet and resin will start to flow from the resin bucket to spiral tube and then to the preform.
6. When resin reaches the outlet spiral tube and the preform is fully impregnated with resin, resin inlet is clamped and the vacuum pump was kept running for 15 minutes to take out all excess resin and air (bleeding).
7. Then the vacuum pump was turned off and sample was kept on the table at least 24 hours for curing.

Appendix D: POF Connection Tests

During testing, variation in the signals was noted. In order to determine the origin of the variation, a test was conducted to determine the effect of the connection of the POF on the consistency of the POF signal. The POF (not embedded in a composite) was connected, signal measured, disconnected, and then reconnected. This was repeated 10 times to identify changes in the signal after each reconnection. The results, Figure D1 show variation in the signals observed when the connection is the only variable. Attenuation loss does not appear to be not specific order: E > J > A > F > C > I > G > H > B > D. There is no drop observed in the first reflection peak, however in the second there is a distinctive separation. Again there does not appear to be a specific order to the separation. Signals A, C, E, F, I, J, and K appear is the higher peak and signals B, D, G, and H appear in the lower peak. There for the variation in the earliest tests, where the POF was connected and disconnected after each impact event does not appear to have significant meaning.

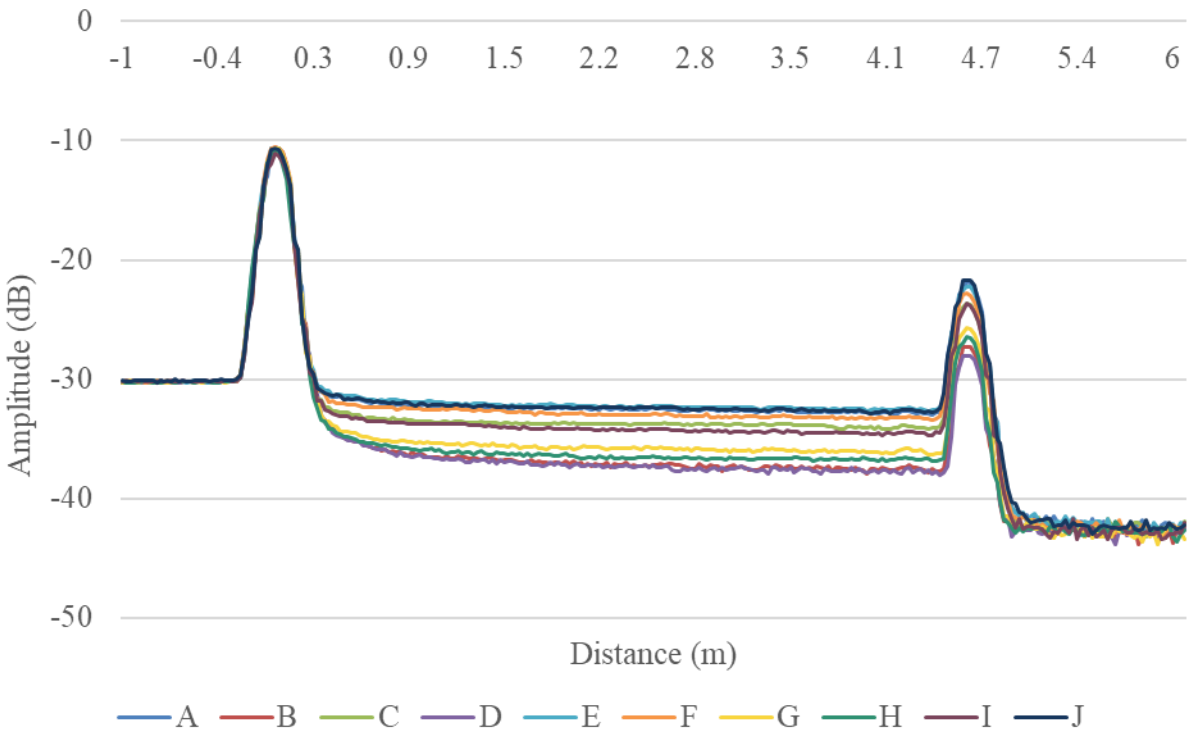

Figure D1. Connection test for POF not embedded in the composite

The test was also conducted with the POF embedded in the composite material. The drop noticed in the first reflection peak, after the first two signals is consistent with POF embedded in composites which are reconnected. Typically, the first few signals tested will have a higher reflection peak than later signals tested. The drop noticed on the right side of the end reflection appears to be also inherent to reconnecting the POF to the OTDR. For the first 3 signals recorded (A-C) the dynamic range is about 6.2 dB, and for the remaining signals the dynamic range increases to between 7.6 and 8.6 dB. Again, the drop in attenuation is not consistent with the order that it was tested (A > E > G > I > C > D > H > J > B > F) indicating that the POF is likely not being damaged as it is reconnected.

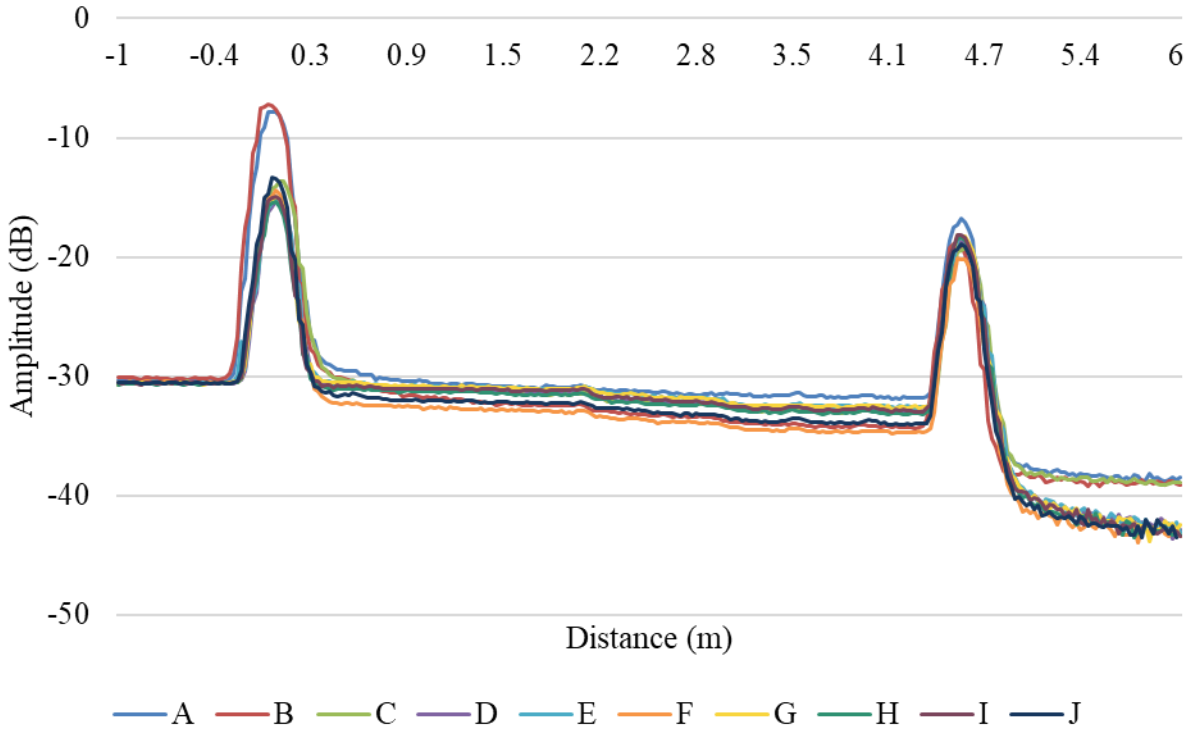

Figure D2. Connection test for POF embedded in the composite

As expected, when the bare POF (not embedded in the composite) remains connected to the OTDR, the signal variation is minimal. Figure D2 shows a difference of about 0.1 dB in the attenuation of the 10 test signals.

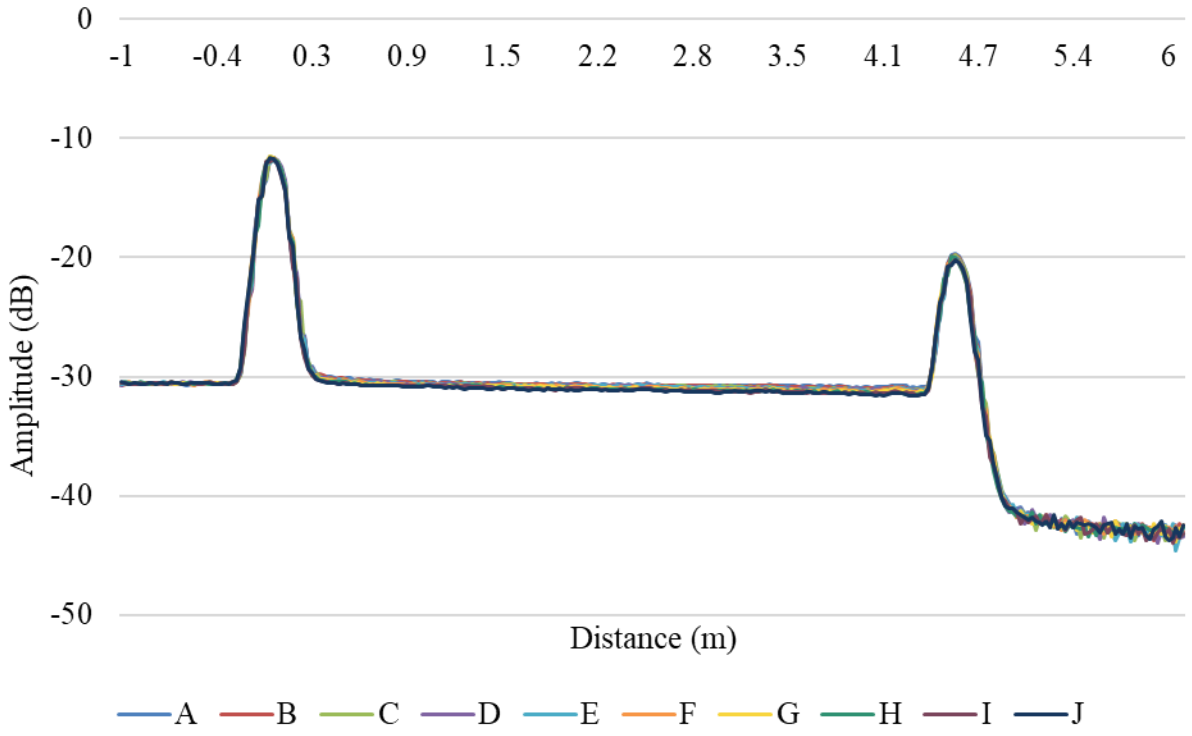

Figure D3. Connection test for POF which remained connection during record of the signals

It's concluded that a lot of the signal noise observed in the repeated impact tests is dependent on the connection to the OTDR. Many factors affect the POF signal these include, how far the end of the POF is placed in connector, that the connector is properly screwed onto the OTDR, the amount/ use of fiber optic cleaner, etc. The best way to conduct the repeated impact test was to leave the POF connect during the duration of repeated impacts to minimize variation in the signals.

Appendix E: Extra POF Signals

The following are specimens which were not used in the analysis due to premature damage, but they may still be able to provide useful information.

The POF shown in Figure E1 appears to be sensitive to damage, only surviving until impact 7 at 9 J impact energy. Impacts 1, 3, and 5 show a decrease in attenuation at the impact location site. The biggest drop around 3.3 m experienced at impact 7 seems to show that damage occurred closer to the edge of the composite rather than at the impact site. It was unclear if the damage experienced by the POF was related to damage at the edge of the composite or related to the impact damage, thus this specimen was not included in the larger analysis.

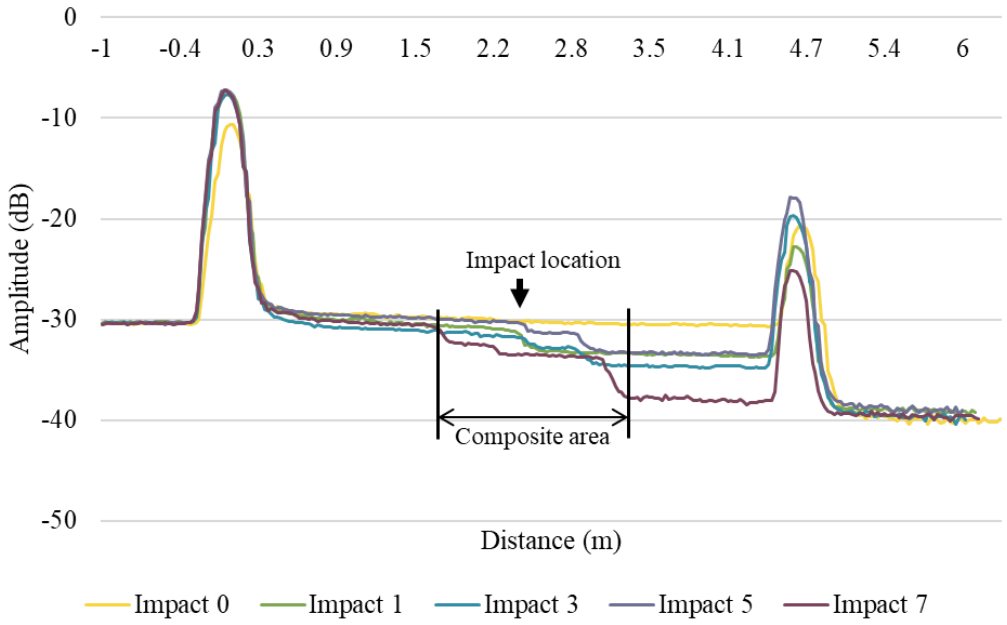

Figure E1. Signal of POF embedded in the top layer of the 4.72 picks/cm preform and impacted at a 9 J energy level

The exit point of the POF from the composite is a very sensitive area that is prone to damage such as bending. Given that there is a large peak near the edge of the composite, it is concluded that the POF in Figure E2 most likely experienced an event which caused the fiber to break, unrelated to the damage experienced by impact testing.

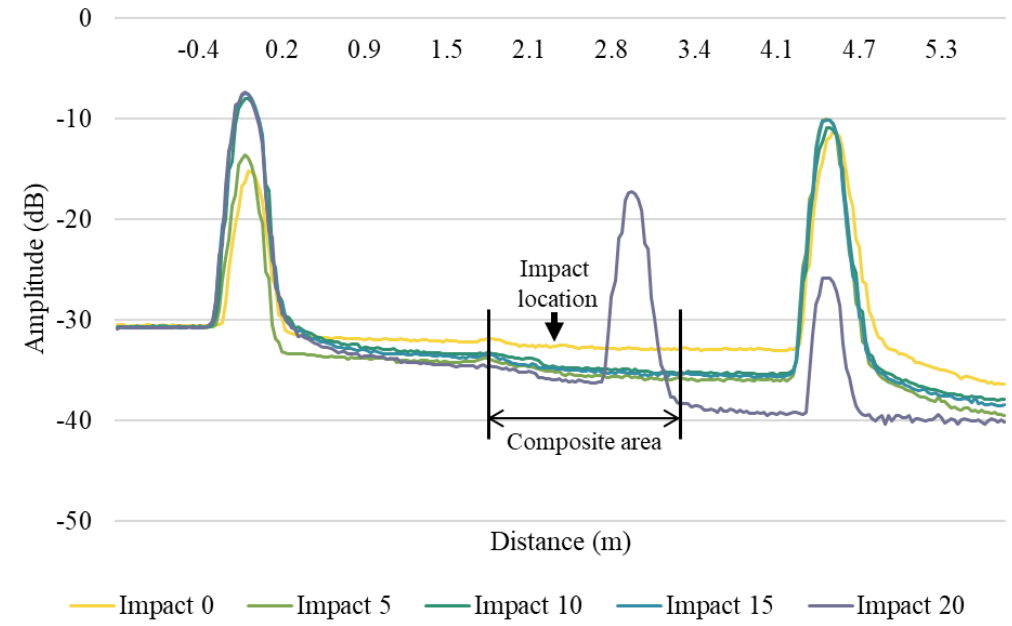

Figure E2. Signal of POF embedded in the middle layer of the 4.72 picks/cm preform and impacted at a 9 J energy level, failed at the edge of composite, not at the impact location

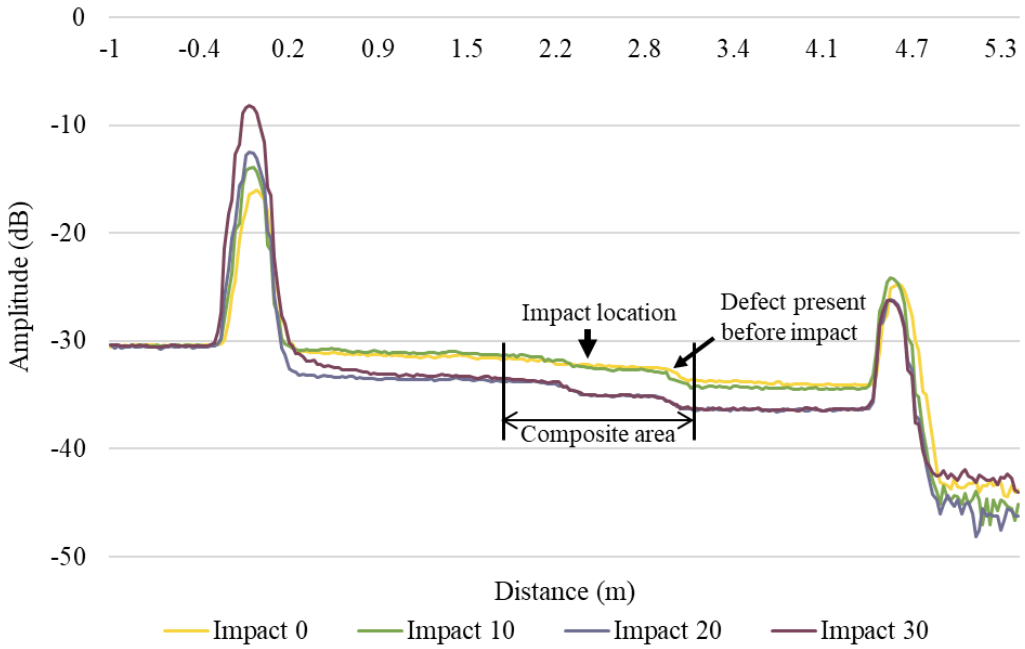

Figure E3. Signal of POF embedded in the bottom layer of the 4.72 picks/cm preform and impacted at an 18 J energy level

The POF in Figure E4 was impacted at an energy level of 9 J 1 cm away from the POF location. Unfortunately, the POF experienced damage outside of the composite area identified by the large

peak around 3.7 m. The interesting thing in this spectra is that the peak grows very nicely with each impact, indicating more damage to the POF each time the fiber is impacted.

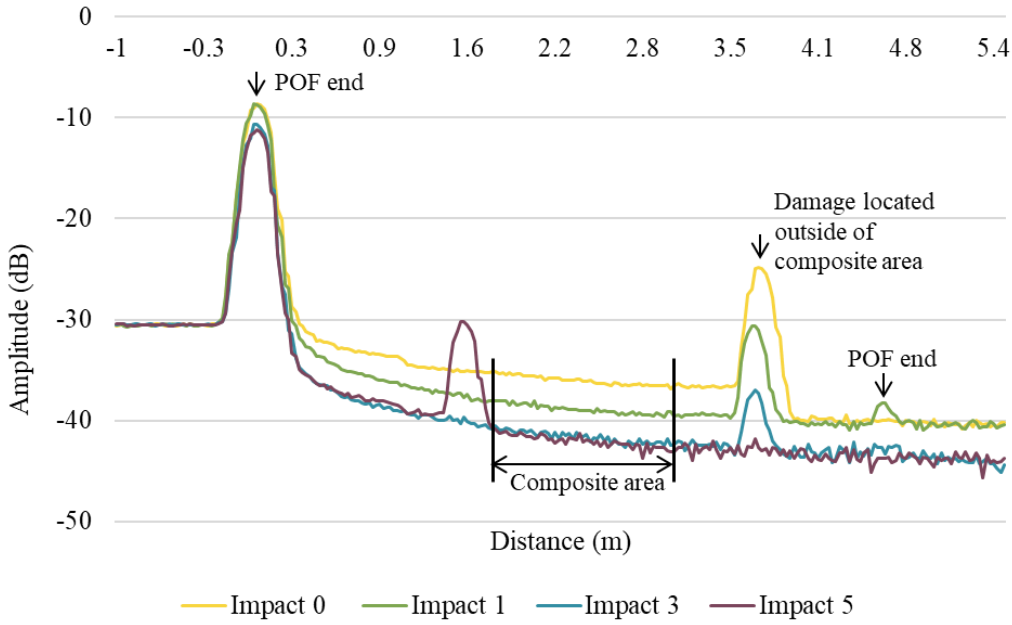

Figure E4. Signal of POF embedded in the top layer of the 4.72 picks/cm preform and impacted at a 9 J energy level, 1 cm from the POF location.

Specimens that had small defects after VARTM were also tested to create more repetition of each test condition. The POF in Figure E3 provides more date on specimens with the POF embedded in the bottom layer of the 4.72 picks/cm preform and impacted at an 18 J energy level. This test was conducted while being disconnected from the OTDR between impact events which accounts for the inconsistency in the reflection peaks at the ends of the POF. The signal shows a drop in attenuation of about 2.5 dB over 30 impacts, which is consistent with the test done under similar conditions in Figure 7.11.

Appendix F: Corning Flexible Glass, Multimode Fibers Testing

In conventional glass production, the silicon and oxygen bonds are very strong, rigid, and reinforced. This means that the weak point is typically a microcrack, scratch or impurity introduced to the glass. The conventional glass will bend a little before it breaks because of these impurities and physical flaws. Corning has a process of creating very pure glass with no impurities. Corning optical fiber is made out of special glass called high purity fused silica. The process takes place in a clean-room environment in a patented process of combusting very pure silicon-containing flammable gas. In this process, silicon tetrachloride gas is converted to silicon dioxide. Optical fibers also have the benefit of being a thin material which results in less stretching of the outer curve. The optic fiber is then coated with a layer of plastic to add extra protection against external damage.

Two optic fibers manufactured in this way, the Infinicor® 300 and ClearCure®, were obtained and a preliminary OTDR test was performed to determine if they are compatible with this measuring device. Both are Multimode fibers and have a small bending radius. Table F1 shows the specifications of each fiber. The OTDR setting used for each test are provided in table F2.

Table F1. Parameters of Corning OF

Parameters	Infinicor® 300	ClearCurve®
Core diameter (µm)	62.5	50
Cladding diameter	125	125
Coating diameter	242	242
Coating type	Acrylate	Acrylate

Table F2. OTDR settings

OTDR Setting	Value
Wavelength (nm)	670
Distance Range (km)	1.25
Refractive Index	1.496
Backscatter Coefficient (dB)	-68

The spectra for each OF, Figure F1a and b, show minimal attenuation and thus both are good candidates for embedding in composite materials in future projects.

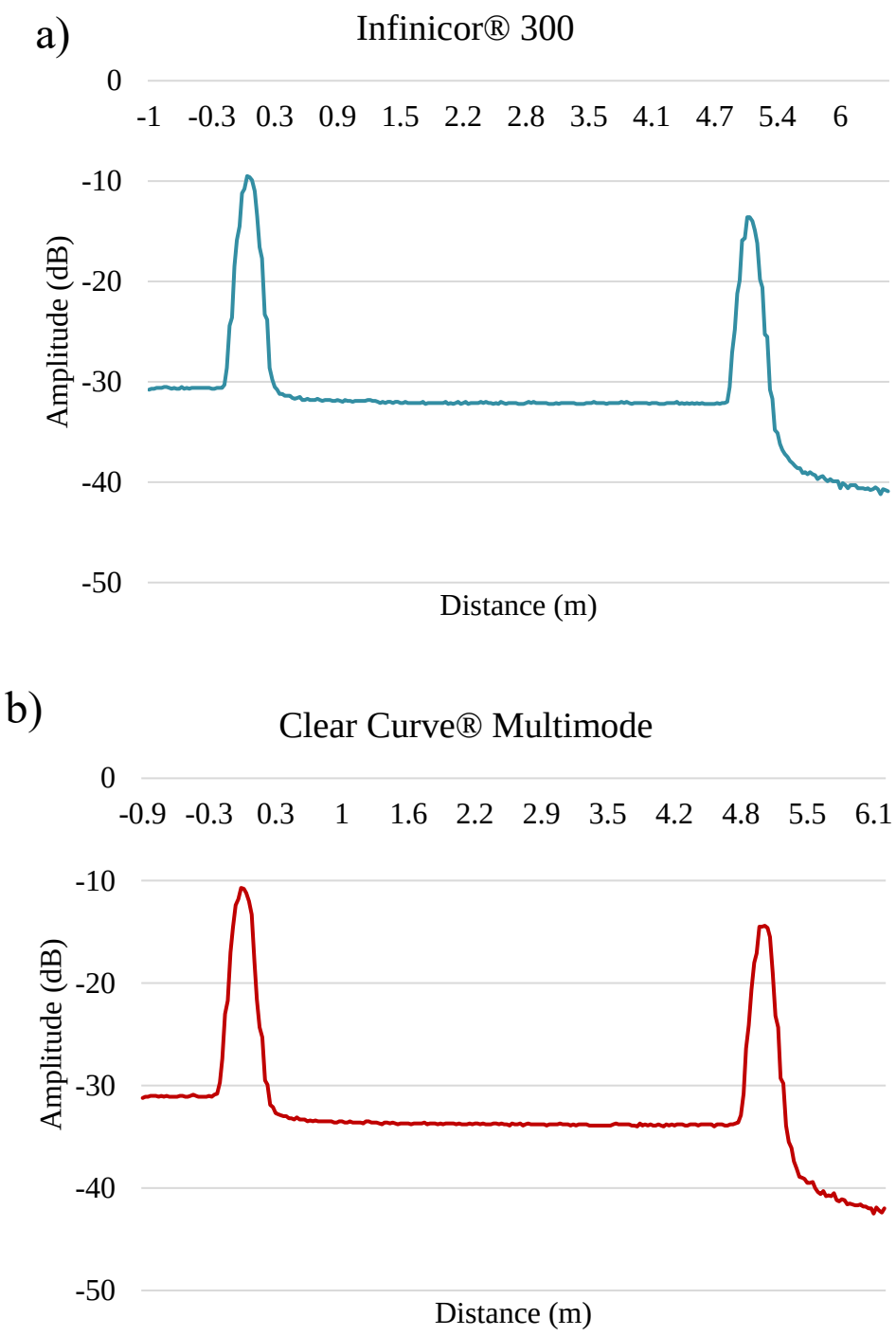

Figure F1. OTDR signal for a) Infinicor® 300 and b) ClearCure®

Appendix G: Additional Stop Words

01	accounted	apr	change
02	accounted	area	changes
03	accounted	article	chart
04	accountid	assembly	chemical
05	active	assets	circuit
06	activities	associated	cladding
07	addition	aug	claim
08	advanced	automation	close
09	ag	available	communication
1000	ago	average	companies
12725	ago	avg	company
1515	apparatus	b.market	company’s
1q	al	baker	compared
263	analysis	based	component
2q	analytics	beam	components
500	analyzed	ber	compositions
6.2	angle	billion	comprises
6702	announced	bites	comprising
a.market	annual	body	computing
a1	apparatus	brdf	condition
abstract	appl	business	conditions
access	application	cagr	configured
according	applications	cell	contact

control
controller
controlling
copyright
core
corp
corporate
corporation
corresponding
cost
coupled
current
customers
damage
data
date
dec
december
demand
description
design
detect
detection
detector
detectors
determine
determining
developed
development
device
devices
different
digital
display
distributed
distribution
document
docview
downhole
dundee
dynamic
ebitda
effect
electronic
electronics
elements
end
engineering
ensure
epo
equipment
equity
et
example
expected
factors
feb
feeds
fiber
fibers
fibre
field
figure
figures
flow
forecast
form
formation
forming
frequency
fujitsu
future
ge
general
generate
generated
generation
global
gm
graph
group
growing
growth
hal
halliburton
hanover
having
high
higher
highest
historic
hole
home
http
https
hughes
ibm
ii
iii
image

imaging
improved
include
includes
including
increase
increased
increasing
index
index.php
industrial
industries
industry
information
input
integrated
interface
interference
international
issue
issued
jan
january
January
jul
jun
june
key
kitco
kvh
large
largest
laser
layer
leading
length
level
light
like
line
location
login
long
loss
low
major
making
making
manufacturing
mar
march
margin
market
markets
material
materials
matrix
may
mcap
measure
measurement
measurements
media
metal
method
methods
million
million control
mode
model
modes
monitoring
month
months
multi
multiple
mz
mz
naics
net
network
new
news
nm
noise
non
nov
number
nyse
Ѳ
obtained
oct
october
office
operating
operation
operations
operations
optic
optical

optics
opticsensors
order
original
outlook
output
page
parameters
past
patent
patents
pcs
pdf
percent
performance
period
phase
photonic
photonics
plurality
point
portion
position
potential
power
pp
present
press
previous
price
process
processing
product
production
products
profit
properties
proquest
provide
provided
provided
provided
provides
providing
proxying.lib.ncsu.edu
pto
pts
publication
pv
quarter
range
rank
rate
real
received
receiver
recent
redox
reference
region
related
relative
release
report
reports
research
researchers
response
rest
results
return
revenue
review
safety
said
sales
sample
schlumberger
search.proquest.com
second
section
sector
security
segment
sensing
sensitive
sensitivity
sensor
sensors
sensuron
sep
services
set
share
shown
side
signal
signals

size
small
solution
solutions
source
speed
spending
state
states
stock
stocks
storage
stryker
study
support
surface
syk
systems
table
technologies
technology
technology
test
text
time
title
titled
today
tool
tools
top
total
trademark
transmission
trends
type
u.s
u.s.
unit
united
url
usd
use
used
user
using
uspto
utilization
value
valve
various
view
voice
vol
volume
wavelength
wellbore
wire
wireless
world
www.reserachandmarkets.com
year
years
yield
yrs
ytd

Appendix H: Stress-Strain Curves for Tensile and Compression Testing

Tensile Testing

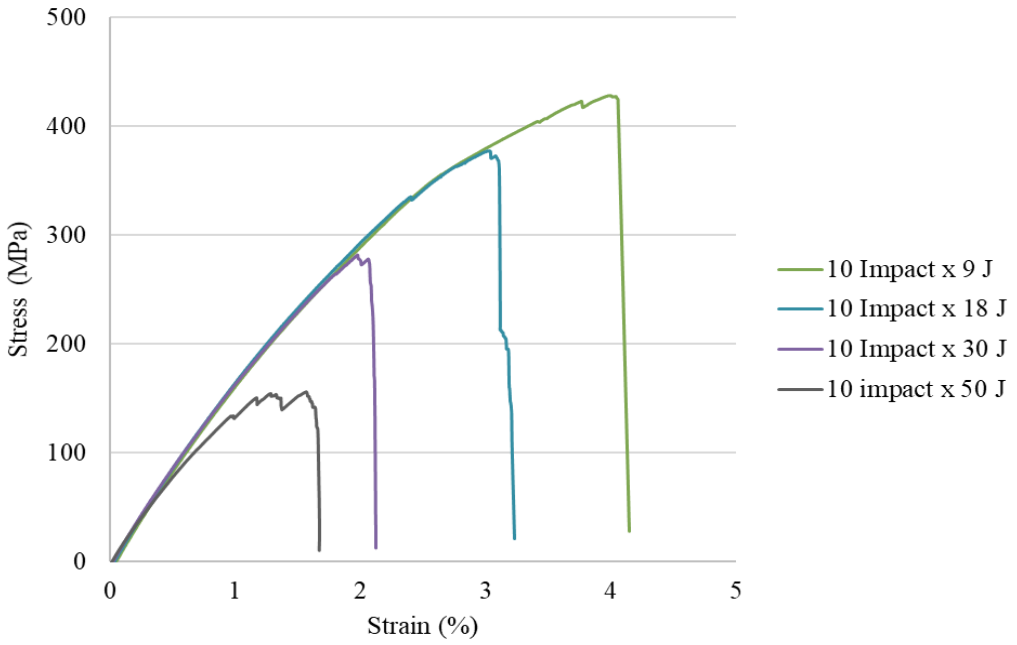

Figure H1. Tensile after impact test results for the 10th impact at various impact energies, pick density: 4.72 picks/cm

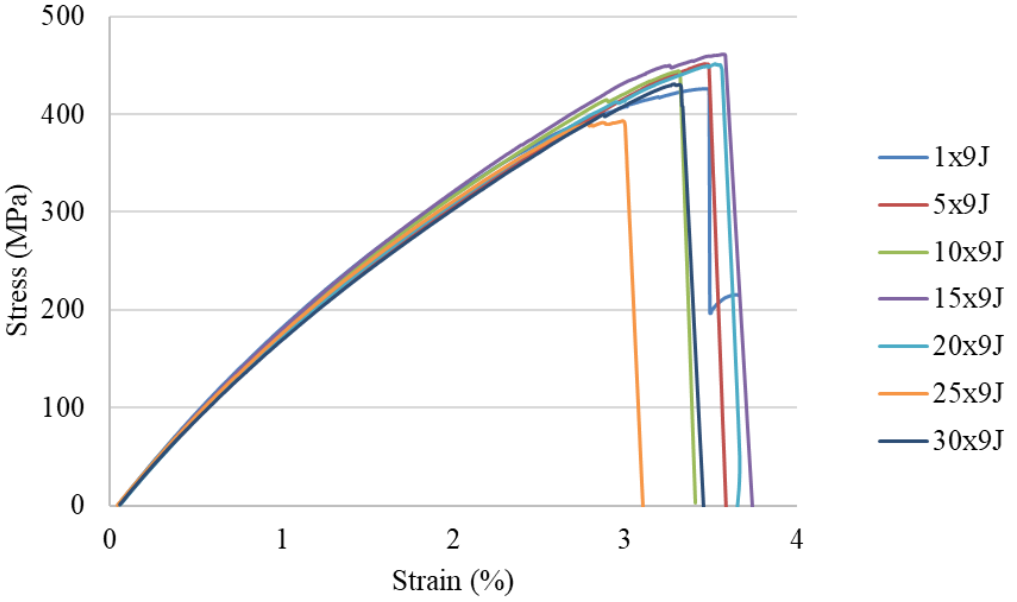

Figure H2. Tensile after impact test results for impact energy: 9 J, pick density: 4.72 picks/cm

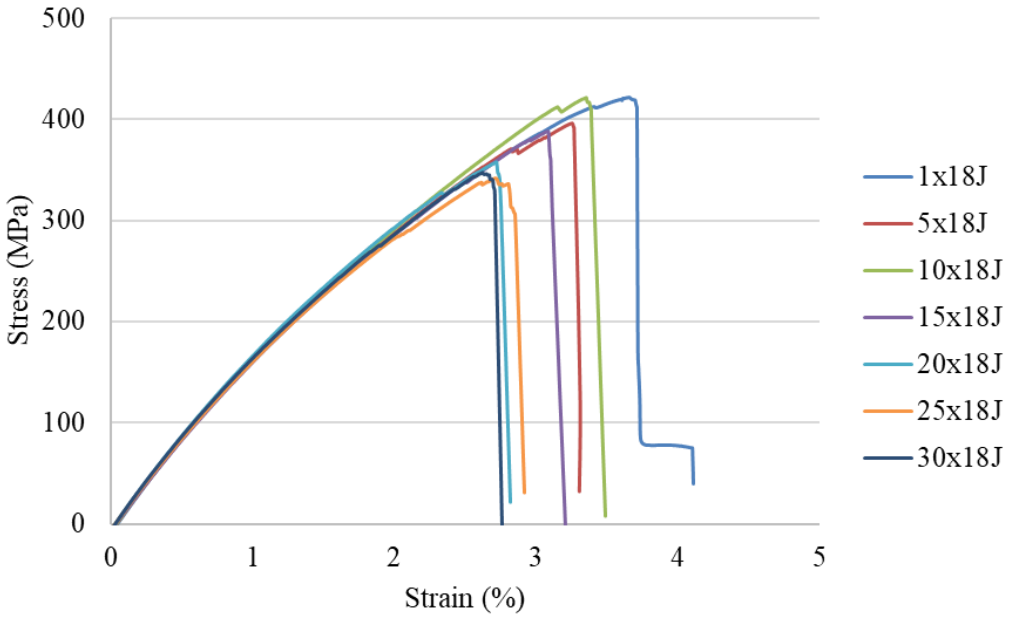

Figure H3. Tensile after impact test results for impact energy: 18 J, pick density: 4.72 picks/cm

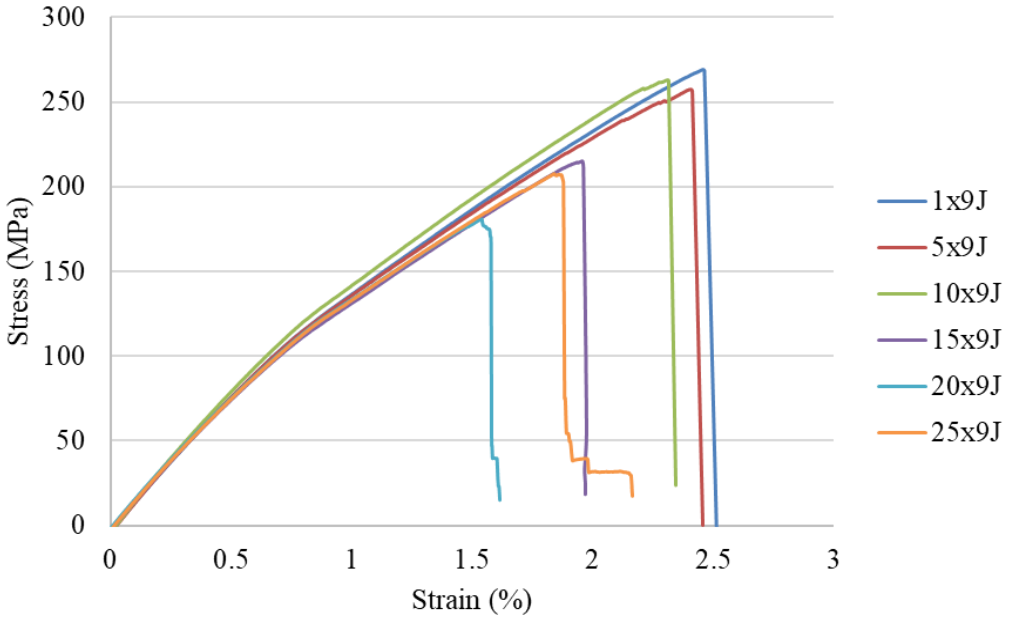

Figure H4. Tensile after impact test results for impact energy: 9 J, pick density: 1.57 picks/cm

Combined loading compression testing

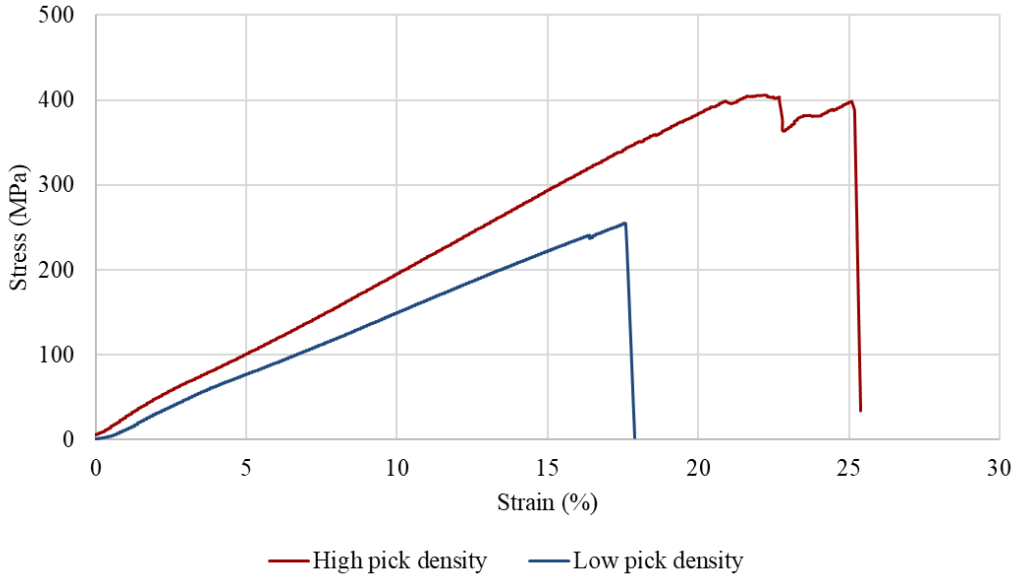

Figure H5. Combined loading compression test results for high pick density (4.72 picks/cm) and low pick density (1.57 picks/cm) specimens

Compression after impact testing

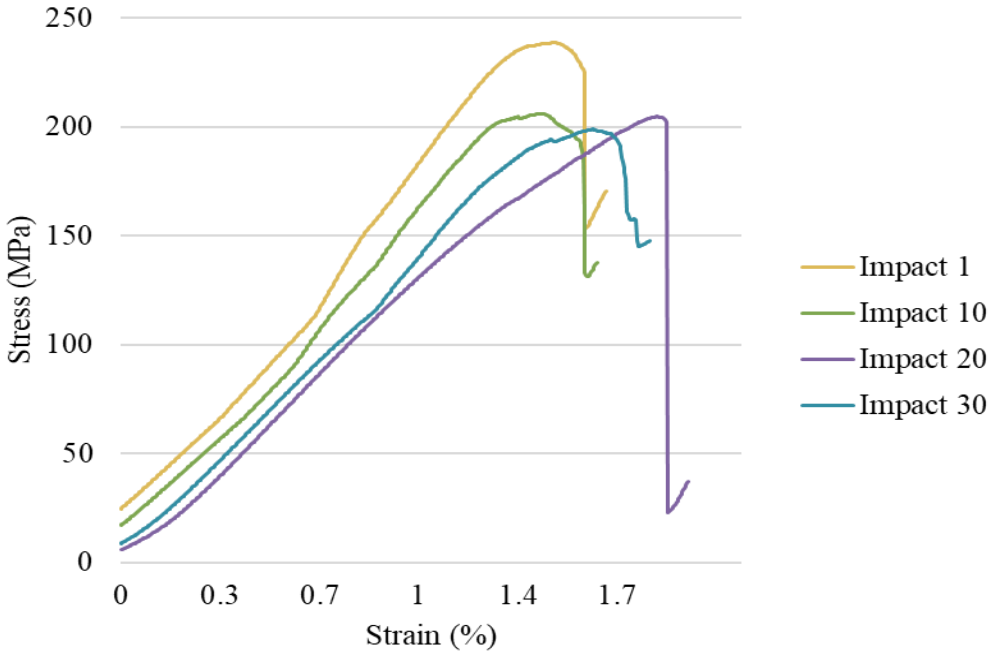

Figure H6. Compression after impact test results for impact energy: 9 J, pick density: 4.72 picks/cm

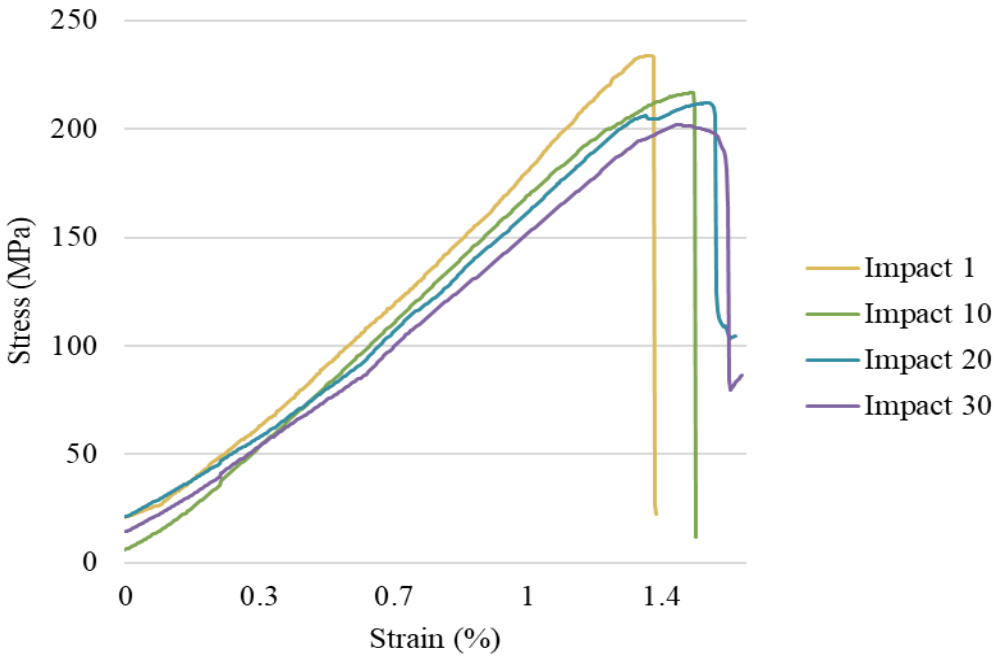

Figure H7. Compression after impact test results for impact energy: 18 J, pick density: 4.72 picks/cm

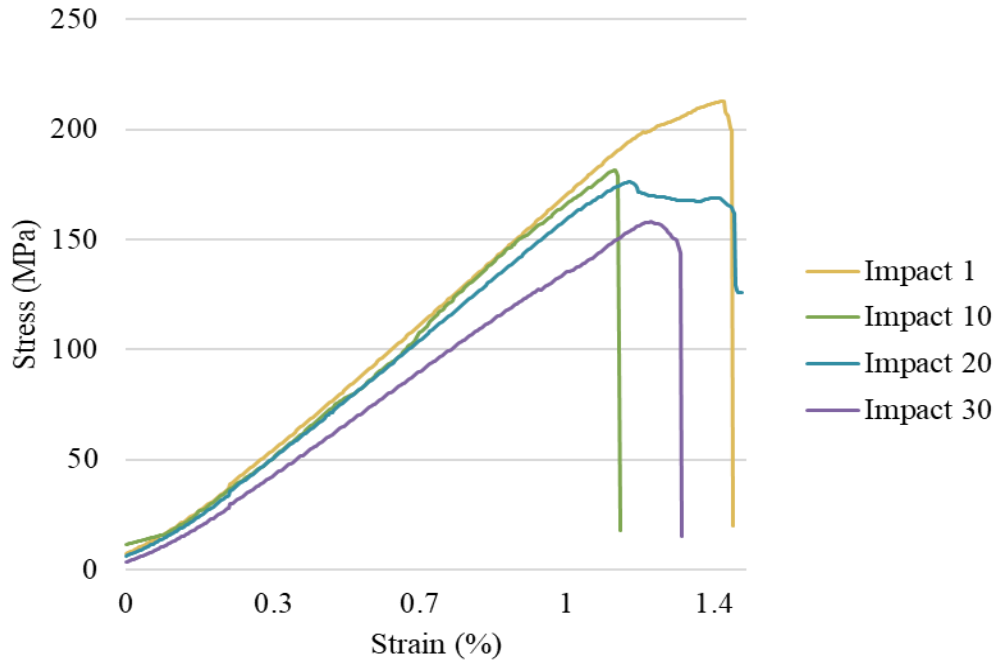

Figure H8. Compression after impact test results for impact energy: 27 J, pick density: 4.72 picks/cm

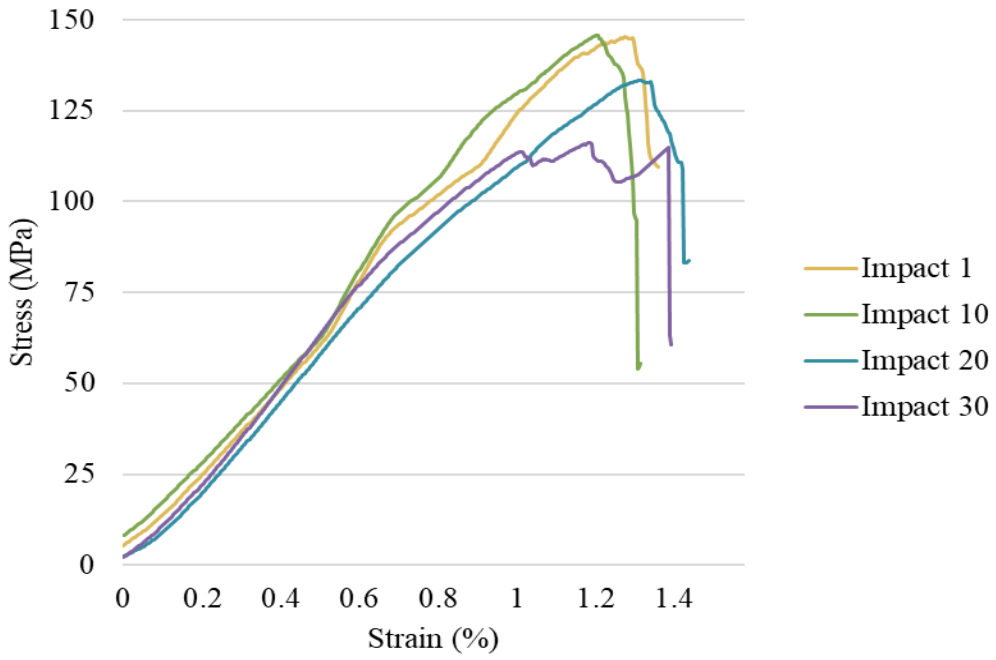

Figure H9. Compression after impact test results for impact energy: 9 J, pick density: 1.57 picks/cm

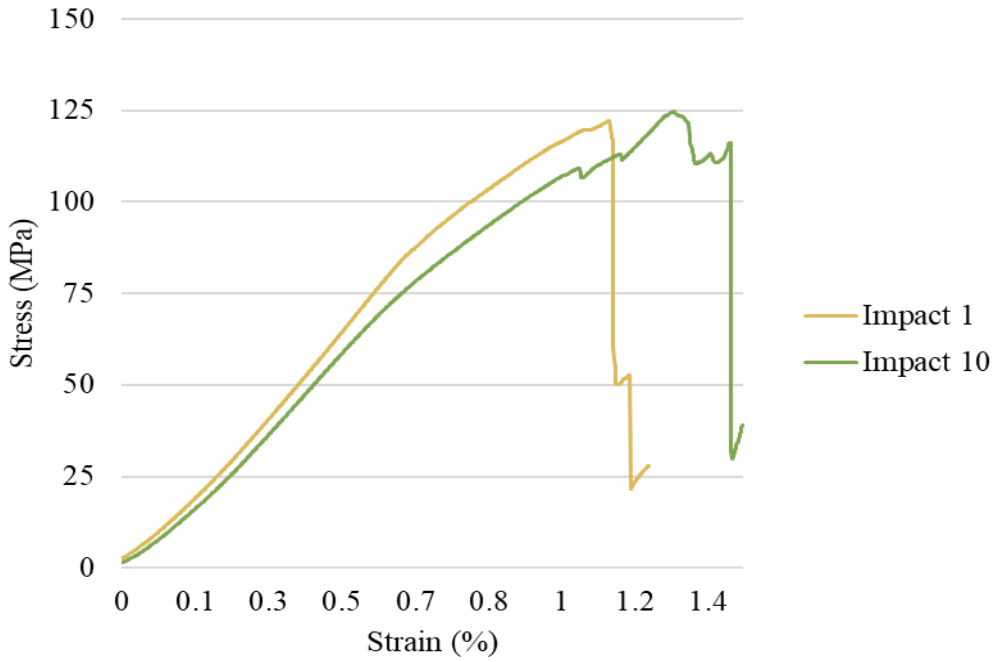

Figure H10. Compression after impact test results for impact energy: 18 J, pick density: 1.57 picks/cm